Office of Naval Research
Contract N00014-67-A-0298-0006 NR-372-012

STUDIES OF HUMAN LOCOMOTION VIA OPTIMAL PROGRAMMING

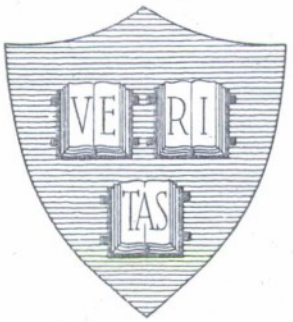

By

C. K. Chow and D. H. Jacobson

October 1970

Technical Report No. 617

Division of Engineering and Applied Physics
Harvard University • Cambridge, Massachusetts

Office of Naval Research

Contract N00014-67-A-0298-0006

NR-372-012

STUDIES OF HUMAN LOCOMOTION VIA OPTIMAL PROGRAMMING

By

C. K. Chow and D. H. Jacobson

Technical Report No. 617

October 1970

The research reported in this document was made possible through support extended the Division of Engineering and Applied Physics, Harvard University by the U. S. Army Research Office, the U. S. Air Force Office of Scientific Research and the U. S. Office of Naval Research under the Joint Services Electronics Program by Contracts N00014-67-A-0298-0006, 0005, and 0008.

Division of Engineering and Applied Physics

Harvard University · Cambridge, Massachusetts

STUDIES OF HUMAN LOCOMOTION VIA OPTIMAL PROGRAMMING†

By

C. K. Chow and D. H. Jacobson

Division of Engineering and Applied Physics

Harvard University · Cambridge, Massachusetts

ABSTRACT

Research to-date towards an understanding of human biped locomotion has been primarily experimental in nature, largely due to the complexity of the process. In view of the new, exciting possibilities of programmed electro-stimulation of paralyzed extremities to restore locomotion, a critical study at the theoretical level is greatly warranted. Optimal programming and modern control theory offer a new approach to the study. First, it is proposed that normal walking obeys a certain "principle of optimality". Next, at the dynamic level, modern control theory is used to derive the optimal moment profiles which actuate the locomotor elements to synthesize the observed patterns of the normal gait.

Development of the problem structure relies closely on the functional characteristics of the biped gait, particularly the ideas of distinct phasic activities and the associated temporal patterns of a walking cycle. The result is a multi-arc programming problem with three stages. Each stage involves dynamic constraints which reflect the particular nature of the phasic activity. Activity in the stance phase is described

† This work is partially supported by the Joint Services Electronics Program under Contract No. N00014-67-A-0298-0006.

by equality constraints on the "states" while the swing phase is characterized by inequality state constraints. A novelty of the approach is that the theory could be used to study walking behavior under different environmental conditions, such as walking up-stairs or over a hole. Joining of the arcs is arranged in such a way as to maintain continuity of certain trajectories as well as repeatability of motion.

A distinct feature of the present approach which differs from other studies is the presence of a minimizing performance criterion. Based on external characteristics of muscles and certain assumptions regarding normal locomotion, a simple quadratic type of performance index is proposed. This performance criterion is meaningful in that it is shown to be proportional to the mechanical work done during normal walking.

Invoking the necessary conditions of optimal control theory, a multi-point boundary value problem is obtained. A penalty function technique is then employed for iterative numerical solution on a digital computer. Using the parameters available in the literature, simulation results are obtained which agree well with the experimental studies performed by Eberhart and his associates. Furthermore, certain refined features are obtained which are not available in previous studies. Success in applying optimal programming techniques to human locomotion could yield better design procedures for prostheses and could allow eventual realization of the dream of programmed stimulation of many paralyzed persons.

TABLE OF CONTENTS

LIST OF FIGURES

A. Preliminary Considerations

1. Motivation.

Human locomotion displays a high degree of complexity, organization, and efficiency. The versatility and "gracefulness" of the motion has fascinated man for a long time. According to Bernstein [1], Leonardo da Vinci was probably the first to make scientific observations about human locomotion although real quantitative studies are only of recent vintage. In addition to scientific curiosity, the phylogenetic development of the biped gait from the push-pull mechanism of the quadruped is also of interest to the physical anthropologist. How much better is a biped adapted to its living patterns than, say, its quadruped counterpart To answer this question adequately, one has to explore the functional characteristics of the biped gait.

An important, practical goal of locomotion study is a better design of prostheses for disabled persons. In this and other areas dealing with human limbs and their substitutes, a common consensus is that the end products should duplicate the performance of their normal human counterparts as closely as possible. Thus, quantitative knowledge of the normal biped gait serves as a common denominator for performance evaluation and improvement of the various innovations.

The modern study of human locomotion began in the 1930's and has drawn greater attention since then. Significant contributions during this time include the works of Fenn [2, 3], Steindler [4], Elftman [5-8], Liberson [9], Wilson [10], Close [11], and the Eberhart-Inman group at Berkeley [12, 13]. Largely due to the complexity of the subject, results obtained so far have been experimental in nature. However, in view of

the recent exciting possibilities of restoring the locomotion ability of certain paralyzed limbs through programmed electro-stimulation [14-20], a critical study of biped locomotion at the theoretical level is greatly warranted. After all, the very fundamental question of " what is the basic mechanism of locomotion?" or "what are the laws governing locomotion?" cannot be answered in its completeness by experimental study. A theory which attempts to embody the known facts about the human gait would be an important step in this field.

Research activities to-date appear to fall into two broad areas. The first area is concerned with the functional structure and operational behavior of the locomotor system and its gait. The second studies energy expenditure, oxygen consumption and metabolism in general associated with walking. These two areas describe the important aspects of a very complicated process. With the tools of modern control theory, it appears possible to weld these two areas into a "functional" theory of human locomotion. Such a study leads to quantitative investigation and useful design procedures for prosthetic devices. To this end, the relevant physiological information and gait features are summarized. This, then, sets up the framework of our theoretical study.

2. Quantitative Features of the Biped Gait

a. Physiological Factors [21]

Locomotion activity and other voluntary efforts usually involve decision and supervision by the "higher centers" in the brain. Fig. 1 illustrates a typical skeletal muscle and its neural pathways. The skeletal muscle is the actuating unit for all locomotion activities. The α-motor input along the spinal cord represents a direct input from the

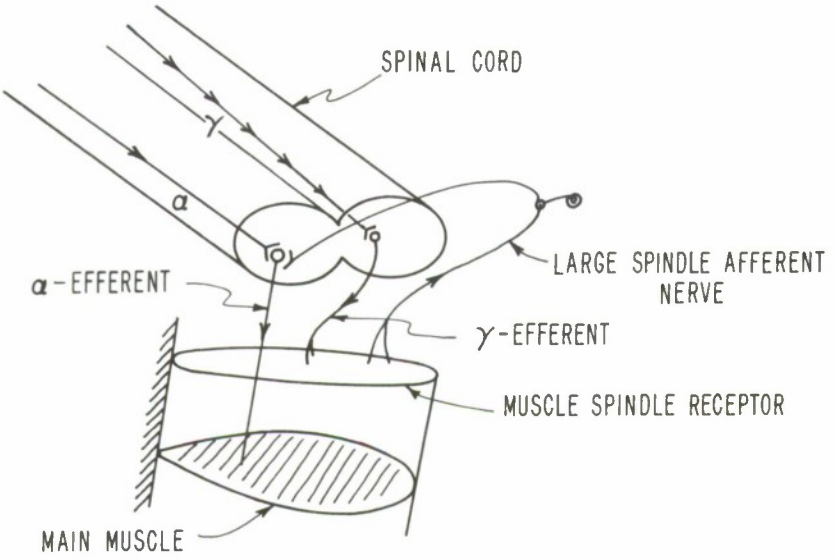

FIG. 1 SKELETAL MUSCLE AND NEURAL PATHWAYS.

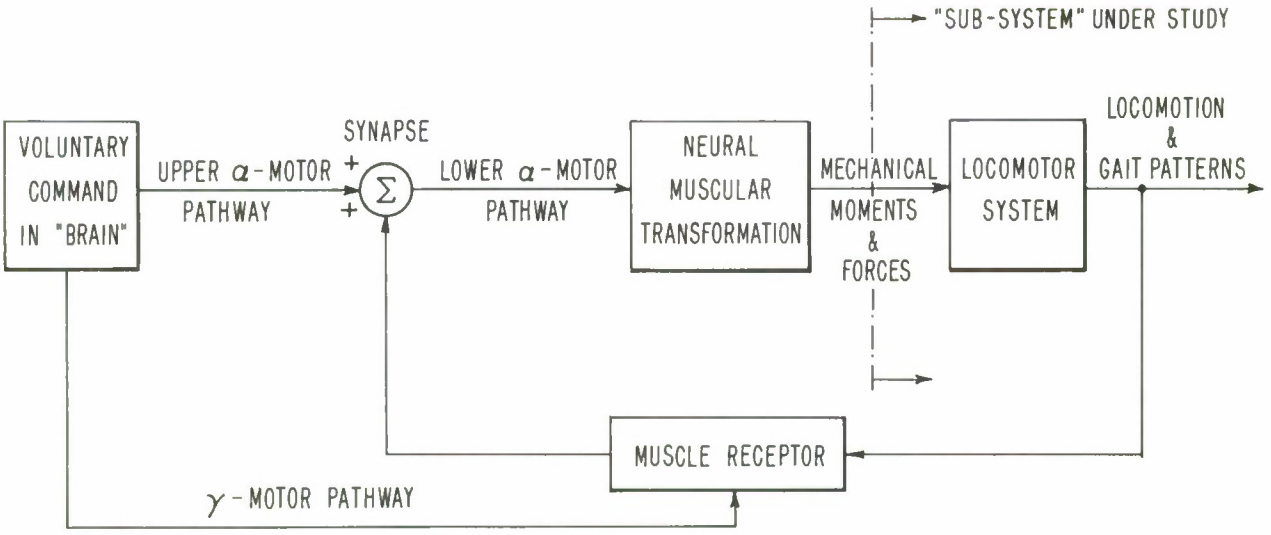

FIG. 2 BLOCK DIAGRAM FOR NEURAL-MUSCULAR CONTROL ACTION.

higher centers to the muscle by which the desired action can be initiated. It is believed that the α-motor input is the signal used for voluntary actions. A voluntary action exists in the conscious thought in terms of a functional rather than a specific description. "Lower" in the brain, the concept of "voluntary actions" is translated into a programmed sequence of individual muscle actions, based on the person's experience in the past in performing the task. The "activation" signal travels along the α-motor pathway. A muscle spindle receptor is shown inserted in a parallel position to the skeletal muscle. This is a transducer device which measures the length of the muscle and its sensitivity is adjusted by the upper γ-motor neuron. Results of the measurement are fed back to the thick lower α-motor neuron at the synapse where further integration of activity is taken. Thus the upper α-motor neuron as well as the peripheral sensory neuron of the muscle receptor control the lower α-motor neuron and subsequent muscular activity.

The simple picture of neural muscular action can be shown functionally in a block diagram in Fig. 2. The present study is primarily concerned with the various mechanical moments which actuate the locomotor system and the resulting gait patterns it produces. By knowing the moment histories, one can then concentrate on the neural-muscular transformation (E. M. G. activity and the like) for the electrical patterns of activity and eventually the neural action. This amounts to working outwards from the inner-most loop rather than studying the entire system in aggregate.

b. The Compass Gait [9, 22]

Under the action of the actuating moments, the motion of the locomotor system produces the patterns of the biped gait which can be studied experimentally to various degrees of accuracy. The principal feature underlying the biped gait is the compass motion of the two lower extremities about alternate centers of rotation. Such a rotation of the body about alternate centers brings about an overall translatory motion. In Fig. 3, suppose that the left leg has just completed its foreward swing and come into the restraining portion of the support (stance) phase. The deploy action of the right leg pushes the body forward with the hip describing a circular arc $\overset{\frown}{ABC}$ about the supporting left foot. At passing point B, the center of gravity of the body is directly above the femural head of the thigh. After that, the hip prescribes the segment $\overset{\frown}{BC}$ with the right leg in swing motion under gravity. At C, the swinging right leg restrains the falling tendency and goes into the stance phase of activity. Concurrently, the left leg in the late stance undergoes deploy and continues into swing. This results in a second arc $\overset{\frown}{CDE}$ for the hip with the role of the left and right legs interchanged. When this is completed, the entire cycle of the "double-step" is repeated. The compass gait results in a series of intersecting circular arcs for the hip trajectory in level walking. In actual motion, the gait is made more graceful and efficient during transfer between adjacent arcs by additional motion of the legs and pelvic adjustment. The smoothed action results in an almost sinusoidal trajectory for the hip.

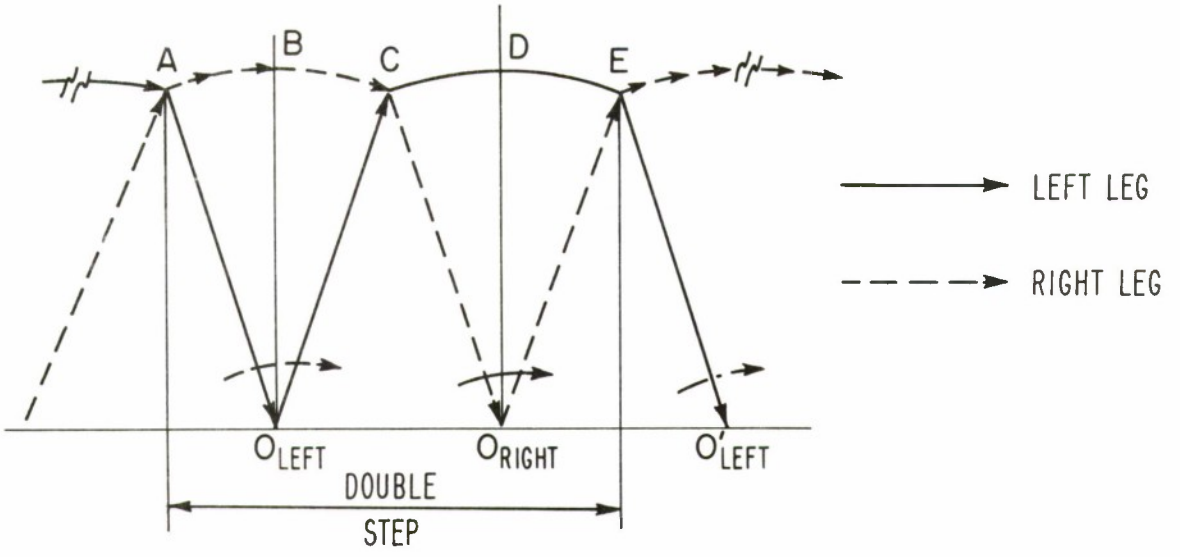

FIG. 3 THE COMPASS GAIT.

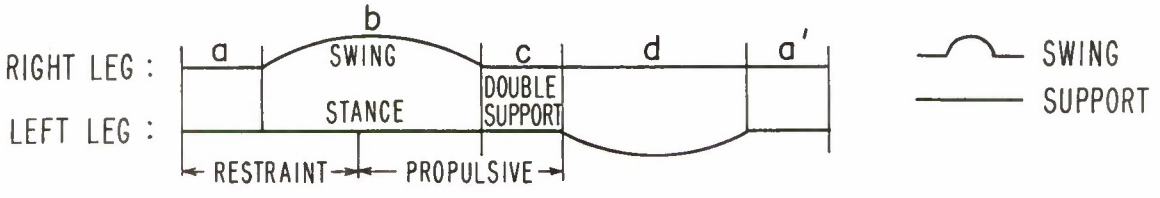

FIG. 4 TEMPORAL PATTERNS OF BIPED GAIT.

c. Phasic Activities and Temporal Patterns [4]

The smoothed pattern of the biped gait requires a good deal of coordination in the activities of the two lower extremities. The result is that there are two characteristic phases of activity in a "double-step" - the stance (restraint, support and deploy) and swing. In normal walking, the phasic activities of one leg occur with regularity and are coordinated with those of the other leg. Fig. 4 illustrates such a temporal pattern. Note that there is a brief double stand period (restraint/deploy) when both legs are in contact with the ground. In fast walking, approaching running, the double stand becomes shorter. In running, there is even a brief period when both legs are in the air. The mechanism of the striding mode in normal walking is different from that of the running mode. Using a foot-switch method, it has been measured that the stance phase occupies roughly 60% of the time required for a double-step. The remaining 40% is swing motion. The deploy (or restraint) portion in stance takes 10 to 15% of a double-step period [4, 19].

d. Postural Control and Stability [22, 23]

The foregoing paragraphs describe the behavior of the lower extremities in level walking. As far as the upper part of the body is concerned, the center of gravity of the trunk is imparted on an oscillatory path as a result of the alternate bipedalism of the gait. As one leg serves as support while the other goes through swinging motion, there is imbalance of moments and forces in the frontal and horizontal planes. These tend to destabilize the trunk from the upright position, as it resembles an inverted pendulum mounted on a moving platform.

To maintain upright position and minimize undesirable oscillations, coordination of various muscle activity is needed. From a locomotion standpoint, the progressive translation of the body is of main concern. The associated unstable tendency of the trunk is an unfortunate consequence inherent in the biped gait.

e. A Hierarchical Control System for Biped Locomotion

From the temporal, phasic and stability properties of the biped gait, it is quite apparent that the locomotion process is involved indeed. It has been postulated that the control system possesses a hierarchical structure, with two or more levels of decision, coordination and regulation for a desired gait and adaptation within a given environment. Important objectives of the control system would be:

(1) determination of speed, step length parameters and direction of progression

(2) synchronization of the motion of the two extremities to achieve coordinated phasic activities and temporal patterns

(3) adaptation to ground profile within a double-step

(4) maintenance of up-right posture.

With the exception of (1), the gait features we have described fit into the objectives of the controller. From an organizational viewpoint, the goals (3) and (4) are realized by a control system under the supervision of a higher level controller connected to (1) and (2). A schematic diagram of the locomotion system would appear as shown in Fig. 5.

Such a functional structure for the control system possesses the advantages described by Tomovic [24]:

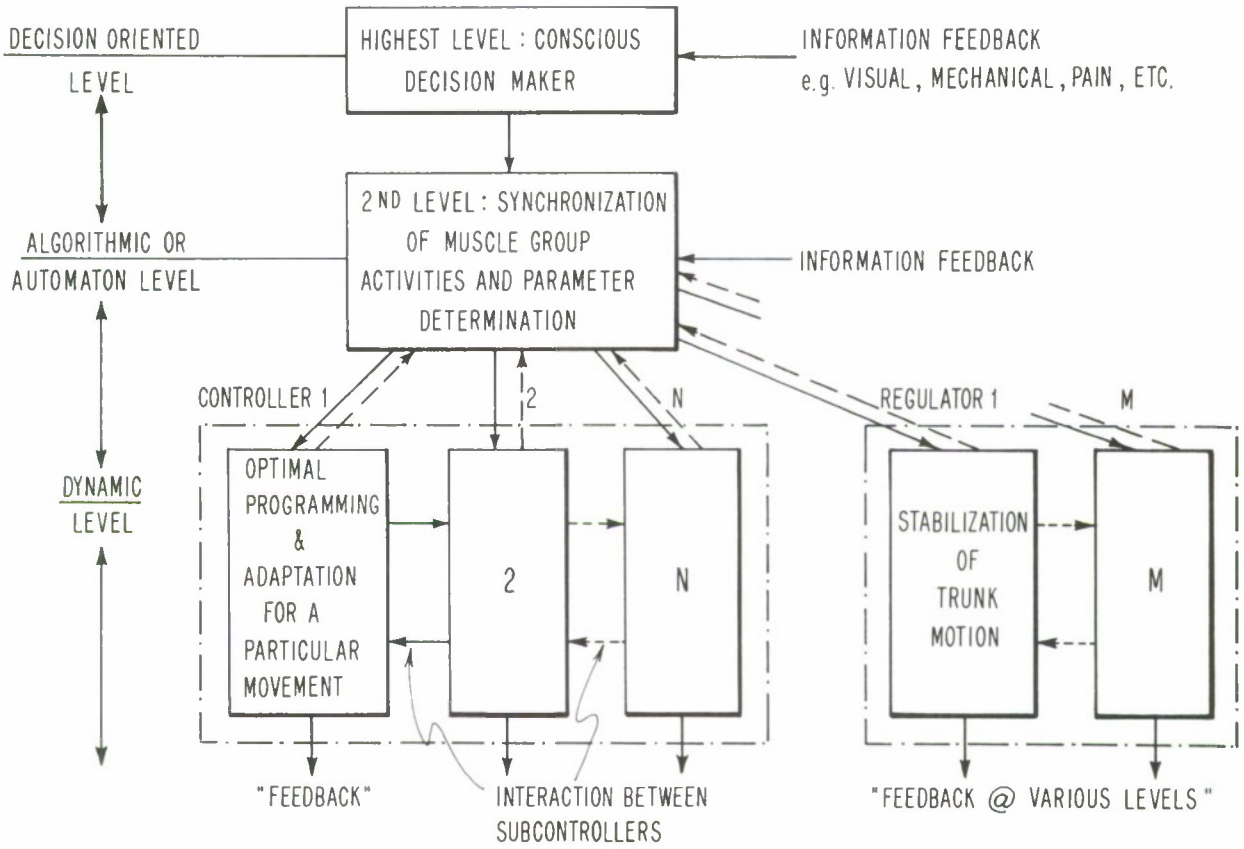

FIG. 5 HIERARCHY STRUCTURE FOR THE LOCOMOTION CONTROL SYSTEM.

(1) A minimal amount of supervision required on the part of controllers at the algorithmic and higher levels in executing well-learned tasks such as normal level walking.

(2) Flexibility at the dynamic level to adapt to a particular environment within a double-step.

The present interest is in finding out the various actuating moments to simulate the biped gait. This implies that the analysis is performed at the dynamic level of the hierarchical system. The choice of speed of walking, step-length, direction and other relevant parameters are the goals of the algorithmic controller, as is the coordination of muscle group activities.

3. Energy Expenditure and "Optimality" in Locomotion

Besides the broad study of the functional characteristics of the biped gait, the ergonomics of locomotion forms another important area of research. An average person walks over a million steps in a year and certainly many times more over the span of his lifetime. In situations such as level walking where speed is not an important factor, it is thus very appealing to think that the walking activity would involve minimization (optimization) of some type of energy performance criterion. In search for such an "optimality" in locomotion, experimental studies in energy expenditure, oxygen consumption associated with locomotion have been performed. Significant contributions include the works of Fenn, Elftman [7], Ralston [25], Cotes and Meade [26]. Earlier results were obtained by Atzler and Herbst. Theoretical attempts to formulate or demonstrate a "minimal" principle were made by Nubar and Contini [27] and Beckett and Chang [28].

By far the most interesting result has been the measurement of mechanical work done by the various body members during walking as a function of speed, step-length and pace frequency parameters. In the experiments by Atzler and Herbst as reported in Elftman [5], they plotted energy expenditure for different speeds and step lengths. A minimum expenditure curve exists for the appropriate combinations of speed and step-length. In a more recent study by Coates and Meade, similar results were obtained and various expressions were obtained from experimental data by interpolation. Milner [20] and his associates performed quantitative study of EMG activity of the muscles of the lower extremities in connection with the programmed electro-stimulation problem. In particular, they showed that the EMG activity is minimum when their human subject is allowed to walk at a pace frequency of his own choice for a given speed of walking. Whether human locomotion does indeed obey an optimality principle has not been proved by experiment or theory, but the results gathered to-date do support the suggestion.

4. The Optimal Programming Approach

We have briefly summarized the two important areas of locomotion research. To cast the biped gait in an optimization context, the underlying hypothesis is that the locomotion activity follows a principle of optimality. In the subsequent analysis, an appropriate minimizing performance criterion is developed which reflects or measures the mechanical work done by the muscles of the lower extremities during walking. The system dynamics and auxiliary constraints will be developed on the basis of gait information mentioned earlier.

Numerical solution of the resulting optimization problem leads to specification of the various moment quantities and the simulation of gait patterns on the basis of minimum mechanical energy expenditure.

This approach, using modern control theory, attempts to unite the two areas of experimental work. It differs from the other studies in that the actuating moments are not predetermined on experimental or intuitive grounds. The programming approach, if proved fruitful, opens a new way to study the locomotion problem and quantify prosthetic design. To formulate the problem structure, specification is required of the following:

(1) An appropriate mathematical model for simulating the functional behavior of the locomotor system.

(2) Auxiliary constraints - kinematic and dynamic on the basis of gait information.

(3) Initial, terminal and "inflight" conditions.

(4) An optimality criterion which can be extremized to yield the actuating moments and other quantities of motion.

B. Mathematical Modelling of the Biped Gait

1. Introduction.

In a quantitative study of the biped gait, the important moving units are not the various bones which support the surrounding tissues but the total mass of the segments which rotate about their respective joint axes. The central straight line which extends between two axes of rotation is called a link. This may be longer or shorter than the particular bone it represents. For example, the femur and humerus are longer than their respective links while the tibia and radius are shorter. Functionally, the human body is an articulated system of links. Although the overall displacement of the body is translatory, motion is achieved by angular displacements of the links about their respective axes. The compass motion as mentioned earlier is the basic mechanism of biped locomotion. The objective of mathematical modelling is to describe the angular motions and relate them to the overall translatory process of locomotion. Such a mechanical description is separated from the action of the muscles and other physiological considerations.

The multi-linkage models have been studied by Nubar and Contini [27]; Vukobratovic and his associates [22, 23, 29]; Beckett and Chang [28]; and Hill [30]. Complexity of the models developed depends on the assumptions made about the gait and degrees of freedom allowed in the motion. In a paper by Nubar and Contini, a system of linear differential equations was derived for small angle dynamics. However, they set pertinent derivatives to zero and studied only static configurations of the gait. Maric and Vukobratovic formulated the leg in level walking as a two link system. The assumptions on the gait were that the hip was

stationary and the foot in continuous contact with the ground during a double-step. There was no mention of the reactional and internal forces. In two joint papers by Vukobratovic, Frank and Juričič, the stability problem of the trunk was studied on the basis of a compass gait for the lower extremities. In the same vein, Beckett and Chang studied the kinematics of swing phase motion under a "minimum energy" hypothesis, but the interesting point is that they obtained the moment profiles without any optimization procedure. Lastly, Hill proposed a nine degrees of freedom model for postural study. The dynamic equations are apparently too lengthy to derive! Thus it appears that realistic efforts in modelling are still lacking. The works done to-date share the following features:

(a) They are multi-linkage type mechanical models.

(b) The analysis is confined to motion in the sagittal plane.

(c) Only the case of level walking has been treated. Other configurations such as walking upstairs, downstairs, or over rough terrain have not been considered at all.

(d) The models have been much simplified to render the problem tractable. The result is that they embody little or none of the described properties of the actual biped gait.

2. Development of the Mathematical Model.

The present model emerges as a compromise between complex high order models and the simple two-link type. Under suitable assumptions, a high order model is decoupled into two parts. The part relevant to lower extremity is still of a two-link type. However, appropriate constraints are imposed to insure realistic simulation of the gait

patterns. Modern control theory can handle constraints effectively while the classical methods cannot. The development of such a "constrained" mechanical model takes place in the following stages.

a. Two Basic Configurations.

Based on the qualitative features of the biped gait, the actual process can be visualized as being made up of two basic configurations or modes of motion. Fig. 6 illustrates the basic configurations. The first is referred to the double-stand period when both legs are in contact with the ground. One leg supports the body, restraining its falling tendency as a result of the previous swing motion. The other leg starts its deploy action through rotation of the foot about its toes (more precisely, the ball of the foot). We call this the deploy/restraint configuration. The second mode follows the first in that the restraining leg now takes up complete support of body weight while the other leg, previously in deploy, is in its swing motion. We call this the support/swing mode. Thus, the biped gait is an alternating sequence of these two basic configurations, with the role of the two lower extremities interchanged during a double-step.

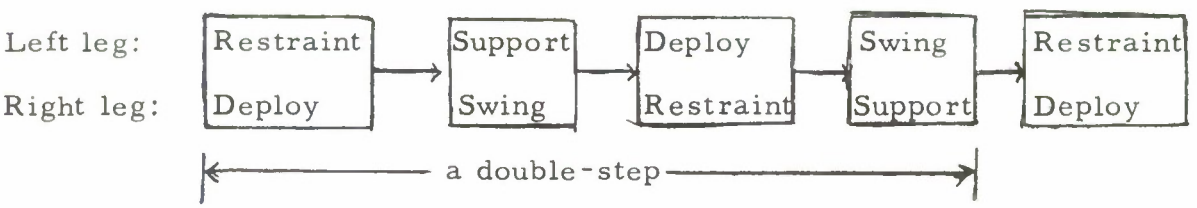

The idea of two basic configurations introduces symmetry into the biped gait. It excludes singular behavior such as one leg starting in deploy while the other is still in the last stage of swing motion. In the actual case, such singular modes, if they exist, usually occur for a very

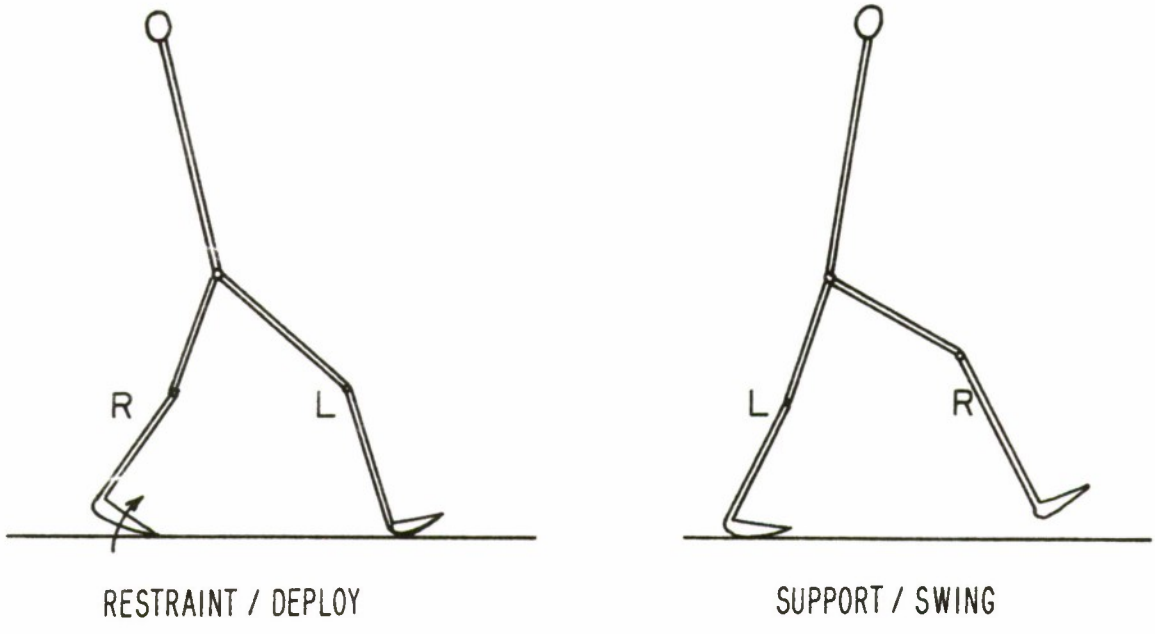

FIG. 6 TWO BASIC CONFIGURATIONS OF BIPED GAIT.

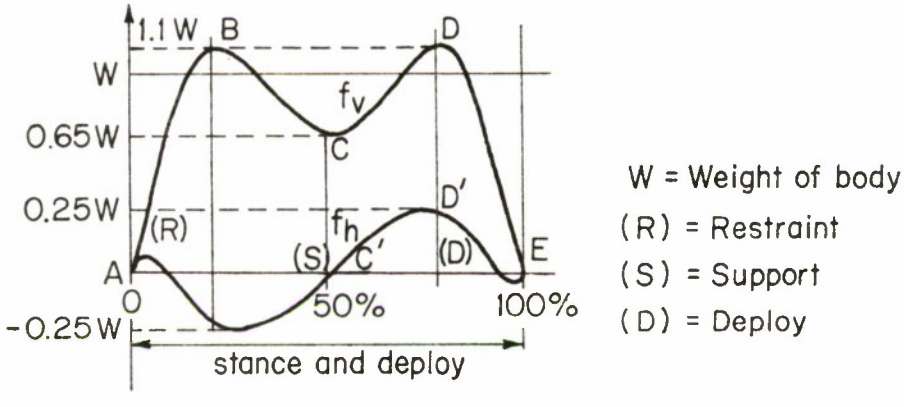

[31]

FIG. 7 GROUND REACTION PROFILES (FROM INMAN).

brief interval so that they can be neglected in a first study. In the current literature, the restraint, support, and deploy portions are collectively known as the stance phase of activity. In our formulation, we will refer to restraint and support collectively as the "stance" portion.

b. Derivation of the Model.

Fig. 8 depicts a high degree of freedom model for motion in the sagittal plane. Considering the locomotor system as a whole, the inertial and gravitational effects of the foot are small in comparison with those of the shank or the thigh. The average weight of a foot is about 1 to 1.5% of the body and its dimensions are also small (approximately $\frac{1}{3}$) as compared to the thigh or the shank. Furthermore, its behavior is more or less specified in a double-step. This is so because, in the stance position, the foot is almost stationary except for a brief moment following heel strike to absorb impact. In deploy, the ankle of the foot describes a circular arc with the center of rotation located about the ball of the foot. In swing, the foot is locked with the shank at an approximately constant angle. Such a kinematic behavior of the foot can be described by appropriate constraints on the thigh and shank variables. Dynamically, the foot is subjected to large ground reaction forces which exceed body weight in the stance position. Characteristic profiles of the forces are shown in Fig. 7. The actual "shape" of these forces depends primarily on the gravitational and inertial effects of the motion of the upper part of the body. The internal forces X, Y at the ankle joint in turn depend almost entirely on the ground reactions. The up-shot of all this is that the behavior of the foot can be alternatively described by appropriate

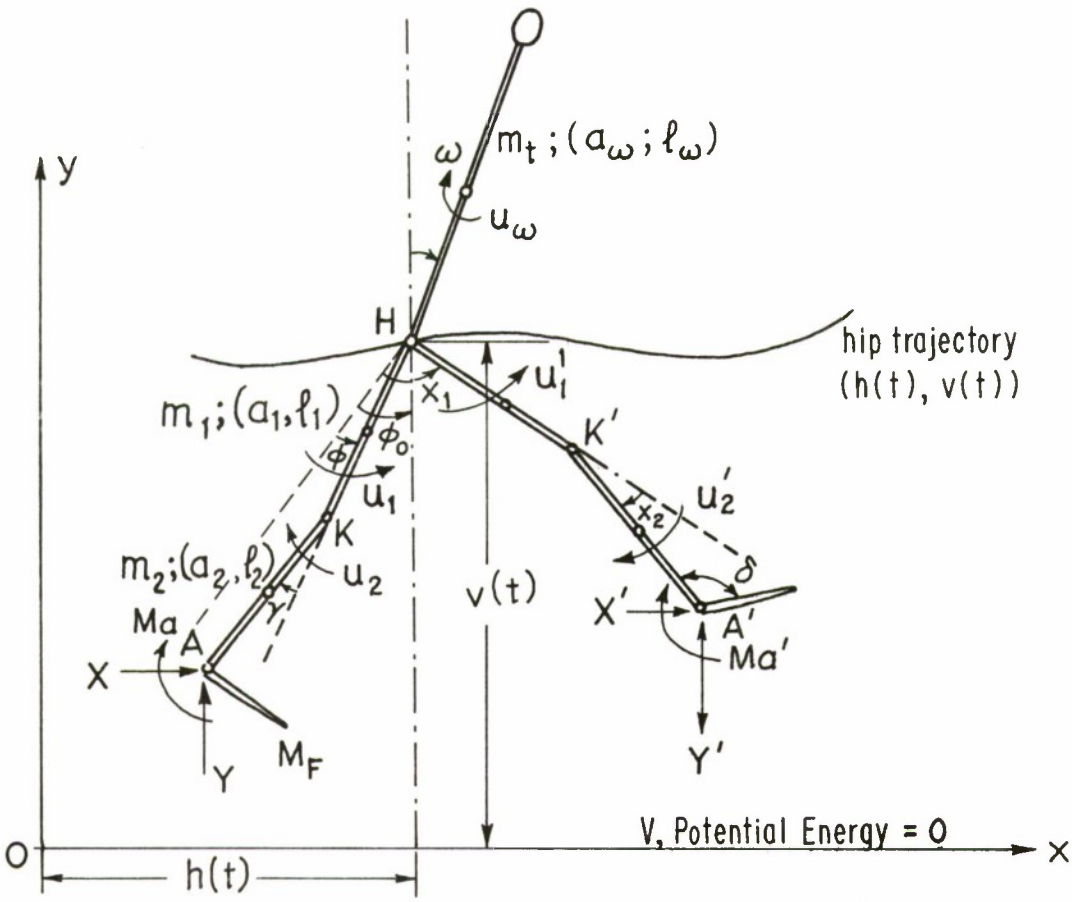

FIG. 8 COORDINATE SYSTEM FOR THE HUMAN LOCOMOTOR SYSTEM MODEL.

NOTATION: a_1 = distance of center of gravity of the thigh segment from hip joint (H)
a_2 = " " " " " " " shank " " knee " (K)
ℓ_1 = length of the thigh segment
ℓ_2 = " " " shank "
$m_i \triangleq$ mass of the i-th segment (i = 1 ⇒ thigh ; i = 2 ⇒ shank ; i = t ⇒ HAT section)
Y, X = vertical and horizontal reactions at the ankle
Ma = ankle moment
u_i = effective moment for the i-th link

constraints and equivalent forces at the ankle. This device reduces the order of the system dynamics.

With the motion of the foot considered, we are now in a position to derive the mathematical model for the locomotor system. To achieve symmetry in the equations, let (h(t), v(t)) denote the horizontal and vertical position of the hip. Let the variables ϕ and γ be assigned to describe the leg in the stance portion. The leg in deploy and swing is described by the angles x_1 and x_2. The head, upper extremities and trunk portions are collectively considered as a single link described by the variable ω. Note that the hip position (h(t), v(t)) is a function of the variables ϕ, γ. This is also dependent on x_1 and x_2 in the deploy portion, i.e.:

$$h = x_A - \ell_1 \sin(\phi - \phi_o) + \ell_2 \sin(\gamma - \phi + \phi_o) \tag{1}$$

$$v = y_A + \ell_1 \cos(\phi - \phi_o) + \ell_2 \cos(\gamma - \phi + \phi_o)$$

where (x_A, y_A) denote the position of the ankle. Similar expressions hold for the x_1 and x_2 variables in the deploy portion. To carry out the derivation by use of Lagrange's equations, expressions for the kinetic and potential energies of the various links are needed. The centers of gravity for the respective links are:

(1) thigh in stance portion

$$\tilde{x}_\phi = h + a_1 \sin(\phi - \phi_o)$$

$$\tilde{y}_\phi = v - a_1 \cos(\phi - \phi_o) \tag{2}$$

(2) shank in stance portion

$$\tilde{x}_\gamma = h + \ell_1 \sin(\phi - \phi_o) - a_2 \sin(\gamma - \phi + \phi_o)$$

$$\tilde{y}_\gamma = v - \ell_1 \cos(\phi - \phi_o) - a_2 \cos(\gamma - \phi + \phi_o) \tag{3}$$

(3) thigh in deploy and swing portions

$$\tilde{x}_1 = h + a_1 \sin(x_1 - \phi_o)$$
$$\tilde{y}_1 = v - a_1 \cos(x_1 - \phi_o) \tag{4}$$

(4) shank in deploy and swing portions

$$\tilde{x}_2 = h + \ell_1 \sin(x_1 - \phi_o) - a_2 \sin(x_2 - x_1 + \phi_o)$$
$$\tilde{y}_2 = v - \ell_1 \cos(x_1 - \phi_o) - a_2 \cos(x_2 - x_1 + \phi_o) \tag{5}$$

(5) trunk motion for all portions

$$\tilde{x}_\omega = h + a_\omega \sin\omega$$
$$\tilde{y}_\omega = v + a_\omega \cos\omega \tag{6}$$

The velocity of the center of gravity for each link is obtained through differentiation with respect to time. From this, the total kinetic energy of a link is the sum of translation component due to motion of C.G. and rotation about the C.G., i.e.:

$$(T)_{\text{i-th link}} = (T_{\text{C.G.}} + T_{\text{Rot.}})_{\text{i-th link.}} \tag{7}$$

The total kinetic energy of the link system is

$$T = T_\phi + T_\gamma + T_{x_1} + T_{x_2} + T_\omega \ . \tag{8}$$

After manipulation, rearranging and regrouping terms, the total kinetic energy expression can be concisely expressed as

$$\begin{aligned} T = {} & \tfrac{1}{2} A_o(\dot{h}^2 + \dot{v}^2) + \tfrac{1}{2} A_1\dot{\phi}^2 + \tfrac{1}{2} A_2(\dot{\gamma} - \dot{\phi})^2 + \tfrac{1}{2} A_1\dot{x}_1^2 + \tfrac{1}{2} A_2(\dot{x}_2 - \dot{x}_1)^2 \\ & + \tfrac{1}{2} A_\omega\dot{\omega}^2 + C_1\dot{x}_1(\dot{h}t_2' + \dot{v}t_1') + C_2(x_2 - \dot{x}_1)(-\dot{h}t_4' + \dot{v}t_3') \\ & - C_3\dot{x}_1(\dot{x}_2 - \dot{x}_1)t_6' + C_1\dot{\phi}(\dot{h}t_2 + \dot{v}t_1) + C_2(\dot{\gamma} - \dot{\phi})(-\dot{h}t_4 + \dot{v}t_3) \\ & - C_3\dot{\phi}(\dot{\gamma} - \dot{\phi})t_6 + C_5\dot{\omega}(\dot{h}\cos\omega - \dot{v}\sin\omega) \end{aligned} \tag{9}$$

where $A_o = 2(m_1 + m_2) + m_\omega$

$A_1 = I_1 + m_1 a_1^2 + m_2 \ell_1^2$

$A_2 = I_2 + m_2 a_2^2$

$A_\omega = I_\omega + m_\omega a_\omega^2$

$C_1 = m_1 a_1 + m_2 \ell_1$

$C_2 = m_2 a_2$

$C_3 = m_2 a_2 \ell_1 = C_2 \ell_1$

$C_5 = m_\omega a_\omega$

$t_1 = \sin(\phi - \phi_o)$ $\qquad$ $t_1' = \sin(x_1 - \phi_o)$

$t_2 = \cos(\phi - \phi_o)$ $\qquad$ $t_2' = \cos(x_1 - \phi_o)$

$t_3 = \sin(\gamma - \phi + \phi_o)$ $\qquad$ $t_3' = \sin(x_2 - x_1 + \phi_o)$

$t_4 = \cos(\gamma - \phi + \phi_o)$ $\qquad$ $t_4' = \cos(x_2 - x_1 + \phi_o)$

$t_5 = \sin(\gamma)$ $\qquad$ $t_5' = \sin(x_2)$

$t_6 = \cos(\gamma)$ $\qquad$ $t_6' = \cos(x_2)$

Similarly, the total potential energy of the system is

$$\frac{V}{g} = (A_o v - C_1 t_2 - C_2 t_4 - C_1 t_2' - C_2 t_4' + C_5 \cos \omega) \tag{10}$$

The equations of motion are obtained by substituting the T and V expressions into

$$\frac{d}{dt}\left(\frac{\partial T}{\partial q_i}\right) - \frac{\partial T}{\partial q_i} + \frac{\partial V}{\partial q_i} = M_i \tag{11}$$

where q_i represents the angular variables and M_i the effective moment for the appropriate link. The result is a system of five nonlinear,

coupled second order differential equations. Implicitly, the system of equations can be expressed as

$$\left\{\begin{array}{l} F_{\phi}(\phi, \dot{\phi}, \ddot{\phi}; \gamma, \dot{\gamma}, \ddot{\gamma}; x_1, \dot{x}_1, \ddot{x}_1; x_2, \dot{x}_2, \ddot{x}_2; \omega, \dot{\omega}, \ddot{\omega}; h, v) = M_{\phi} \\ F_{\gamma}(\phi, \dot{\phi}, \ddot{\phi}; \text{ --- }; h, v) = M_{\gamma} \\ F_1(\phi, \dot{\phi}, \ddot{\phi}; \text{ --- }; h, v) = M_1 \\ F_2(\phi, \dot{\phi}, \ddot{\phi}; \text{ --- }; h, v) = M_2 \\ F_{\omega}(\omega, \dot{\omega}, \ddot{\omega}; h, v) = M_{\omega} \end{array}\right\} \qquad (12)$$

Explicitly, we have

(i) Leg in stance portion.

$$A_o(\ddot{v}\cdot \dot{v}_{\phi} + \ddot{h}\cdot \dot{h}_{\phi}) + A_1\ddot{\phi} - A_2(\ddot{\gamma} - \ddot{\phi}) + C_1(\ddot{h}t_2 + \ddot{v}t_1) + C_1\ddot{\phi}(\dot{h}_{\phi}t_2 + \dot{v}_{\phi}t_1)$$

$$+ C_1\dot{\phi}^2(-\dot{h}_{\phi}t_1 + \dot{v}_{\phi}t_2) - C_2(-\ddot{h}t_4 + \ddot{v}t_3) + C_2(\ddot{\gamma} - \ddot{\phi})(-\dot{h}_{\phi}t_4 + \dot{v}_{\phi}t_3)$$

$$+ C_2(\dot{\gamma} - \dot{\phi})^2(\dot{h}_{\phi}t_3 + \dot{v}_{\phi}t_4) - C_3t_6(\ddot{\gamma} - 2\ddot{\phi}) + C_3t_5\dot{\gamma}(\dot{\gamma} - 2\dot{\phi})$$

$$+ C_1\ddot{x}_1(\dot{h}_{\phi}t_2' + \dot{v}_{\phi}t_1') + C_1\dot{x}_1^2(-\dot{h}_{\phi}t_1' + \dot{v}_{\phi}t_2') + C_2(\ddot{x}_2 - \ddot{x}_1)(-\dot{h}_{\phi}t_4' + \dot{v}_{\phi}t_3')$$

$$+ C_2(\dot{x}_2 - \dot{x}_1)^2(\dot{h}_{\phi}t_3' + \dot{v}_{\phi}t_4') + C_5\ddot{\omega}(\dot{h}_{\phi}\cos\omega - \dot{v}_{\phi}\sin\omega) - C_5\dot{\omega}^2(\dot{h}_{\phi}\sin\omega + \dot{v}_{\phi}\cos\omega)$$

$$+ \left(A_o\frac{\partial v}{\partial \phi} + C_1t_1 - C_2t_3\right)g = M_{\phi} \qquad (13)$$

$$A_o(\ddot{v}\cdot \dot{v}_{\gamma} + \ddot{h}\cdot \dot{h}_{\gamma}) + A_2(\ddot{\gamma} - \ddot{\phi}) + C_1\ddot{\phi}(\dot{h}_{\gamma}t_2 + \dot{v}_{\gamma}t_1) + C_1\dot{\phi}^2(-\dot{h}_{\gamma}t_1 + \dot{v}_{\gamma}t_2)$$

$$- C_2(-\ddot{h}t_4 + \ddot{v}t_3) + C_2(\ddot{\gamma} - \ddot{\phi})(-\dot{h}_{\gamma}t_4 + \dot{v}_{\gamma}t_3) + C_2(\dot{\gamma} - \dot{\phi})^2(\dot{h}_{\gamma}t_3 + \dot{v}_{\gamma}t_4)$$

$$- C_3t_6\ddot{\phi} + C_3t_5\dot{\phi}^2 + C_1\ddot{x}_1(\dot{h}_{\gamma}t_2' + \dot{v}_{\gamma}t_i') + C_1\dot{x}_1^2(-\dot{h}_{\gamma}t_1' + \dot{v}_{\gamma}t_2')$$

$$+ C_2(\ddot{x}_2 - \ddot{x}_1)(-\dot{h}_{\gamma}t_4' + \dot{v}_{\gamma}t_3') + C_2(\dot{x}_2 - \dot{x}_1)^2(\dot{h}_{\gamma}t_3' + \dot{v}_{\gamma}t_4')$$

$$+ (A_o \frac{\partial v}{\partial \gamma} + C_2 t_3)g = M_\gamma \tag{14}$$

where $\dot{h} \triangleq \frac{d}{dt} h$; $\ddot{h} = \frac{d^2}{dt^2} h$; $\dot{h}_{\dot{\phi}} = \frac{\partial}{\partial \dot{\phi}} \dot{h}$ and similar expressions hold for

$\dot{v}_{\dot{\phi}}$, $\dot{v}$, $\ddot{v}$, etc. The effective moments M_ϕ and M_γ are given by

$$M_\phi = u_1 + M_\phi + Y(\ell_1 t_1 - \ell_2 t_3) + X(\ell_1 t_2 + \ell_2 t_4) \tag{15}$$

$$M_\gamma = u_2 - M_\gamma + Y\ell_2 t_3 - X\ell_2 t_4 \tag{16}$$

u_1 = Moment generated by muscle action about the hip joint

u_2 = Moment generated by muscle action about the knee joint

M_a = Ankle moment

Y = Vertical component of the internal reaction force at the ankle joint

X = Horizontal internal reaction at the ankle.

Specification of the quantities X, Y and M_a will be considered later.

(ii) Leg in deploy portion.

$$\begin{aligned}
&A_o(\ddot{v}\cdot \dot{v}_{\dot{x}_1} + \ddot{h}\cdot \dot{h}_{\dot{x}_1}) + A_1 \ddot{x}_1 - A_2(\ddot{x}_2 - \ddot{x}_1) + C_1(\ddot{h}t_2' + \ddot{v}t_1') \\
&+ C_1 \ddot{x}_1(\dot{h}_{\dot{x}_1} t_2' + \dot{v}_{\dot{x}_1} t_1') + C_1 \dot{x}_1^2(-\dot{h}_{\dot{x}_1} t_1' + \dot{v}_{\dot{x}_1} t_2') - C_2(-\ddot{h}t_4' + \ddot{v}t_3') \\
&+ C_2(\ddot{x}_2 - \ddot{x}_1)(-\dot{h}_{\dot{x}_1} t_4' + \dot{v}_{\dot{x}_1} t_3') + C_2(\dot{x}_2 - \dot{x}_1)^2(\dot{h}_{\dot{x}_1} t_3' + \dot{v}_{\dot{x}_1} t_4') \\
&- C_3 t_6'(\ddot{x}_2 - 2\ddot{x}_1) + C_3 t_5' \dot{x}_2(\dot{x}_2 - 2\dot{x}_1) + C_1 \ddot{\phi}(\dot{h}_{\dot{x}_1} t_2 + \dot{v}_{\dot{x}_1} t_1) \\
&+ C_1 \dot{\phi}^2(-\dot{h}_{\dot{x}_1} t_1 + \dot{v}_{\dot{x}_1} t_2) + C_2(\ddot{\gamma} - \ddot{\phi})(-\dot{h}_{\dot{x}_1} t_4 + \dot{v}_{\dot{x}_1} t_3) \\
&+ C_2(\dot{\gamma} - \dot{\phi})^2(\dot{h}_{\dot{x}_1} t_3 + \dot{v}_{\dot{x}_1} t_4) + C_5 \ddot{\omega}(\dot{h}_{\dot{x}_1} \cos\omega - \dot{v}_{\dot{x}_1} \sin\omega) \\
&- C_5 \dot{\omega}^2(\dot{h}_{\dot{x}_1} \sin\omega + \dot{v}_{\dot{x}_1} \cos\omega) + (A_o \frac{\partial v}{\partial x_1} + C_1 t_1' - C_2 t_3')g = M_1
\end{aligned} \tag{17}$$

$$A_o(\ddot{v}\cdot \dot{v}_{\dot{x}_2} + \ddot{h}\cdot \dot{h}_{\dot{x}_2}) + A_2(\ddot{x}_2 - \ddot{x}_1) + C_1\ddot{x}_1(\dot{h}_{\dot{x}_2}t_2' + \dot{v}_{\dot{x}_2}t_1') + C_1\dot{x}_1^2(-\dot{h}_{\dot{x}_2}t_1' + \dot{v}_{\dot{x}_1}t_2')$$

$$- C_2(-\ddot{h}t_4' + \ddot{v}t_3') + C_2(\ddot{x}_2 - \ddot{x}_1)(-\dot{h}_{\dot{x}_2}t_4' + \dot{v}_{\dot{x}_2}t_3') + C_2(\dot{x}_2 - \dot{x}_1)^2(\dot{h}_{\dot{x}_2}t_3' + \dot{v}_{\dot{x}_2}t_4')$$

$$- C_3t_6'\ddot{x}_1 + C_3t_5'\dot{x}_1^2 + C_1\ddot{\phi}(\dot{h}_{\dot{x}_2}t_2 + \dot{v}_{\dot{x}_2}t_1) + C_1\dot{\phi}^2(-\dot{h}_{\dot{x}_2}t_1 + \dot{v}_{\dot{x}_2}t_2)$$

$$+ C_2(\ddot{\gamma} - \ddot{\phi})(-\dot{h}_{\dot{x}_2}t_4 + \dot{v}_{\dot{x}_2}t_3) + C_2(\dot{\gamma} - \dot{\phi})^2(\dot{h}_{\dot{x}_2}t_3 + \dot{v}_{\dot{x}_2}t_4)$$

$$+ (A_o\frac{\partial v}{\partial x_2} + C_2t_3')g = M_2 \quad . \tag{18}$$

The effective moments M_1 and M_2 are given by

$$M_1 = u + M_a' + Y'(\ell_1t_1' - \ell_2t_3') + X'(\ell_1t_2' + \ell_2t_4') \tag{19}$$

$$M_2 = u_2 - M_a' + Y'\ell_2t_3 - X'\ell_2t_4 \tag{20}$$

where M_a', Y', X' are moments and internal reactions about the ankle joint for the deploying leg. These quantities calculated from the tail portions DE and D'E of the reaction profiles in Fig. 7.

(iii) Leg in swing motion.

$$A_1\ddot{x}_1 - A_2(\ddot{x}_2 - \ddot{x}_1) + C_1(\ddot{h}t_2 + \ddot{v}t_1) - C_2(-\ddot{h}t_4 + \ddot{v}t_3) - C_3t_6(\ddot{x}_2 - 2\ddot{x}_1)$$

$$+ C_3t_5'\dot{x}_2(\dot{x}_2 - 2\dot{x}_1) + (C_1t_1' - C_2t_3')g = M_1 \tag{21}$$

$$A_2(\ddot{x}_2 - \ddot{x}_1) + C_1(-\ddot{h}t_4 + \ddot{v}t_3) - C_3t_6\ddot{x}_1 + C_3t_5\dot{x}_1^2 + C_2t_3g = M_2 \tag{22}$$

where $M_1 = u_1$

$M_2 = u_2$.

(iv) Motion of the Trunk.

$$A_\omega\ddot{\omega} + C_5(\ddot{h}\cos\omega - \ddot{v}\sin\omega) - C_5g\sin\omega = M_\omega \tag{23}$$

where

$$M_\omega = u_\omega - u_1 \tag{24}$$

u_ω = effective moment due to muscle actions of the trunk and upper extremities.

Equation groups (i) and (ii) form a system of coupled equations describing the motion in the restraint/deploy configuration. Note that the expressions are identical except for the interchange of variables - x_1 and x_2 for ϕ and γ. This is reasonable as both legs are in contact with the ground and the (h, v) - description for the hip position introduces symmetry into the expressions. In state variable language, the system of equations is equivalent to an eight-dimensional vector differential equation. Equation groups (i) and (iii) describe the support/swing mode of motion. The swing equations are comparatively simple and contain no ϕ, γ variables explicitly. Equation (iv) describes the trunk motion in the sagittal plane.

c. Decoupling and Simplification of the Model.

The foregoing equations describe the complete behavior in the sagittal plane and no approximations have been introduced. Motion of the body in the frontal and horizontal planes will introduce additional equations but no modification in the present ones. However, such a "high order" model is very complex to handle. Although the differential equations can be numerically integrated as an initial value problem, what is at hand is a multi-point boundary value problem from the optimal programming formulation. Simplification of the model is necessary to render the problem tractable and to obtain insight into the problem. The major complexity of the model is in the coupling of motion between the two lower extremities as expressed in (h, v) and their various derivatives.

The central idea in simplification is to decouple the motion of the two legs. In level walking over the range of normal speeds, pace frequency and step-length, the hip position (h, v) describes a characteristic trajectory. The horizontal component, h, is uniform motion while the vertical component describes a double period sinusoid about some mean value. Thus, to obtain a realistic simulation of lower extremity motion, one may introduce the auxiliary constraints

$$h \triangleq x_A - \ell_1 \sin(\phi - \phi_o) + \ell_2 \sin(\gamma - \phi + \phi_o) = \tilde{f}(t) \tag{25}$$

$$v \triangleq y_A + \ell_1 \cos(\phi - \phi_o) + \ell_2 \cos(\gamma - \phi + \phi_o) = \tilde{g}(t) \tag{26}$$

for the leg in stance and where f(t) and g(t) are prescribed time functions for the hip trajectory. Similar expressions hold for the leg in deploy. The auxiliary constraints simplify the equation groups (i), (ii) and (iii) somewhat but we still have a high order model as h_{ϕ}, h_{γ}, h_{x_1}, h_{x_2}, etc. are non-zero. To obtain further simplification, it is assumed that all the partial derivatives are zero, i.e. $h_{\phi} = 0$, $v_{\phi} = 0$ and so on. Such a step amounts to the consideration of the hip as the origin of a moving coordinate system, prescribing the characteristic trajectory of the hip. Useful expressions for the hip position are

$$\tilde{f}(t) = v_o(t + t_o) \quad ; \quad [\text{ft}] \tag{27}$$

$$\tilde{g}(t) = e_o - \frac{0.9}{12} \sin \frac{4\pi}{T}(t + \beta \cdot T) \quad ; \quad [\text{ft}] \tag{28}$$

where v_o = velocity of level walking

t_o = constant based on the initial configuration of the system

e_o = average height of the hip above the ground

T = period of a double-step

β = constant dependent on initial conditions of motion.

The device of prescribing a hip trajectory has been used by Galiana [33], Beckett [28] and Wallach [34] in their various studies. From this, we obtain a decoupled model for the optimization problem.

Simplified Dynamics.

(i) Stance Portion.

$$(A_1 + 2C_3t_6)\ddot{\phi} - (A_2 + C_3t_6)\ddot{\gamma} + C_3t_5\dot{\gamma}(\dot{\gamma} - 2\dot{\phi}) + (C_1t_1 - C_2t_3)(\ddot{v} + g)$$

$$= u_1 + M_a + Y(\ell_1t_1 - \ell_2t_3) + X(\ell_1t_2 + \ell_2t_4) \tag{29}$$

$$-(A_2 + C_3t_6)\ddot{\phi} + A_2\ddot{\gamma} + C_3t_5\dot{\phi}^2 + C_3t_6(\ddot{v} + g) = u_2 - M_a + Y\ell_2t_3$$

$$- \ell_2t_4X \tag{30}$$

$$\ddot{v} \triangleq \tilde{\ddot{g}} \tag{31}$$

(ii) Deploy and Swing Portions.

The form of the equations is identical with those of (i) except for the following:

(a) The variables x_1 and x_2 replace ϕ and γ.

(b) The terms M_a', Y', X' replace the corresponding terms in (i) for the deploy portion.

(c) In swing, all terms due to ankle moment and reactions vanish.

Because of the similarity in the equations, we can now adopt a common notation. Let x_1 and x_2 stand for the thigh and shank angles respectively (i.e. for ϕ and γ in stance; x_1 and x_2 in deploy and swing). Define also $x_3 = \dot{x}_1$; $x_4 = \dot{x}_2$, then we obtain the equations in first order canonical form

$$\dot{x}(t) = f(x, \tilde{u}; t) \tag{32}$$

where $x \triangleq (x_1, x_2, x_3, x_4)^T$

$$\begin{cases} \dot{x}_1 = x_3 \\ \dot{x}_2 = x_4 \\ \dot{x}_3 = \frac{1}{\delta} \{(\tilde{R}_3 + \tilde{u}_1) A_2 + t_7(\tilde{R}_4 + \tilde{u}_2)\} \\ \dot{x}_4 = \frac{1}{\delta} \{t_7(\tilde{R}_3 + u_1) + t_8(\tilde{R}_4 + \tilde{u}_2)\} \end{cases} \tag{33}$$

$$\tilde{R}_3 = -C_3 t_5 x_4(x_4 - 2x_3) - (C_1 t_1 - C_2 t_3)(\ddot{\tilde{g}} + g)$$

$$\tilde{R}_4 = -C_3 t_5 x_3^2 - C_3 t_6(\ddot{\tilde{g}} + g)$$

$$\tilde{u}_1 = \begin{cases} u_1 + M_a + Y(\ell_1 t_1 - \ell_2 t_3) + X(\ell_1 t_2 + \ell_2 t_4) & \text{in stance} \\ u_1 + M_a' + Y'(\ell_1 t_1 - \ell_2 t_3) + X'(\ell_1 t_2 + \ell_2 t_4) & \text{in deploy} \\ u_1 & \text{in swing} \end{cases}$$

$$\tilde{u}_2 = \begin{cases} u_2 - M_a + Y\ell_2 t_3 - X\ell_2 t_4 & \text{in stance} \\ u_2 - M_a' + Y'\ell_2 t_3 - X'\ell_2 t_4 & \text{in deploy} \\ u_2 & \text{in swing} \end{cases}$$

$\delta = A_2 t_8 - t_7^2 \triangleq$ determinant of the dynamic coupling matrix

$t_8 = A_1 + 2C_3 t_6$

$t_7 = A_2 + C_3 t_6$

$t_9 = t_8 - t_7$.

d. Comments.

Using the dynamics in first order form, one can study the motion of the two lower extremities by considering only the sequential behavior of a single leg. Although the expressions are similar to those obtained

in two-link models, we have placed into perspective that the simplified model is obtained through decoupling of a high order one. In the model by Beckett and Chang, only the kinematic aspects of the motion are considered by neglecting all reactions and ankle moment contributions. Wallach's [34] paper on knee prosthetics also neglected the forces and moment. In the paper by Galiana [33], the ankle moment term was missing as a result of the "fixed-foot" assumption. The decoupled equations are identical to those derived by Bresler and Frankel [13] using the D'Alembert's principle of dynamic equilibrium for their experimental study. Their important results indicate that the ground reaction forces in the stance portion are the most significant quantities and gravitational and inertial effects of the thigh and shank variables are small compared to these. Thus it appears that the simplified model should yield realistic results provided appropriate consideration of the foot motion is taken.

e. Kinematic Constraints.

In the deploy portion, the ankle of the foot describes a circular arc about the ball of the foot. With the hip motion prescribed, the angles x_1 and x_2 are no longer independent but subjected to an equality constraint relationship. Suppose that deploy starts at time $\bar{t}_1$ and ends at $\bar{t}_2$. Vertical displacement is summed to yield

$$e_o = \tilde{g}(\bar{t}_1) + \ell_1 \cos(x_1(\bar{t}_1) - \phi_o) + \ell_2 \cos(x_2(\bar{t}_1) - x_1(\bar{t}_1) + \phi_o) + d\sin\alpha(\bar{t}_1)$$

as shown in Fig. 9. The angles $x_1(t_1), x_2(t_1)$ and $\alpha(t_1)$ are specified. Similarly, for $\bar{t}_1 < t \leq \bar{t}_2$, we have

$$e_o = \tilde{g}(t) + \ell_1 \cos(x_1(t) - \phi_o) + \ell_2 \cos(x_2(t) - x_1(t) + \phi_o) + d\cos\alpha(t) .$$

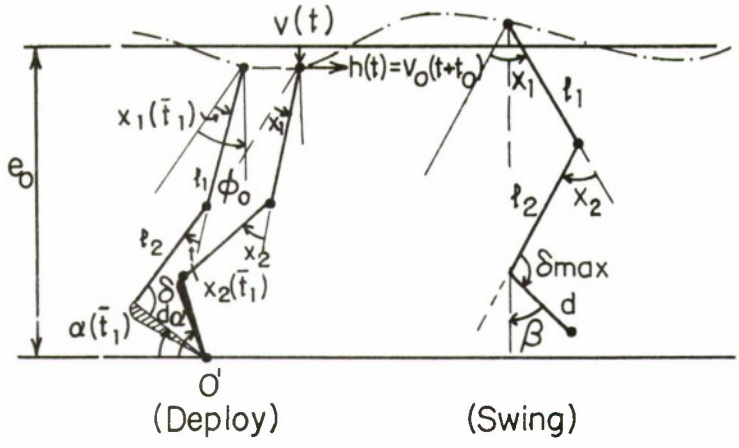

FIG. 9 KINEMATIC CONSTRAINTS IN DEPLOY AND SWING PORTIONS.

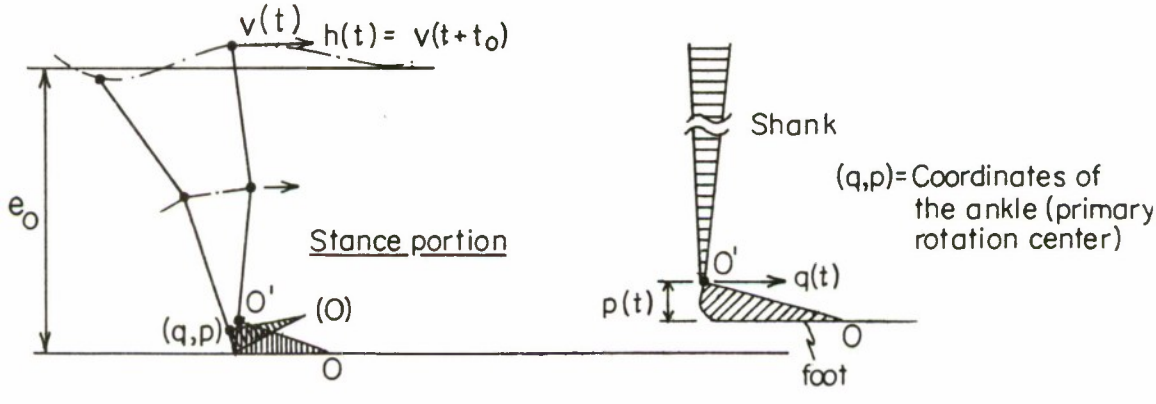

FIG. 10 KINEMATIC CONSTRAINTS IN STANCE PORTION.

Eliminating e_o between the two expressions, we have

$$d \sin \alpha(t) = e_1 - \tilde{g}(t) - \ell_1 t_2 - \ell_2 t_4 \triangleq S_1 = y_A \tag{34}$$

$$e_1 = \tilde{g}(\bar{t}_1) + (\ell_1 t_2 + \ell_2 t_4)\bar{t}_1 + d \sin \alpha(\bar{t}_1).$$

Summation of horizontal displacements gives

$$v_o(\bar{t}_1 + t_o) + \ell_1 \sin(x_1(\bar{t}_1) - \phi_o) - \ell_2 \sin(x_2(\bar{t}_1) - x_1(\bar{t}_1) + \phi_o)$$

$$+ d \cos \alpha(\bar{t}_1) = v_o(t + t_o) + \ell_1 \sin(x_1(t) - \phi_o) - \ell_2 \sin(x_2(t) - x_1(t) + \phi_o)$$

$$+ d \cos \alpha(t)$$

or

$$d \cos \alpha(t) = e_2 - v_o t - \ell_1 t_1 + \ell_2 t_3 = S_2 = x_A \tag{35}$$

$$e_2 = v_o \bar{t}_1 + (\ell_1 t_1 - \ell_2 t_3)\bar{t}_1 + d \cos \alpha(t_1) \quad .$$

Eliminating $\alpha(t)$ between S_1 and S_2, we obtain the desired relationship

$$S^d(x;t) = \ell_1^2 + \ell_2^2 - d^2 + (e_1 - \tilde{g})^2 + (e_2 - v_o t)^2 + 2\ell_1 \ell_2 t_6$$

$$-2(e_1 - \tilde{g})(\ell_1 t_2 + \ell_2 t_4) - 2(e_2 - v_o t)(\ell_1 t_1 - \ell_2 t_3) = 0. \tag{36}$$

At time $\bar{t}_2$, the angle δ between the shank and foot approaches a limiting maximum value, δ max. During <u>swing</u> motion, $\delta = \delta$ max (i.e. foot-locking) while the toes of the foot are kept above the ground. From Fig. 9, we thus have the inequality constraint

$$S^s(x;t) = \tilde{g}(t) + \ell_1 t_2 + \ell_2 t_4 + d \cos \beta(t) - e_o \leqslant 0 \tag{37}$$

$$\beta = \pi - \delta \max - \phi_o + x_1(t) - x_2(t) \tag{38}$$

for $\bar{t}_2 \leqslant t \leqslant \bar{t}_3$, $\bar{t}_3$ being the end of swing (i.e. $\bar{t}_3 = T + \bar{t}_1$; T = period of a double-step).

In addition to state variable inequality constraint (37), the angle $x_2(t)$ has to be positive ($x_2 > 0$) during the swing. However, the multi-linkage mechanical model does not take into account such a restriction.

This aspect of model limitation does not appear to have been noticed in previous investigations. A useful device to alleviate the difficulty is to adjoin a "soft" penalty [35] to the performance criterion J_o under optimization†, i.e. define

$$J_s \triangleq J_o + \gamma_s \int_{t_2}^{t_3} \frac{dt}{x_2(t)} \tag{39}$$

for a sequence of γ_s: $\gamma_o > \gamma_1 > \gamma_2 \text{ --- } > \gamma_s \rightarrow 0_+$. The penalty becomes effective as $x_2 \rightarrow 0_+$ but smaller as $x_2(t)$ becomes more positive. A restriction is that in iterative computation, the trajectory $x_2(t)$ has to remain feasible, i.e. $x_2(t) > 0 \ \forall t \in [\bar{t}_2, \bar{t}_3]$. Intuitively, the factor $\frac{\gamma_s}{x_2(t)}$ is equivalent to a nonlinear spring placed about the knee joint and the parameter γ_s measures its stiffness.

In the stance portion, the foot is more or less stationary except for the brief moment following heel strike. The dynamic behavior is difficult to describe because a rigid link cannot describe the behavior of a "round" foot. Fig. 10 illustrates the roll-over situation where the weight bearing leg rotates about its ankle ($0'$) - the primary rotation center. The pressure center where the ground reaction forces are acting is gradually transferred from the heel towards the toe. The effective kinematic constraints in this period are that the ankle (x_A, y_A) coordinates follow a prescribed trajectory, $(q(t), p(t))$. In a rough analysis, $q(t)$ and $p(t)$ can be taken as constant. Thus, we have

$$S_1^{rs}(x;t) = \tilde{g}(t) + \ell_1 t_2 + \ell_2 t_4 - e_o + p(t) = 0 \tag{40}$$

$$S_2^{rs}(x;t) = v_o(t + t_o) + \ell_1 t_1 - \ell_2 t_3 - q(t) = 0 \tag{41}$$

† J_o has yet to be defined.

The particular choice of p and q profiles has to depend on experimental data. Fig. 11 shows the typical profiles. Note that they are almost constant except for the initial restraining moment.

f. Quasi-Static Estimation of Ankle Moment and Reactions.

Having developed the dynamic equations and kinematic constraints, the model is incomplete until the ankle moments and reaction forces are known. Fig. 12 shows a free body diagram of the foot. The forces f_v and f_h represent the vertical and horizontal components of the ground reactions due to weight bearing and trunk motion. These forces have been measured by various investigators using force plates and Fig. 7 shows the typical, normalized profiles over a wide range of level walking speeds and step-lengths. To describe the foot motion, we write the equations for translation motion for the center of gravity (O_F) and rotation about O_F. On summing the vertical forces, we have

$$M_F\ddot{y}_F = f_v - M_F g - Y$$

or
$$Y = f_v - M_F g - (M_F\ddot{y}_F) \quad . \tag{42}$$

Similarly, summing the horizontal forces gives

$$M_F\ddot{x}_F = f_h - X$$

or
$$X = f_h - M_F\ddot{x}_F \quad . \tag{43}$$

Taking moments about O_F and rearranging terms yields

$$M_a = f_v(x_p - x_A) + f_h(y_A - y_p) - M_F g(x_F - x_A) + (M_F\ddot{x}_F)(y_F - y_A)$$
$$- (M_F\ddot{y}_F)(y_F - y_A) + I_F\ddot{\alpha} \tag{44}$$

I_F = Moment of inertia of a foot about its C.G. ($\approx 10^{-2}$ slug-ft^2).

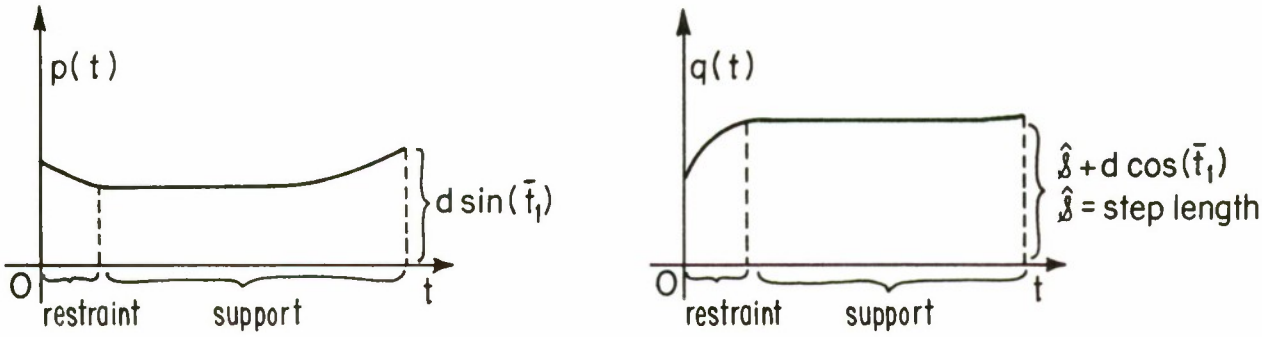

FIG. 11 TYPICAL PROFILES FOR ANKLE COORDINATES IN STANCE PORTION. (FROM BRESLER AND FRANKEL).

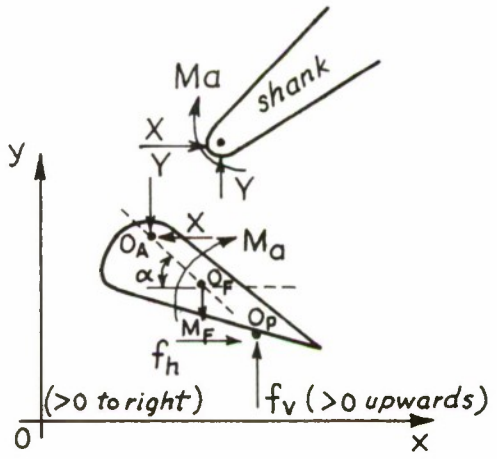

O_P = pressure center (x_p, y_p)

O_F = center of gravity of the foot (x_F, y_F)

O_A = ankle (x_A, y_A)

X,Y = reactions (internal) @ the ankle

f_v,f_h = vertical and horizontal components of ground forces

FIG. 12 FREE BODY DIAGRAM OF THE FOOT.

It is obvious that the ankle reactions and moment depend on the ground reactions. Since $f_v >> (M_F g)$; $f_v >> (M_F \ddot{y}_F)$; $f_h >> (M_F \ddot{x}_F)$; and $(I_F \ddot{\alpha})$ is small because I_F is small, we can obtain a simple "quasi-static" estimate of the dynamic quantities by neglecting the inertial and gravitational terms, i.e.:

$$\begin{aligned} Y &\approx f_v \\ X &\approx f_h \\ M_a &\simeq f_v(x_p - x_A) + f_h(y_A - y_p) \end{aligned} \tag{45}$$

The ankle coordinates (x_A, y_A) are specified through the kinematic constraints derived in the preceding section. As far as the pressure center (x_p, y_p) is concerned, we have $y_p \equiv 0$ throughout the stance portion. In the report by the Eberhart-Inman group [12], force plate data reveals an approximately linear transfer characteristic in the stance portion, i.e.:

$$x_p \simeq a t + b \tag{46}$$

where a, b are parameters dependent on walking speed, foot length and other parameters. During deploy, x_p is fixed at the ball of the foot. With the dynamic quantities specified, the multi-linkage model with auxiliary constraints is now complete.

3. Discussions.

We have derived, through a succession of steps, an appropriate model for the optimization problem. It is a two-link model with kinematic constraints and ankle forces and moments. Fig. 13 is a flow chart illustrating the development. Note that models at different levels of detail can be obtained by allowing additional degrees of freedom and

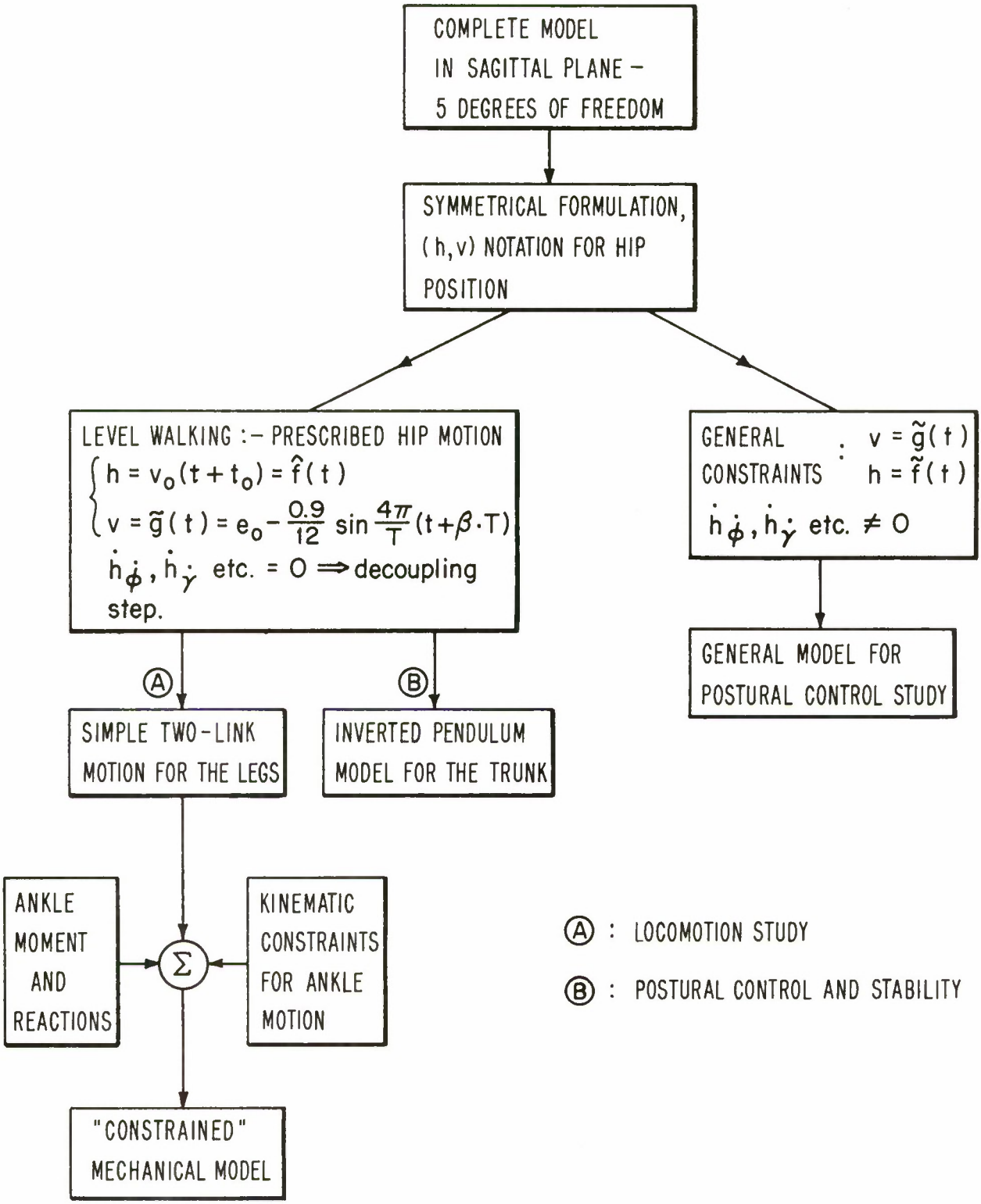

FIG. 13 FLOW CHART OF MODEL DEVELOPMENT.

complexity.

An inherent drawback of the high order model is that the dynamic variables chosen for description are always coupled. This implies the matrix inversion is necessary to convert the equations to first order form. For models with more than two degrees of freedom, matrix inversion with analytic expressions soon becomes too messy to handle. The use of symbolic manipulation language such as FORMAC appears indispensible in the study of complex models in locomotion and bio-engineering in general.

The use of a prescribed hip trajectory and kinematic constraints for ankle motion is a useful device. Locomotion under different conditions such as up an inclined surface or over other terrain only changes the form of the prescribed functions and not the other expressions. Since modern control theory can handle readily auxiliary constraints, it appears very promising in the study of locomotion under various environmental conditions.

C. On an Energy Performance Criterion in Human Locomotion

1. Introduction.

Having developed an appropriate model for the optimal programming problem, the next step is to derive a suitable performance criterion. As mentioned earlier, Atzler and Herbst [5] and Cotes and Meade [26] independently obtained experimental results which show a minimum expenditure of mechanical work for appropriate combination of speed, step-length and pace frequency. Theoretically, Nubar and Contini [27] were probably the first and only thus far to propose a minimal principle for human locomotion.

They hypothesized that energy expenditure under several simultaneous forms (mechanical, heat and chemical) is associated with muscular activity. The muscular effort, an aggregate quantity, is defined quantitatively in terms of the effective moments which actuate the locomotor system. The locomotion process is thought to occur in such a manner as to minimize some "effort" function E_f (performance criterion) consistent with imposed constraints - physiological, physical and geometrical. The effort function they proposed is of a quadratic variety, i.e.

$$E_f = \sum_j \hat{C}_j u_j^2(t)\ \Delta t$$

where $u_j(t)$ represents the effective moment acting on the j-th link; $\hat{C}_j$ being an effectiveness weighing factor; and Δt is the time interval over which optimization is performed.

Their work, however, has two important shortcomings. At that time, optimal control theory and numerical computation were not

developed extensively and the proposed problem was not seriously tackled. A second and more fundamental question is that while the effort function being chosen is selected on the basis of mathematical tractability and physical appeal, there is no apparent connection to the physiology of the muscle actuating system. Our present objective is to derive a simple but physiologically based performance index.

2. Development of the Performance Criterion.

Mechanical energy expenditure is the quantity of interest for the derivation. In general, mechanical work done (by or on) can be evaluated in two ways. One measure is the time integral of the instantaneous power which is the product of the moment about a joint and the angular velocity of the limb with respect to that joint. The other measure is the integral of the product the force generated by the muscle in causing rotation and its velocity of shortening. The latter method is used as it involves naturally the muscle mechanics. Specifically, the external characteristics of the muscle are used.

a. Assumptions.

The neural-viscoelastic model for the muscle is based on the following set of experiments which have been performed on both isolated muscle fibers and the human muscle in vivo.

(i) tension (force) - velocity curves by A. V. Hill [36, 37]

(ii) length - tension curves [36, 37]

(iii) EMG characteristics by Bigland and Lippold [46]

Fig. 14 illustrates these properties. From these, the force generated by a muscle is a function of neural stimulation Z, muscle length ℓ and velocity v. The functional form is given as [38, 39]

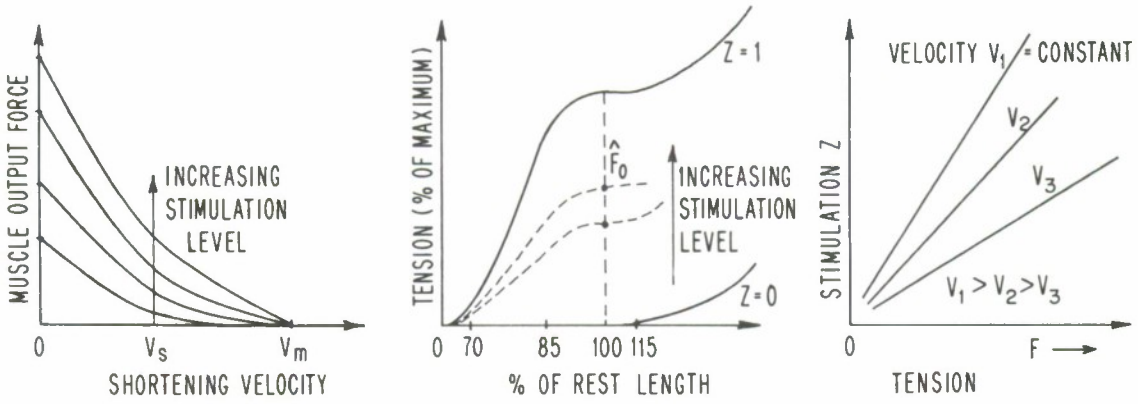

FIG. 14 EXPERIMENTAL CHARACTERISTICS OF SKELETAL MUSCLES [36,37]

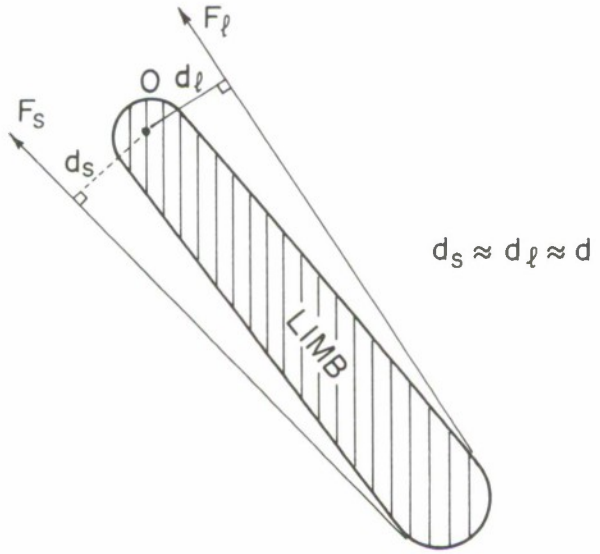

FIG. 15 AGONIST / ANTAGONIST MUSCLE SYSTEM.

$$F(\ell, v, Z) = ZF_o(\ell) \frac{1 - \frac{v}{v_m}}{1 + \frac{v}{bv_m}} \qquad (1)$$

where $F_o(\ell)$ = maximum isometric force at length ℓ

Z = neural stimulation level ($0 \leq Z \leq 1$)

v_m = maximum velocity for isotonic case (i.e. when $F = 0$)

b = constant (typical values between 0.25 and 0.3).

Thus, F is a function of three variables, ℓ, v, Z. By holding one variable constant, the muscle length ℓ in this case, F can be graphically portrayed as a surface. This we call the characteristic surface of the muscle.

The derivation is confined to one joint agonist/antagonist muscle system. The actual muscle system involved in almost any complex limb motion is seldom that simple. We assume that the same principles hold for each agonist/antagonist pair involved, and thus the discussion represents an average behavior of all pairs contributing to the actual limb motion. The human locomotor system is equipped with an abundance of two joint muscles; however, Steindler [4], Eberhart et al [10] have shown how two joint muscles can be functionally decomposed into the one joint variety.

b. Derivation.

Consider a limb being acted upon by an agonist/antagonist muscle system (Fig. 15). With the two moment arms approximately equal, there is no net rotation of the limb when each muscle exerts an equal force $F_o = Z_o F_o(\ell_o)$. The presence of static forces is to maintain joint stability and body posture. When one muscle exerts more force than the other, a net rotation results. The amount of mechanical work

done by the muscle actuating system is given by.

$$W = \int (\hat{F}_o + \delta F_s) \cdot v_s dt + \int (\hat{F}_o + \delta F_\ell) \cdot v_e dt \qquad (2)$$

$$= \int \hat{F}_o (v_s + v_e) dt + \int \delta F_s \cdot v_s dt + \int \delta F_\ell \cdot v_e dt$$

where δF_s and δF_e are the incremental forces above the static component $\hat{F}_o$ in shortening and lengthening respectively. The corresponding shortening and lengthening velocities are $v_s (> 0)$ and $v_e (< 0)$. In normal locomotion, it is taken that $|v_s| \approx |v_e|$ and so the static dependent term $\hat{F}_o (v_s + v_e) \approx 0$, contributing little or nothing to W.

Muscle in Shortening.

From (1), the "shortening" force is

$$F_s = Z F_o(\ell) \frac{1 - \frac{v_s}{v_m}}{1 - \frac{v_s}{v_m}} \qquad (3)$$

For normal locomotion activity, F_s is not significantly different from the static component so that it can be satisfactorily represented as

$$\delta F_s = F_s - \hat{F}_o$$

$$= \left(\frac{\partial F_s}{\partial Z}\right)_{Z_o} (Z - Z_o) + \left(\frac{\partial F_s}{\partial \ell}\right)_{\ell_o} (\ell - \ell_o) + \left(\frac{\partial F}{\partial v_s}\right)_{v_o} (v - \cancel{v_o}) \qquad (4)$$

$$\text{"}0\text{"}$$

and $\left(\frac{\partial F_s}{\partial Z}\right) = F_o(\ell_o)$

$$\left(\frac{\partial F}{\partial v_s}\right)_{v_o} = - Z_o F_o(\ell_o)(1 + \frac{1}{b}) \Big/ v_m$$

$$\left(\frac{\partial F}{\partial \ell}\right)_{\ell_o} \approx 0 \quad \text{(small)} \quad .$$

The fact that the linear terms constitute the main contribution is

supported by experimental results obtained in normal walking.

(i) The stimulation level Z appears linearly in (1) and so there is no approximation in (4).

(ii) The term due to length contribution $\left(\frac{\partial F}{\partial \ell}\right)(\ell - \ell_o)$ is considered small compared to the other two; consequently it is omitted Results by Elftman on the soleus muscle indicated that the muscle length change is small during the shortening cycle (Fig. 16). Also, from the length-tension diagram the shape of the curve is almost flat in the vicinity of the rest length. In the EMG experiment by Galiana [33], satisfactory results were obtained under a length independence assumption.

(iii) The effect of shortening velocity v_s on F_s is essentially linear in the range of interest. The expansion generates a linear approximation to the hyperbolic curve of Hill. It is interesting to observe that the stimulation level Z is multiplicative rather than additive, so that it controls the damping as well as the isometric force effectively. Physically, the linear approximation replaces a velocity dependent damper by a constant one whose magnitude depends on the isometric conditions. Stark [41] and Houk [42] had used linearization in their modelling of muscle actuators; their results appear satisfactory.

By neglecting the length contribution, we have

$$\begin{aligned} \delta F_s &= F_s - F_o \\ &\tilde{=} F_o(\ell_o)(Z - Z_o) - B_{m_s} v_s \end{aligned} \tag{5}$$

where $B_{m_s} = Z_o F_o(\ell_o)(1 + \frac{1}{b}) / v_m$.

The next crucial step is to obtain a relationship between stimulation increment $\Delta Z = Z - Z_o$ and velocity v_s. Bigland and Lippold

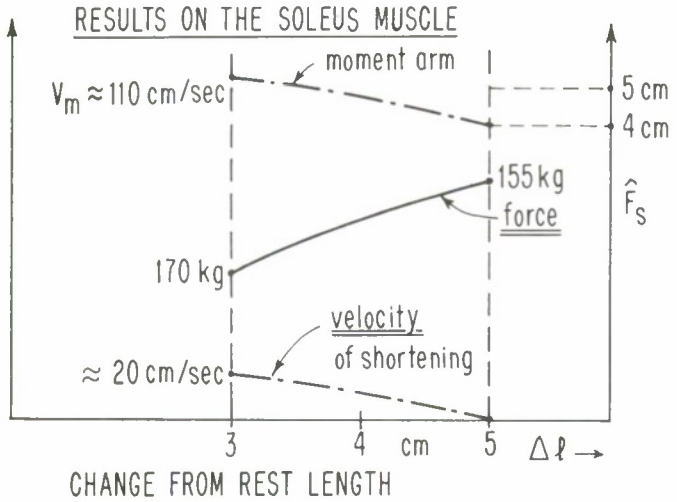

FIG. 16 VELOCITY-LENGTH CHARACTERISTICS (from Elftman[7]).

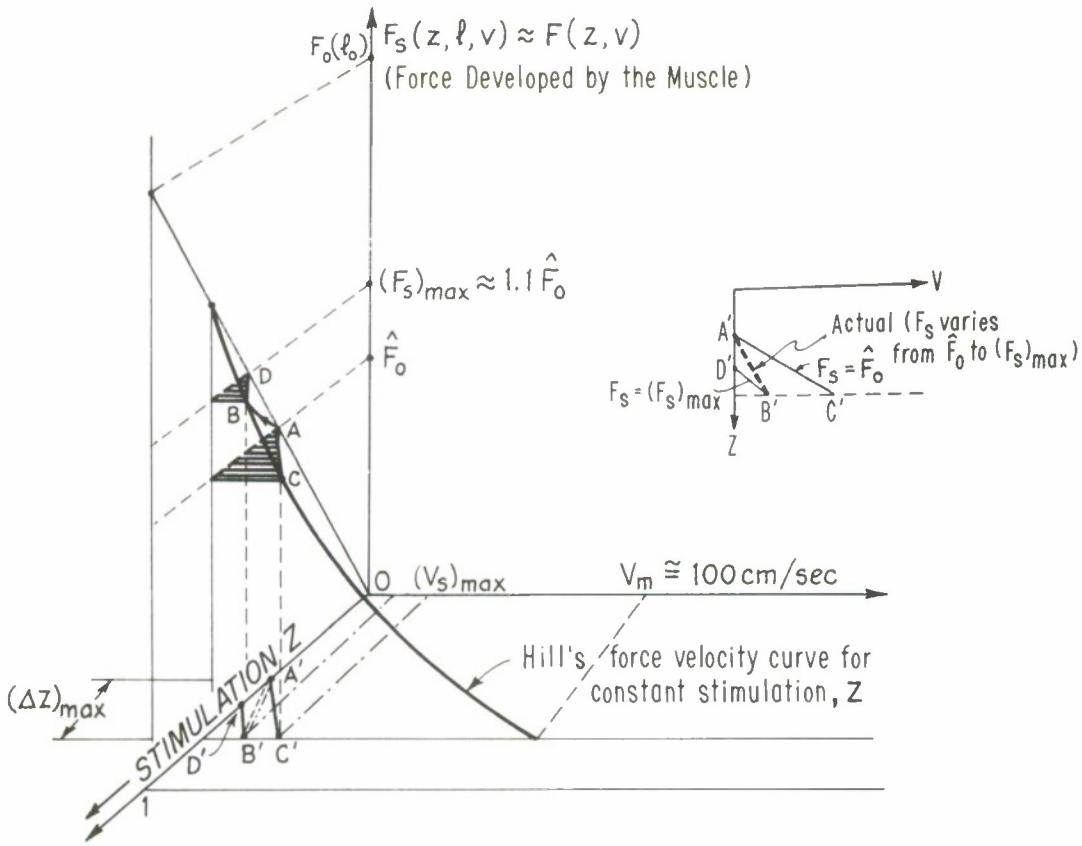

FIG. 17 CHARACTERISTIC SURFACE OF A SKELETAL MUSCLE.

showed that for approximately constant F_s, v_s and ΔZ are linearly related for small velocities. This is easy to verify from (3):

$$\Delta Z \cong \frac{F_s}{F_o(\ell)}(1 + b)\frac{v_s}{v_m} \propto v_s \text{ for} \left(\frac{v_s}{v_m}\right) << 1 \tag{6}$$

In the normal range of locomotion activity, a linear relationship between ΔZ and v_s still holds but with a slightly larger slope dependent on the maximum value of F_s. The "equivalent linearization" is clear from the characteristic surface as illustrated in Fig. 17. The surface is a graphical representation of the functional relationship (1) for ℓ = constant. As the muscle length changes are fairly small in normal locomotion, the locus of F_s lies within two characteristic surfaces lying close together. For F_s = constant, increasing stimulation ΔZ lies on paths AC or DB on the characteristic surface. With F_s varying from $\hat{F}_o$ to $(\hat{F}_s)\max \approx 1.1\hat{F}_o$ (estimated from Elftman's result), the locus is the curve $\overset{\frown}{AB}$ on the surface. When projected onto the Z - v plane, we have an almost linear segment A'B'. Thus, we have an operating relationship of the form

$$\Delta Z = k_s((\hat{F}_s)\max; \hat{F}_o) \cdot v_s \tag{7}$$

Note that if one uses the line A'C' instead (i.e. no correction for F_s changing), the error is approximately 10% for the range of F_s variation. Combining (5) and (7), we have

$$\delta F_s = (\hat{F}_o k_s - B_{m_s}) \cdot v_s \quad . \tag{8}$$

Since $(F_s - F_o) > 0$ for a shortening muscle, then $(F_o k_s - B_{m_s}) > 0$. The work done by a muscle in shortening is then

$$W_s = \int_{t_o}^{t_f} \frac{(F_s - F_o)^2}{(F_o k_s - B_{m_s})}\, dt$$

$$= \int_{t_o}^{t_f} \frac{u_s^2(t)\, dt}{(\hat{F}_o k_s - B_{m_s}) \cdot d_s^2(t)} = \frac{1}{2} \int_{t_o}^{t_f} r_s(t) u_s^2(t) dt \qquad (9)$$

where $u_s(t)$ is the moment generated by the shortening muscle and $d_s(t)$ the moment arm.

$$\frac{1}{2} r_s(t) \triangleq \frac{1}{(F_o k_s - B_{m_s}) d_s^2} \qquad (10)$$

Muscle in Lengthening.

When the other member of the agonist/antagonist pair is being stretched, mechanical work is done on it. The Hill's force-velocity curve holds for the lengthening muscle up to a maximum allowable force which is roughly twice $F_o(\ell_o)$. For larger forces, the Golgi tendon organs reflexly cause the muscle to yield.

Following the same procedure as in the preceding case, the force in lengthening is given by

$$\delta F_\ell = F_\ell - \hat{F}_o$$

$$= \hat{F}_o \Delta Z - B_{m_\ell} v_\ell \qquad (11)$$

where $v_\ell < 0$ and $\frac{B_{m_\ell}}{B_{m_s}} \approx 6$ according to Stark, Galiana. Thus, the linear approximation to the characteristic surface is a piecewise

one with the damping during lengthening (B_{m_ℓ}) much larger than that in shortening. Fig. 18 illustrates that below saturation, ΔZ and v_ℓ are linearly related, i.e.

$$\Delta Z = k_\ell((F_\ell)_{max};\ F_o)v_\ell \tag{12}$$

The work done on the muscle is

$$W_e = -\int_{t_o}^{t_f} \frac{(F_\ell - \hat{F}_o)^2}{(B_{m_\ell} - \hat{F}_o k_\ell)}\,dt$$

$$= -\tfrac{1}{2}\int_{t_o}^{t_f} \frac{(2)\cdot u_\ell^2(t)dt}{(B_{m_\ell} - \hat{F}_o k_\ell)\cdot d_\ell^2(t)}$$

$$= -\tfrac{1}{2}\int_{t_o}^{t_f} r_\ell(t)u_\ell^2(t)dt \tag{13}$$

where $r_\ell(t) = \dfrac{2}{(B_{m_\ell} - \hat{F}_o k_\ell)d_\ell^2(t)}$ and $d_\ell(t) \triangleq$ moment arm for the lengthening muscle ($\approx d_s(t)$).

Total Mechanical Work.

The total work done is the sum of lengthening and shortening contributions

$$W = W_\ell + W_s$$

$$= \tfrac{1}{2}\int_{t_o}^{t_f} (r_s u_s^2 - r_\ell u_\ell^2)dt. \tag{14}$$

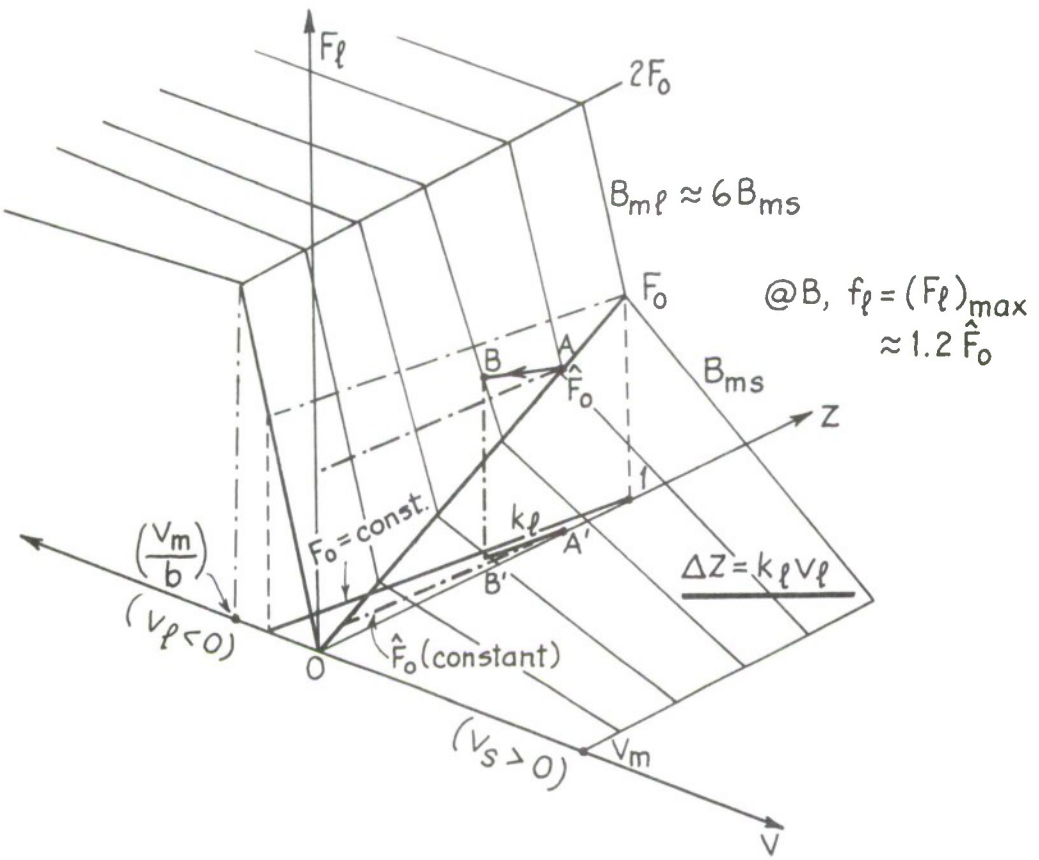

FIG. 18 PIECEWISE APPROXIMATION OF CHARACTERISTIC SURFACE (HOUK[42], STARK[41], GALIANA[33]).

The net moment acting on the limbs is given by

$$u = \frac{F_s - F_\ell}{d_s}$$

$$= \frac{(F_s - \hat{F}_o) - (F_e - \hat{F}_o)}{d_s}$$

$$= u_s - (\frac{d_\ell}{d_s})u_e$$

$$\approx u_s - u_\ell \quad \text{for} \quad (\frac{d_\ell}{d_s}) \approx 1 \quad . \tag{15}$$

Now, $u^2 = (u_s - u_\ell)^2 = u_s^2 + u_\ell^2 - 2u_s u_\ell \leq 2(u_s^2 + u_\ell^2)$.

But, $u_s^2 - u_\ell^2 \leq u_s^2 + u_\ell^2$

$$\therefore \quad u^2 = \frac{k}{2}(u_s^2 - u_\ell^2); \quad k = \text{constant factor}$$

$$W = \frac{1}{2}\int_{t_o}^{t_f} (r_s u_s^2 - r_\ell u_\ell^2)dt$$

$$\simeq \text{constant} \cdot \int_{t_o}^{t_f} u^2(t)dt \quad . \tag{16}$$

Hence, in the normal range of activity, the sum total of mechanical energy expenditure by the muscle activating system is proportional to the integral of the square of the net moment.

3. Discussions.

In the present derivation, mechanical energy expenditure by the muscle system is the physical quantity being identified. Although other quantities such as total energy expenditure by the muscles or total

"active states" of the muscles have been suggested as bases for a performance index, it appears not straight-forward to develop these. The mechanical work done by (and on) the muscles has been of most concern in experimental work done to-date.

As to the form of the effort function, generalization can be made of the form

$$J = \frac{1}{2} \int_{t_o}^{t_f} \sum_i r_i |u_i|^p \, dt \; ; \; r_i \geq 0$$

where p is some appropriate integer; u_i the net moment acting on the i-th link and r_i the weighing factor. Physiologically, justification for one particular choice may be more difficult than for another. For the case $p = 0$ and t_f treated as unspecified, the criterion leads to a "minimum time" problem and appears applicable to fast walking. The $p = 1$ case corresponds to the "minimum fuel" problem in optimal control theory. For $p = 2$, we have the quadratic criterion considered in the preceding sections.

D. Optimization in Biped Locomotion

1. Problem Formulation [43]

The constrained mechanical model and performance criterion form the core of the optimization problem for biped locomotion. Based on the simplified model, simultaneous motion of the two legs is reduced to the sequential behavior of a single leg. Let deploy, swing and stance portions describe in order the phasic activities in a walking cycle (i.e. double-step). Mathematically, the optimization problem can be stated as follows:

Let t_f be the time required for a double-step and t_1 and t_2 partition $[0, t_f]$ into the respective phasic portions. It is proposed that level locomotion is realized by programming the hip and knee moments $(u_1; u_2)$ so as to minimize the quadratic criterion.

$$J_o = \frac{1}{2}\int_o^{t_f}(r_1u_1^2+r_2u_2^2)dt = \frac{1}{2}\int_0^{t_1} + \int_{t_1}^{t_2} + \int_{t_2}^{t_f}(r_1u_1^2 + r_2u_2^2)dt \quad (1)$$

for $r_1, r_2 > 0$; $0 < t_1 < t_2 < t_f$ and subject to

a. dynamic equations.

$$\dot{x}(t) = f(x, u; t) \quad (2)$$

i.e., equations (32), (33) of the modelling section.

b. kinematic constraints.

$$\left.\begin{aligned} S^d(x;t) &= S_1^2 + S_2^2 - d^2 = 0 \\ S_1 &\triangleq e_1 - \tilde{g}(t) - \ell_1 t_2 - \ell_2 t_4 \\ S_2 &\triangleq e_2 - v_o t - \ell_1 t_1 + \ell_2 t_3 \end{aligned}\right\} \quad \text{for } 0 \leq t \leq t_1 \quad (3)$$

$$\left.\begin{aligned} S^s(x;t) &= \tilde{g}(t) + \ell_1 t_2 + \ell_2 t_4 + d\cos\beta - e_o \leq 0 \\ \beta &\triangleq \pi - \delta_{max} - \phi_o + x_1 - x_2 \\ x_2 &> 0 \end{aligned}\right\} \text{for } t_1 < t \leq t_2 \qquad (4)$$

$$\left.\begin{aligned} S_1^{rs}(x;t) &= \tilde{g}(t) + \ell_1 t_2 + \ell_2 t_4 + p(t) - e_o = 0 \\ S_2^{rs}(x;t) &= v_o(t + t_o) + \ell_1 t_1 - \ell_2 t_3 - q(t) = 0 \end{aligned}\right\} \text{for } t_2 < t \leq t_f \qquad (5)$$

c. Initial and terminal conditions.

$$x(0) = \hat{x}_o \quad \text{(specified)} \qquad (6)$$

$$\left.\begin{aligned} \Psi_1(x(t_1);t_1) &\triangleq [S^d(x;t)]_{t=t_1} = (S_1^2 + S_2^2 - d^2)_{t_1} = 0 \\ \Psi_2(x(t_1);t_1) &\triangleq x_2(t_1) - x_1(t_1) + \phi_o + \delta_{max} - \frac{\pi}{2} - \alpha(t_1) = 0. \end{aligned}\right\} \qquad (7)$$

These are the terminal hypersurface constraints for deploy.

$$x(t_2) \triangleq \hat{x}_2 = \tilde{d} \quad \text{(specified)} \qquad (8)$$

$$x(t_f) = x(0) \quad \text{(repeatability in walking)} \qquad (9)$$

Note 1.

Conditions (6), (7) and (8) describe the configuration of the leg at heel off, toe off and heel strike respectively. In our study, the values $x(0)$ and $x(t_2)$ are specified from experimental data, as they together depict the deploy/restraint configuration at the starting instant. Such a specification appears more natural than Beckett's case where $x(t_2)$ remains unspecified.

Note 2.

A hypersurface type of constraint is used to describe the toe off condition at the end of deploy. Although the state equality constraint $S^d(x;t)$ is binding throughout the deploy portion, the additional condition

$\Psi_1 = 0$ is a device used to eliminate possible jumps for the influence equations in numerical simulation. The $\Psi_2 = 0$ condition describes "foot-locking" for the subsequent swing; and δ max, $\alpha(t_1)$ are set at 110° and 70° for simulation [10].

Note 3.

The condition (9) describes repeatability of motion in normal level walking.

Note 4.

From the kinematic constraints (3) describing deploy motion and Fig. 12, we can write

$$S_1 = e_1 - \tilde{g}(t) - \ell_1 t_2 - \ell_2 t_4 = d \sin\alpha$$

$$S_2 = e_2 - v_o t - \ell_1 t_1 + \ell_2 t_3 = d \cos\alpha$$

where $d \triangleq$ effective length of the foot between the ankle joint and the ball of the foot (i.e. center of rotation)

$$\therefore \quad \tan\alpha = \left(\frac{S_1}{S_2}\right) \Longrightarrow \alpha(t) = \tan^{-1}\left(\frac{S_1}{S_2}\right)$$

$$\dot{\alpha}(t) = \frac{\dot{S}_1}{S_2}$$

$$\ddot{\alpha}(t) = \frac{\ddot{S}_1}{S_2} - \frac{\dot{S}_1 \dot{S}_2}{S_2^2}$$

2. Characteristics of the Problem Formulation

a. It is a programming approach as opposed to the direct approach taken in other studies.

b. The formulation results in a multi-arc programming problem with three stages on account of the varied nature of the ankle reactions and moments; kinematic constraints; initial and terminal conditions.

c. Computationally, the multi-arc problem is decomposable into three problems for solution. Continuity in the state variable histories (angular displacements and velocities) is ensured by matching the trajectories between two adjacent stages.

d. The programming formulation is very flexible. Although emphasis has been on the human case, the formalism and approach are certainly applicable to practical designs such as above-knee prosthetics and remotely controlled manipulators utilized in a hostile environment.

e. The splitting up of the multi-arc programming problem for independent numerical solutions links to the important concept of sub-optimality in our solution. For the present simulation, the intermediate times t_1 and t_2 are specified from experimental data and it is implicitly assumed that

$$\underset{\substack{u(\cdot)\\ 0\leq t\leq t_f}}{J_o} \approx \underset{\substack{u(\cdot)\\ 0\leq t\leq t_1}}{J^{(\text{deploy})}} + \underset{\substack{u(\cdot)\\ t_1\leq t\leq t_2}}{J^{(\text{swing})}} + \underset{\substack{u(\cdot)\\ t_2\leq t\leq t_f}}{J^{(\text{stance})}}; \qquad 0<t_1<t_2<t_f .$$

In general, the optimal control strategy over the entire interval $[0, t_f]$ is not equal to the concatenation of the optimal strategies over the successive sub-intervals. However, it appears that the very special nature of the locomotion problem renders the sub-optimal solution close to the optimal one. In both the deploy and stance portions, the contributions due to the ankle moment and reactions are the major determinants in the control moment $u(\cdot)$ calculation. In addition, the moments in the stance portion are determined by an algebraic method without an optimization procedure and so the

contribution $J^{(stance)}$ is essentially constant, irrespective of optimization. The cost $J^{(deploy)}$ is a small fraction of the total cost because the subinterval $[0, t_1]$ is short (i.e. $\frac{t_1}{t_f} \approx 0.1$ to 0.15) and the control moments are also influenced by the ankle moment and reactions. Only the term $J^{(swing)}$ can be significantly minimized via optimization. Thus, it appears that the sub-optimal solution should be very close to the true optimal.

3. Necessary Conditions of Optimality; Method of Solution.

With the problem formulation completed, the next step is to invoke the necessary conditions of optimality. Solution for the deploy and swing portions are first considered as they are of a similar nature. The technique is to convert the original constrained optimization problem into a sequential unconstrained problem. Let $S(x;t)$ denote the state constraint (equality or inequality) in either portion. Define an extra state variable $x_5(t)$ such that it satisfies the differential equation

$$\dot{x}_5(t) = \text{sgn}(S) \cdot S^2(x;t) \tag{10}$$

$$\text{sgn}(S) \triangleq \begin{cases} 1 \text{ if } S = 0 \\ 0 \text{ if } S \leq 0 \end{cases} \tag{11}$$

for $0 \leq t \leq t_1$; $t_1 \leq t \leq t_2$. The original state vector satisfies, of course, the dynamic equation

$$\dot{x}(t) = f(x, u; t) \; ; \; x = (x_1, x_2, x_3, x_4)^T \quad . \tag{12}$$

With the initial condition set to zero, i.e. $x_5(t_1) = 0$ for swing, $x_5(0) = 0$ for deploy respectively, then

$$\text{Min } x_5(t_f^i) = \int_{(0);(t_1)}^{(t_1);(t_2)} \text{Sgn}(S)S^2(x;\eta)d\eta = 0 \qquad (13)$$

$$\Rightarrow \text{Sgn}(S) \cdot S^2(x;\eta) = 0 \quad \forall \eta \epsilon [0, t_1] \text{ or } \eta \epsilon [t_1, t_2] \quad .$$

The state constraint is thus satisfied. A mathematical proof of the above penalty function technique is given by Lele and Jacobson [44]. As far as the initial and terminal conditions are concerned, a quadratic penalty function is used. With these, the necessary conditions of optimality can be separately derived for the deploy and swing portions.

In deploy, we have the modified performance criterion for the sequential unconstrained problem, i.e.

$$\text{Min}_u \hat{J}_d = \sigma_k \{x_5(t_1) + \psi_1^2(x(t_1);t_1) + \psi_2^2(x(t_1);t_1) + (x_3(t_1)-d_3)^2 + (x_4(t_1) - d_4)^2\} + \frac{1}{2}\int_0^{t_1} (r_1u_1^2 + r_2u_2^2)dt \quad . \qquad (14)$$

Specifically, we solve (14) for a monotonically increasing sequence $0 < \sigma_1 < \sigma_2 < \text{---} < \sigma_k$ and subject to the equations

$$\left.\begin{array}{l} \dot{x}(t) = f(x,u;t) \; ; \quad x(0) = x_o \\ \\ \dot{x}_5(t) = (S^d(x;t))^2; \quad x_5(0) = 0 \end{array}\right\} \quad . \qquad (15)$$

The signum function $\text{Sgn}(S^d) = 1$ because the state equality constraint is effective throughout the interval. Define a variational Hamiltonian $H^d(x, u, \lambda, \sigma_k; t)$ as

$$H^d \triangleq \frac{1}{2}(r_1u_1^2 + r_2u_2^2) + \sum_{j=1}^{4} \lambda_j f_j(x,u;t) + \lambda_5(t)\,(S^d(x;t))^2 \qquad (16)$$

The λ's are the influence functions or the adjoint variables of the

optimization problem. The extremal condition is

$$\frac{\partial H^d}{\partial u_i} = 0 \Longrightarrow r_i u_i + \sum_{j=1}^{4} \lambda_j \frac{\partial f_j}{\partial u_i} = 0 \text{ for } i = 1, 2 \quad . \tag{17}$$

$$\therefore \quad \begin{cases} r_1 u_1 + \frac{1}{\delta}(A_2\lambda_3 + t_7\lambda_4) = 0 \\ r_2 u_2 + \frac{1}{\delta}(t_7\lambda_3 + t_8\lambda_4) = 0 \quad . \end{cases} \tag{17a}$$

Note: $\frac{\partial^2 H^d}{\partial u_i^2} = r_i > 0$ for $r_i > 0$; $i = 1, 2$. The influence equations and their terminal conditions at t_1 are

$$\left\{ \begin{array}{l} -\dot{\lambda}_i = \frac{\partial H^d}{\partial x_i} \\ \qquad = \sum_{j=1}^{4} \lambda_j \frac{\partial f_j}{\partial x_i} + 2\lambda_5 \cdot S^d(x;t) \frac{\partial S^d}{\partial x_i}; \quad i = 1, ---, 4 \\ -\dot{\lambda}_5 = 0 \\ \lambda_1(t_1) = \partial\sigma_k(\psi_1 \frac{\partial \psi_1}{\partial x_1} + \psi_2 \frac{\partial \psi_2}{\partial x_1}) \\ \lambda_2(t_1) = 2\sigma_k(\psi_1 \frac{\partial \psi_1}{\partial x_2} + \psi_2 \frac{\partial \psi_2}{\partial x_2}) \\ \lambda_3(t_1) = 2\sigma_k(x_3(t_1) - d_3) \\ \lambda_4(t_1) = 2\sigma_k(x_4(t_1) - d_4) \\ \lambda_5(t_1) = \sigma_k \end{array} \right. \tag{18}$$

Explicitly, expressions for the λ-equations and $\frac{\partial S^d}{2x_i}$ are given as follows:

$$-\dot{\lambda}_1 = \frac{1}{\delta}\{(A_2R_{31}+t_7R_{41})\lambda_3 + (t_7R_{31}+t_8R_{41})\lambda_4\} + 2\lambda_5 S^d \cdot \frac{\partial S^d}{\partial x_1}$$

$$-\dot{\lambda}_2 = \frac{\lambda_3}{\delta}\cdot\{A_2R_{32} - C_3t_5(R_4+u_2) + t_7\cdot R_{42} - \frac{\delta}{\delta}^2\cdot[A_2(R_3+u_1)+t_7(R_4+u_2)]\}$$

$$+\frac{\lambda_4}{\delta}\cdot\{t_7R_{32} - C_3t_5(R_3+u_1) + t_8R_{42} - 2C_3t_5(R_4+u_2)$$

$$+\frac{\delta}{\delta}^2\cdot[t_7(R_3+u_1)+t_8\cdot(R_4+u_2)]\} + 2\lambda_5 S^d\cdot\frac{\partial S^d}{\partial x_2}$$

$$-\dot{\lambda}_3 = \lambda_1 + \frac{1}{\delta}\{(A_2\lambda_3+t_7\lambda_4)\cdot R_{33} + (t_7\lambda_3+t_8\lambda_4)\cdot R_{43}\}$$

$$-\dot{\lambda}_4 = \lambda_2 + \frac{R_{34}}{\delta}\cdot\{A_2\lambda_3+t_7\lambda_4\}$$

$$-\dot{\lambda}_5 = 0$$

$$R_3 = -C_3t_5x_4(x_4 - 2x_3) - (C_1t_1 - C_2t_3)(g + \ddot{\tilde{z}}g)$$

$$R_4 = -C_3t_5x_3^2 - C_3t_6(g + \ddot{\tilde{z}}g)$$

$$R_{31} = -(C_1t_2 + C_2t_4)t_{10} \quad ; \; t_{10} \triangleq g + \ddot{\tilde{z}}g$$

$$R_{41} = C_2t_4t_{10} + \ell_1t_2Y - \ell_1t_1X$$

$$R_{32} = -C_3t_6x_4(x_4 - 2x_3) + C_2t_4\cdot t_{10}$$

$$R_{42} = -C_3t_6x_3^2 - C_2t_4t_{10}$$

$$R_{33} = 2C_3t_5x_4$$

$$R_{43} = -2C_3t_5x_3$$

$$R_{34} = -2C_3t_5(x_4 - x_3)$$

$$S^d = S_1^2 + S_2^2 - d^2$$

$$S_1 = e_1 - \ell_1 t_2 - \ell_2 t_4 - \tilde{g}(t)$$

$$S_2 = e_2 - \ell_1 t_1 + \ell_2 t_3 - v_o t$$

$$\frac{\partial S^d}{\partial x_1} = 2S_1(\ell_1 t_1 - \ell_2 t_3) - 2S_2(\ell_1 t_2 + \ell_2 t_4)$$

$$\frac{\partial S^d}{\partial x_2} = 2\ell_2(S_1 t_3 + S_2 t_4)$$

$$\delta = A_2 t_8 - t_7^2$$

$$\delta_2 \triangleq \frac{\partial S}{\partial x_2} = 2C_3^2 t_5 t_6 \quad .$$

Similarly, in the <u>swing</u> portion, we have the augmented performance criterion

$$\underset{u}{\text{Min}}\ \hat{J}_s = \sigma_k\{x_5(t_2) + \sum_{i=1}^{4}(x_1(t_2) - \tilde{d}_i)^2\} + \gamma_k \int_{t_1}^{t_2} \frac{dt}{x_2(t)}$$

$$+ \frac{1}{2}\int_{t_1}^{t_2}(r_1 u_1^2 + r_2 u_2^2)dt \tag{19}$$

for $0 < \sigma_1 < \text{---} < \sigma_k \rightarrow \infty$ and $\gamma_1 > \gamma_2 > \text{---} > \gamma_k \rightarrow 0_+$. The dynamic equations are now

$$\begin{cases} \dot{x}(t) = f(x, u; t)\ ;\ x(t_1)\ \text{s.t.}\ \psi_1 = 0,\ \psi_2 = 0\ \text{from deploy} \\ \dot{x}_5(t) = \text{Sgn}(S^s) \cdot (S^s(x; t))^2\ ;\ x_5(t_1) = 0. \end{cases} \tag{20}$$

The presence of the "soft" penalty is to ensure that $x_2(t) > 0$ during the entire swing portion. This requires that the initial and all iterative trajectories be feasible. Similar to the deploy portion, define a variational Hamiltonian as

$$H^s(x, u, \lambda; \sigma_k, \gamma_k; t) \triangleq \frac{1}{2}(r_1 u_1^2 + r_2 u_2^2) + \frac{\gamma_k}{x_2(t)} + \sum_{j=1}^{4} \lambda_j f_j(x, u; t)$$

$$+ \lambda_5(t) \cdot \mathrm{Sgn}(S^s) \cdot (S^s(x; t))^2 \quad . \tag{21}$$

Again, the extremal condition implies

$$(H^s)_u = 0 \Longrightarrow r_1 u_1 + \sum_{j=1}^{4} \lambda_j \frac{\partial f_j}{\partial u_i} = 0; \; i = 1, 2 \quad . \tag{22}$$

The equation set (17a) is thus obtained. The influence equations and their appropriate boundary conditions are

$$\left\{ \begin{array}{l} -\dot{\lambda}_i = \displaystyle\sum_{j=1}^{4} \lambda_j \frac{\partial f_j}{\partial x_i} + 2\lambda_5 \mathrm{Sgn}(S^s) \cdot S^s \cdot \frac{\partial S^s}{\partial x_i} - \frac{\gamma_k \cdot \delta(2, i)}{x_2^2(t)} \\ -\dot{\lambda}_5 = 0 \\ \lambda_i(t_2) = 2\sigma_k (x_i(t_2) - \tilde{d}_i) \\ \lambda_5(t_2) = \sigma_k \end{array} \right\} \tag{23}$$

for $i = 1, ---, 4$ and $\delta(2, i) = 1$ if $i = 2$ and 0 otherwise. The expressions for the λ-equations are similar to those for the deploy portion except for the substitution of inequality for equality constraint expressions.

Expressions related to the constraint are

$$\left\{ \begin{array}{l} \dfrac{\partial S^s}{\partial x_1} = -\ell_1 t_1 + \ell_2 t_3 - d \sin\beta(t) \\ \dfrac{\partial S^s}{\partial x_2} = -\ell_2 t_3 + d \sin\beta(t) \\ \dfrac{\partial S^s}{\partial x_3} = 0; \quad \dfrac{\partial S^s}{\partial x_4} = 0 \end{array} \right. \quad . \tag{24}$$

For both the deploy and swing portions, we thus have a two-point boundary value problem (TPBVP) — (15, 17a, 18) and (20, 22, 23) for the respective unconstrained optimization problems.

Solution of the stance portion differs from the other two stages. The leg in stance carries the body weight while the inertia of the trunk and forward motion of the swinging leg carry the entire body forward. The result is a "sinusoidal" trajectory for the hip and the foot is almost stationary during the roll-over. With prescribed motion for the hip and ankle, motion of the thigh and shank are determined through these kinematic constraints. The result is that the effective hip and knee moments can be found without the need of minimization of the performance criterion; an algebraic method is sufficient for the solution in this portion. The equality constraints on the ankle motion are

$$\begin{cases} S_1^{rs}(x;t) = \tilde{g}(t) + \ell_1 t_2 + \ell_2 t_4 + p(t) - e_o = 0 \\ S_2^{rs}(x;t) = v_o(t + t_o) + \ell_1 t_1 - \ell_2 t_3 - q(t) = 0 \end{cases} \tag{5'}$$

for $t_2 \leq t \leq t_f$. Differentiating once with respect to t, we have

$$\begin{cases} \dot{S}_1^{rs}(x;t) = \dot{\tilde{g}}(t) + \dot{p}(t) + z_{11}x_3 + z_{12}x_4(t) = 0 \\ \dot{S}_2^{rs}(x;t) = v_o - \dot{q}(t) + z_{21}x_3(t) + z_{22}x_4(t) = 0 \end{cases} \tag{25}$$

where

$$Z \triangleq \begin{pmatrix} z_{11} & z_{12} \\ z_{21} & z_{22} \end{pmatrix} = \begin{pmatrix} -\ell_1 t_1 + \ell_2 t_3 & -\ell_2 t_3 \\ \ell_1 t_2 + \ell_2 t_4 & -\ell_2 t_4 \end{pmatrix} .$$

The equation sets (5') and (25) form a decoupled system of four equations in the state variables $(x_1, \cdots, x_4)$ at each instant of time in

the stance interval. Note that (5') is a nonlinear equation set in x_1 and x_2 while (25) is linear in x_3 and x_4 with the coefficients z_{ij} $(i, j = 1, 2)$ as functions of x_1 and x_2. Differentiating once more with respect to time,

$$\begin{pmatrix} \ddot{S}_1^{rs} \\ \ddot{S}_2^{rs} \end{pmatrix} = \begin{pmatrix} \ddot{\tilde{g}} + \ddot{p} \\ -\ddot{q} \end{pmatrix} + Z \begin{pmatrix} \dot{x}_3 \\ \dot{x}_4 \end{pmatrix} - L \begin{pmatrix} x_3^2 \\ (x_4 - x_3)^2 \end{pmatrix} = 0 \qquad (26)$$

where

$$L \triangleq \begin{pmatrix} \ell_1 t_2 & \ell_2 t_4 \\ \ell_1 t_1 & -\ell_2 t_3 \end{pmatrix} .$$

Now, $\dot{x}_3$ and $\dot{x}_4$ contain the actuating moments u_1 and u_2 explicitly from the original dynamic equations

$$\begin{cases} \dot{x}_1 = x_3 \\ \dot{x}_2 = x_4 \\ \dot{x}_3 = \frac{1}{\delta}\{A_2(\tilde{R}_3 + u_1 + M_a + (\ell_1 t_1 - \ell_2 t_3)Y + (\ell_1 t_2 + \ell_2 t_4)X) + t_7(\tilde{R}_4 \\ \qquad + u_2 - M_a + \ell_2 t_3 Y - \ell_2 t_4 X)\} \\ \dot{x}_4 = \frac{1}{\delta}\{t_7(\tilde{R}_3 + u_1 + M_a + (\ell_1 t_1 - \ell_2 t_3)Y + (\ell_1 t_2 + \ell_2 t_4)X) + t_8(\tilde{R}_4 + u_2 \\ \qquad - M_a + \ell_2 t_3 Y - \ell_2 t_4 X)\} \end{cases} \qquad (27)$$

or

$$\begin{pmatrix} \dot{x}_3 \\ \dot{x}_4 \end{pmatrix} = \begin{pmatrix} \hat{R}_3 \\ \hat{R}_4 \end{pmatrix} + A^{-1} \begin{pmatrix} u_1 \\ u_2 \end{pmatrix} ; \quad A^{-1} = \frac{1}{\delta} \begin{pmatrix} A_2 & t_7 \\ t_7 & t_8 \end{pmatrix} ; \delta = A_2 t_8 - t_7^2 . \qquad (27')$$

Combining (26) and (27'), the moments can be expressed as:

$$u = -A \begin{pmatrix} \hat{R}_3 \\ \hat{R}_4 \end{pmatrix} + AZ^{-1} \left\{ L \begin{pmatrix} x_3^2 \\ (x_4 - x_3)^2 \end{pmatrix} + \begin{pmatrix} -(\ddot{\tilde{g}} + \ddot{p}) \\ \ddot{q}(t) \end{pmatrix} \right\} \tag{28}$$

and

$$\begin{pmatrix} \dot{x}_3 \\ \dot{x}_4 \end{pmatrix} = Z^{-1} \left\{ L \begin{pmatrix} x_3^2 \\ (x_4 - x_3)^2 \end{pmatrix} + \begin{pmatrix} -(\ddot{\tilde{g}} + \ddot{p}) \\ \ddot{q}(t) \end{pmatrix} \right\} \tag{29}$$

To generate the trajectories in the stance portion, we proceed forward from $t = t_2$ to $t = t_f$ in small positive increments, Δ. At each instant, solve equation set (5') for x_1 and x_2 numerically (this is essentially finding the roots of nonlinear equations). With the x_1 and x_2 values determined, the matrix Z is known and so the variables x_3 and x_4 can be computed from (25). Equation (28) then generates the hip and knee moment profiles.

E. Numerical Simulation and Results

1. Parameters and Pertinent Data

Having formulated an optimal programming theory for biped locomotion, the next step is to perform a numerical simulation of the gait based on the proposed theory. This is a crucial step because only the results can demonstrate the validity and relevance of the theory. In general, the walking pattern of each individual is a little different from that of another person because of the skeletal structure and physiological conditions. However, there are characteristic, qualitative features which are observable in the human gait for non-pathological cases. The objective of the numerical experiment is to simulate these common features.

a. Physical Parameters.

The values of the parameters used in the present computation are based on those used by Galiana and Milsum [33] in their EMG-experiment. Typical values for the mass, length and moment of inertia for the two segments of the lower extremity are listed as shown below. It is noted that their values are derived from the commonly used "percentage" values of Fisher and Dempster in Lissner [32]. Values of the composite parameters used in the mathematical model are also listed.

Parameter	Value	Remarks
Body Weight, W	130 pounds	
Mass, A_o	4.05 slugs	$A_o = W/g$
Mass of Thigh, M_1	0.389 slugs	9.6% of A_o
Mass of Shank, M_2	0.2595 slugs	6.4% of A_o (includes mass of foot)

Parameter	Value	Remarks
Moment of Inertia of Thigh, I_1	1.4×10^{-2} slugs	
Moment of Inertia of Shank, I_2	1.882×10^{-2} slugs	(shank-foot combination)
Link Length of Thigh, ℓ_1	1.3524282 ft.	
Link Length of Shank, ℓ_2	1.2618726 ft.	
Distance from Hip Joint to C.G. of Thigh, a_1	0.586 ft.	Dempster's average data
Distance from Knee Joint to C.G. of Shank, a_2	0.547 ft.	Dempster's data
Length of Foot	0.55 ft. (*)	Effective length in deploy
	0.65 ft.	Effective length in swing

Composite Parameters in Simulation

$$A_1 = I_1 + m_1 a_1^2 + m_2 \ell_1^2 = 0.5993547648 \text{ slug-ft.}^2$$

$$A_2 = I_2 + m_2 a_2^2 = 0.1414525055 \text{ slug-ft.}^2$$

$$C_1 = m_1 a_1 + m_2 \ell_1 = 0.564730024 \text{ slug-ft.}^2$$

$$C_2 = m_2 a_2 = 0.1735743239 \text{ slug-ft.}^2$$

$$C_3 = C_2 \cdot \ell_1 = 0.2347468104 \text{ slug-ft.}^2$$

b. Initial and Terminal Conditions.

The starting values for the angular displacements and velocities (i.e. initial states) are derived from Beckett's [28] numerical experiment These are

(*) During deploy, the foot rotates about its ball. The distance between the ankle joint and center of rotation is shorter than the foot-length during swing when the toes are also taken into consideration.

$x_1(0) = 0.11170107$ radians (6.4°)

$x_2(0) = 0.2268928$ radians (13°)

$x_3(0) = x_1(0) = 0.$ radians/sec.

$x_4(0) = x_2(0) = 1.68$ radians/sec.

At the end of the double-step, the terminal values are chosen as

$x_1(2.0) = 0.799$ radians (46°)

$x_2(2.0) \cong 0.052$ radians (3°)

$x_3(2.0) \cong 0.0$ radians/sec.

$x_4(2.0) \cong 0.0$ radians/sec.

The initial, intermediate and terminal times for the three portions are set at $t_o = 0$; $t_1 = 0.2$ sec (deploy); $t_2 = 1.0$ sec (swing); $t_f = 2.0$ (stance). Here, we assume a 10% interval for deploy and restraint activity. The swing (or support) occupies 40%. Variation in the temporal patterns modify the numerical results but not the methodology.

c. Prescribed Trajectories.

For the hip motion, we have

$\tilde{f}(t) = v_o(t + t_o)$ feet

$v_o = 2.275$ ft./sec.

$t_o = 0.24698953$ sec.

$\tilde{g}(t) = e_o - \frac{0.9}{12} \sin \frac{4\pi}{t_f} (t + \beta \cdot t_f)$ feet

$e_o = 2.7358172$ feet

$t_f = 2.0$ sec.

$\beta = 0.525$

$$e_1 \triangleq e_o = 2.7358172 \text{ feet}$$

$$e_2 \triangleq -v_o t_o = -0.399078 \text{ feet}$$

To describe the almost stationary behavior of the foot in stance portion, we rely on the experimental profiles by Bresler and Frankel [13], and other experimenters [10, 12], (Fig. 11). For the present simulation, simple curve fitting on the experimental data is used as our important objective is to illustrate our approach of study. Better results could be obtained through interpolation or spline function approximation. In the stance portion simulation, the following prescribed trajectories are used for the ankle motion:

$$q(t) = 2.00 + 0.35\,(1 - e^{-6.5\tau}) \; ; \; \tau \triangleq t - 1.0 \; ; \; 1.0 \leq t \leq 2.0 \; .$$

$$p(t) = \begin{cases} 0.17 + 0.15\,\mathrm{Sgn}(\eta) \cdot \eta^2 & 1.0 \leq t \leq 1.3 \\ 0.17 & 1.3 \leq t \leq 1.55 \\ 0.17 + 0.25(t-1.0) + 49.1 \cdot [0.25(t-1)^4 - 0.755(t-1)^3 \\ \qquad + 0.85(t-1)^2 - 0.421(t-1)] & 1.55 \leq t \leq 2.0 \end{cases}$$

$$\eta = t - 0.3 \; ; \; \mathrm{Sgn}(\eta) = \begin{cases} 1 & \eta \leq 0 \\ 0 & \eta > 0 \end{cases}$$

The particular choice of (p, q)-profiles is based on the form of the experimental curves as well as continuity at the matching points.

d. Pressure Transfer Curve.

Equation (46) of mathematical modelling proposes a linear expression for the transfer characteristics of the pressure center in the stance portion. The distance travelled from heel strike to rotation about the ball of the foot is equal to the effective foot length in deploy, i.e. $d = 0.55'$. In approximately mid-stance, the ankle joint is directly above the pressure center. These two pieces of information give us

the required expression:

$$x_p(t) = 2.35 + 0.9\,(t - 1.40) \quad \text{feet} \qquad 1.0 \leq t \leq 2.0$$

2. Numerical Computations.

From the conditions of optimality, a first order algorithm is employed for iterative, numerical solution. The algorithm is coded into Fortran IV programming language to run on the IBM 360/65 digital computer. The program possesses the following features:

a. The program has two options:

(1) a one-dimensional minimization subroutine (QUADCL) used in conjunction with conjugate gradient or steepest descent algorithms.

(2) a simple gradient procedure with a pre-specified improvement step-size.

b. A fourth order Runge-Kutta method with fixed integration step-size is used for integrating the state and adjoint equations. In each integration step, the control histories u(t), state trajectories x(t) and ground reactions (X(t), Y(t)) are represented by their values at the end points. Presumably, such a "discretization" could have effect on the quality and convergence rate of the computation.

c. To satisfy the state constraints, the computation is done in series with increasing positive values of the weighing factor, σ .

d. The computation is carried out in single precision arithmetic.

The numerical computation is involved because the dynamic equations involve five state variables and they are highly non-linear. More efficient algorithms such as second order optimization methods are very complicated to program. In the literature, little has been reported on the computational experience involving problems of such

complexity. Besides, the primary purpose of the computation is to establish the relevance of the theory to biped locomotion and simulate the common features of gait. These considerations prompt the use of the first order algorithm for an adequate, approximate solution to the problem. For each value of σ, the computation involves a large number of iterations before a satisfactory solution is obtained. The procedure with the QUADCL-search option involves more computing time per iteration in general than the simple fixed-step gradient procedure. However, these two options were used more or less alternatively to achieve improvement (cost reduction) because of the non-linearity of the problem. An acceptable solution is obtained with $\sigma = 10^3$ for the deploy portion and $\sigma = 10^2$ for the swing. An interesting observation is that the swing portion with an inequality constraint is comparatively simpler to compute than an equality constraint as in the deploy portion.

3. Results and Discussion.

Results of the simulation are summerized in the various graphs. To facilitate discussion, comparison is made with the often-quoted experimental works of the Eberhart-Inman group at Berkeley [10, 12, 13]. In general, the results can be classified into three groups for discussion.

a. Angular Displacements and Related Results.

Results pertaining to this part are depicted in the graphs No. 1 to No. 7. The state trajectories $x_1(t)$ and $x_2(t)$ together with their time derivatives portray the angular motion of the thigh and shank in the sagittal plane. Note that the curves are so plotted that they begin

at heel strike (i.e. stance portion) for comparison purposes.

The $x_2(t)$-trajectory describes the motion of the shank with reference to the thigh. At heel strike, the knee joint is extended so that the $x_2(t)$ angle is at a small positive value. During the brief restraining portion of stance, the angle x_2 increases so that this flexing of the knee absorbs the impact of body weight passing on to the leg in stance. The angle then decreases until deploy when it starts to increase rapidly. The behavior that the knee is first flexed at heel strike and then flexed again during deploy is known as "knee locking" - a fact well documented in experimental studies. In the swing portion, $x_2(t)$ reaches a peak value of roughly 80^o and then decreases rapidly to almost zero in 0.5 second. The behavior resembles the ballistic action of a pendulum as illustrated clearly by the velocity profile $x_2(t)$ in graph No. 2. In the pioneering works of Fischer, it was conjectured that the action of the leg in swing is purely due to gravity, but this was disputed by others later in connection with muscle activity studies. From the present optimization standpoint, it appears that the effective moments cooperate with gravity for lesser expenditure of work while still satisfying the state constraints. From the graph No. 17, it is apparent that the constraint is well satisfied. The state trajectories (i.e. angular displacements and velocities) are well matched for the multi-arc programming problem. This is achieved by using the terminal conditions of one stage as the initial values for the following in actual computation. However, there exist small discontinuities for the acceleration and moment profiles at the stance/deploy and deploy/swing junctions. The reason for the mismatch is primarily numerical as the

penalty technique used in the computation seldom satisfies the desired conditions exactly. For the purpose of illustrating the theory, the "numerical" discrepancy is not critical. Similarly, another interesting point is that the x_2-acceleration curve (graph No. 3) exhibits a "peaky" behavior in mid-stance. The probable reason is that in our algebraic method of solution, a piecewise polynomial representation is used for the ankle trajectories. Another reason for the slight mis-match of acceleration profiles could be that the overall optimization problem is decomposed into a number of optimization problems over sub-intervals defined by the different phasic periods. This results in an overall sub-optimal solution unless the joins of the sub-intervals happen to occur at exactly optimal locations (which is unlikely since these are experimentally obtained data) and particular care is taken in the matching of the adjoint variables.

The hip trajectory $x_1(t)$ portrays the familiar pattern as observed in experimental studies. In the stance portion, the angle $x_1(t)$ decreases more or less uniformly while the hip joint is describing a sinusoidal path. This characterizes the roll-over action of the upper part of the body (HAT-section) about the weight-bearing leg. During deploy and subsequent swing, the angle $x_1(t)$ shoots up to a maximum value and then coasts until heel strike. The combined motion of the thigh and shank clears the toe sufficiently above the ground for swing motion. As for the $x_2(t)$-trajectories, the $x_1(t)$-trajectories are matched at the junction points except for the acceleration curve. The reason is again numerical as discussed above.

The angle $\alpha(t)$ (Fig. 12) describes the rotation of the foot about

its ball during deploy action. Graph No. 4 shows the result of computation based on the equality constraint relationship. The angle $\alpha(t)$ has a monotonically increasing profile, reaching a limiting value of about 1.2 radians ($\sim 68°$) at the end of deploy. A value of 70° was used for specifying the terminal deploy conditions. The velocity and acceleration curves likewise show a monotonically increasing trend, but the acceleration trajectory appears to be more irregular. This is because the state constraint is satisfied approximately as shown in the residue error curve in graph No. 16.

The angular displacements, velocities and accelerations constitute the main results of the computation upon which related quantities can be calculated. Graph No. 5 shows a phase plane diagram for the angular displacements $x_1(t)$ versus $x_2(t)$ during a double-step. In the paper by Maric and Vukobratovic, a special type of compass gait was considered in which the hip motion is stationary in the vertical direction and the foot is in continuous contact with the ground. The resulting realization of the gait pattern is that the thigh and shank angles are sinusoidal in a double-step. This gives an elliptic phase plane plot with the points equally spaced. The present results simulate much more realistically the biped gait and the plot indicates deformation of the curve in the stance portion. Note that the points are not uniformly spaced, showing different rates of activity in the three portions.

The horizontal and vertical displacements of the joints are plotted in graphs No. 6 and No. 7. A double-step takes two seconds during which there is an overall horizontal displacement of 4.55 feet. This gives a walking speed of about 1.6 miles per hour, a case of slow

level walking. The hip moves at a uniform rate while the knee and ankle move through 4 feet during the swing portion. Graph No. 7 illustrates the vertical displacement of the joints. A double sinusoid with 0.9 inches in amplitude is used to simulate the hip motion. In a more accurate description, a Fourier series representation can be used to fit the experimental profile. In fact, the amplitude and phase of the various components have been studied to reveal the abnormal properties of the pathological gait. In the normal case, the double sinusoid is the principal component. During stance, the knee joint is almost stationary, so is the ankle trajectory as prescribed by the p(t)-profile. The displacement at initial stance is prevailingly restraining action to absorb impact and the gradual increase towards deploy implies the transfer of the pressure center. In subsequent deploy and swing motion, the vertical motion of the knee and ankle is comparatively larger. Note that the overall vertical displacement is almost zero in a double-step.

b. Reaction Forces and Moments at the Joints.

The foregoing section describes the kinematic behavior of the lower extremity in level walking. To complete the description, dynamic quantities such as the forces and moments at the various joints must be determined. It is only with the dynamic information that a realistic description of biped locomotion can be said to have been achieved. In the weight bearing portions, the foot is subjected to very large ground reaction forces due to the weight and acceleration of the upper part of the body (HAT-section). With these large forces appearing at the inputs to the dynamic equations, it is not difficult to realize that they are the dominant quantities in determining the

actuating moments and reaction forces at the various joints. In passing, we note that the numerical integration of differential equations having inputs of a large rapidly varying magnitude is not trivial.

The present model assumes the ground reactions as known inputs to the dynamic equations. This condition amounts to prescribing the behavior of the HAT-section and then investigating the walking patterns of the lower extremities using optimization theory. It is certainly consistent with the concept of decomposing the human postural study into the stability problem of the HAT-section and the locomotion activity study of the two legs, i.e. control through a hierarchy structure. In an analysis using a complete high order model, the ground reactions are determined from the resulting motion of the various segments. For the present study, the experimental profiles by Inman [31] (normalized to body weight) are used as shown in graphs No. 8 and No. 9. Note that the vertical reaction has a double-peak behavior in the stance-deploy portions. The first occurs after heel strike when the body rolls over the weight-bearing leg. The second peak occurs in the deploy portion when the leg pushes the body up in preparation for the swing motion. In both graphs, it is apparent that the reactions at the ankle, knee and hip joints are close to the ground reactions. The differences are due to the inertia and mass of the thigh and shank segments. The ground forces are zero in the swing portion.

Results pertaining to the moment quantities are presented in the graphs No. 10 to No. 12. The ankle moment has the greatest values in the weight bearing portions. The manner in which the ankle moment is calculated is approximate. Based on a "quasi-static"

assumption, the inertial and gravitational effects of the foot are neglected as they are 1% or less of the contribution of the ground reactions. In addition, a linear function is used to describe the transfer of pressure center in stance. Despite the crudeness of the calculation, the ankle moment agrees qualitatively well with the experimental results of Bresler and Frankel [13]. This is encouraging because the approximate calculation avoids the complexity of the high order model. With better representation (e.g. spline polynomial interpolation) of the prescribed trajectories, better results are anticipated. The ankle moment and ground reaction contributions are the dominant quantities in determining the hip and knee moments in the stance and deploy portions (graphs No. 11 and No. 12). This is very interesting because the inertial and gravitational terms are the most complicated to calculateand yet they are only second in importance in the moment calculation. Thus, the use of the simplified decoupled model together with kinematic constraints is not as crude as it may initially appear. However, neglecting the ankle moment and ground reactions makes a big difference in the moment calculation. This, then, should explain the shortcomings of the papers by Beckett, Wallach, Galiana and Vukobratovic et al.

The hip and knee moments are also plotted in graph No. 10. The greatest activity occurs during stance following heel strike and at deploy. Activity in the swing portion is addressed to maintaining the leg above the ground (i.e. to satisfy the state inequality constraints) while utilizing gravity as much as possible).

The knee moment profile shows a typical pattern associated with

the "knee-locking" behavior discussed earlier in a. The sign convention for the moment is such that, when negative, the forces pass behind the knee, tending to flex it; while a positive moment tends to hold the knee in a "locked" position. The present profile agrees fairly well with experiment [13]. At heel strike, the leg is quickly stabilized, then unlocked, and once again locked for the deploy portion. Bresler [13] pointed out that the knee-locking behavior allows one to move forward with a minimum raise of center of gravity, and therefore less expenditure of work.

Like the ankle and knee moments, the hip moment again agrees with the experimental pattern. The negative moment following heel strike is responsible for the roll-over of the body, indicated by a monotonic decrease of the $x_1(t)$-ankle. Toward the deploy, the hip angle starts to increase. The greatest values at initial stance and deploy are opposite in sign. Based on the idea of two basic configurations for the biped gait, the two portions of "maximum" activity correspond to the "restraint/deploy" configuration (Fig. 6). From the dynamic equation for the HAT-section, the trunk of the body is subjected to the action of the hip moments. But the interesting fact that the hip moments of the two legs are more or less of the same order of magnitude but opposite in sign leads to the concept of moment annihilation (i.e. cancelling) of the hip moment's effect on the HAT-section. This consequently requires far less stabilizing moment effort for maintaining up-right posture! In the same vein, the "complementary" † profiles for the hip reaction forces (graphs No. 8 and No. 9) create a couple action in the frontal

† i.e., the profiles at deploy are reflections of those at initial stance.

plane, facilitating the transfer of body weight from the deploying leg to the restraining one following heel strike.

c. "Quality" of Numerical Computation.

As stated earlier, the important objective of the numerical experiment is to demonstrate the validity and relevance of the optimal programming approach to the study of biped locomotion The requirement of an adequate solution together with complexity of programming prompted us to use a first order algorithm and appropriate simplifications. Despite the simplicity of the program, the results agree well with the experimental results. The graphs No. 16 and No. 17 show that the constraints are well satisfied for both the deploy and swing activities. Graph No. 15 depicts the gradient histories for the two control moments in the respective portions. In numerical computation, a commonly used stopping rule is that the integral of the square of the gradients be less than some small positive number, i.e.

$$\int_{(t_i)}^{(t_j)} \left(\sum_{i=1}^{2} g_i^2 \right) dt \qquad < \epsilon \; ; \qquad \epsilon \text{ small}$$

$$g_i \triangleq \frac{\partial H}{\partial u_i} \qquad \text{for both swing and deploy} \quad .$$

The condition that the integral approaches zero implies that the gradient histories become arbitrary close to zero. From graph No. 15, the gradients are certainly not zero. These are the best values obtained from the gradient algorithm as the gradient trajectories tend to fluctuate without evidence of further improvement in the value of

the performance criterion. The greatest deviation from zero occurs at initial deploy, when the ground reactions are at their maximum. Judging from the quality of our results, the gradient histories are acceptable though not as small as one would have hoped. From our computational experience, the cost improvement may be slight in iterative calculations while the gradient histories may change by a wide margin. Thus, the numerical limitations plus the large non-linearity of the cost function account for the gradient fluctuation and difficulty in convergence. In addition, all our computations were carried out in single precision on the IBM 360/65 which offers between 6 and 7 significant decimal places. Double precision could improve the convergence significantly if round off errors are accumulating in the computations.

d. Equivalence of Kinematic and Dynamic Optimality.

An important result of the numerical simulation is the concept of equivalence of kinematic and dynamic optimality. In the absence of the ground reactions and ankle moment (i.e. $M_a = 0, X = 0, Y = 0$), the model is kinematic in that the moment contribution is entirely inertial and gravity. In the graphs No. 13 and No. 14, the $\beta = 0$ curves indicate the optimal moment profiles without any ground reaction forces. This is the kinematic optimal solution. The computation is next made for small increments of the factor β ($0 \leq \beta \leq 1$) which represent different percentages of ground reactions acting on the foot in stance. The graphs illustrate the results for the fractions $\beta = 0.2$, 0.55, 0.8 and 1.0 (the actual dynamic case). For each β, the starting control moments are shown by the dotted lines obtained from a

previous β^* ($\beta^* < \beta$) curve by adding corrections due to incremental ground reactions. The optimal solutions are represented by the solid lines. These solutions, which contain the effect of ground reactions, are the dynamic optimal solutions. On the graphs, the initial and optimal curves are very close together. These curves often differ in the first decimal place in the computer output. Thus, to obtain the optimal moment profiles in the presence of ground reactions, one may first compute the optimal solution with no force present and then add in the contribution from ground reactions and ankle moments. The kinematic solution ($\beta = 0$) is much easier to obtain than the dynamic case ($\beta = 1$) because of the difficulty in handling numerically the large forces. The following table shows the β-series of computations. Note that J increases as the fraction of ground reactions is increased. The higher values in the "norm" of the gradient are probably due to severe non-linearity of the cost surface.

β	Cost, J		$\int_0^{0.2} H_u^2 dt$	
	Initial	Final	Initial	Final
0	4.65354		1.22550×10^{1}	
0.2	5.26159	5.03576	9.21051×10^{3}	1.19315×10^{2}
0.55	32.8768	26.2485	6.26548×10^{8}	1.06064×10^{3}
0.8	75.8608	63.2441	3.50728×10^{9}	1.93208×10^{2}
1.0	135.271	99.7697	1.91357×10^{9}	1.94933×10^{3}

e. Feasible Initial and Terminal Regions.

The starting and terminal values used in the simulation are chosen from experimental curves. In actual locomotion, these values are seldom duplicated either due to parameter sensitivity or environmental changes. Whatever the initial configuration may be, the deploy portion is almost characterized by the same circular arc equality constraint. Thus, it would appear to be very valuable to obtain the initial and terminal feasible regions for adaptation of control programs. For our purposes, the feasible initial region is defined as the set of values which satisfy the constraint and its time derivatives at the initial time, i.e. $\forall\, x_o$ s.t. $S^d(x_o; t = 0) = 0$; $\dot{S}^d(x_o; t = 0) = 0$; $\ddot{S}^d(x_o; t = 0) = 0$, etc. Results of the calculation are shown in graphs No. 18 to No. 21. These are obtained by varying the $x_2(0)$ angle by small increments from the chosen value and computing the corresponding $x_1(0)$ through iteration. The striking fact is that although the equation is highly non-linear, the set of feasible values forms a straight line as shown in No. 18. In No. 19, the velocities are also linearly related. This is very interesting for parameter variation design considerations. For a given set of starting values, the feasible terminal values are shown in No. 20 and No. 21.

f. Design Considerations.

From the foregoing discussions a. through e. on the simulation results, useful ideas are evolved for practical design and quantitative study via the optimal programming approach. Fig. 19 shows a schematic realization of a walking program by means of multi-arc programming. The locomotion behavior for a double-step is first

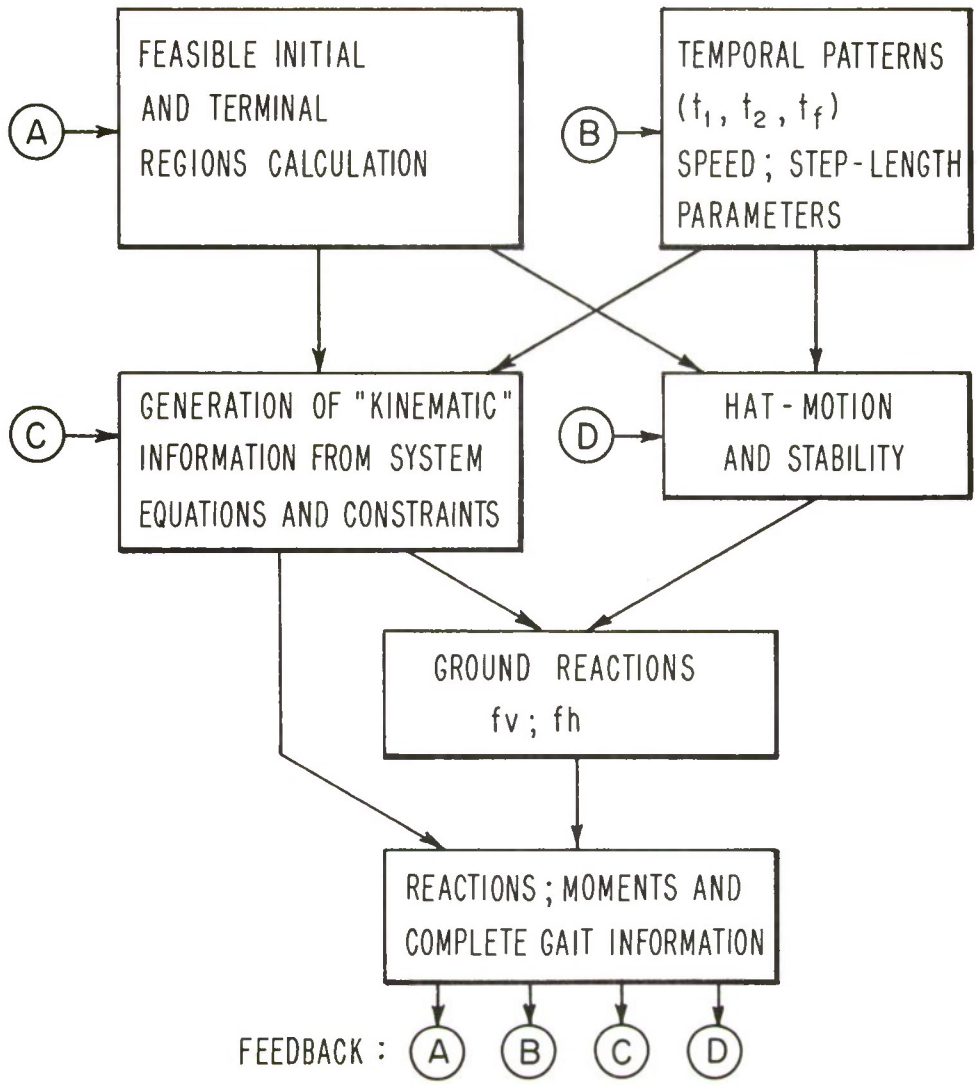

FIG. 19 REALIZATION OF LOCOMOTION PROGRAM VIA MULTI-ARC OPTIMAL PROGRAMMING.

decomposed into pertinent sub-modes or configurations. Information on the feasible initial and terminal conditions, temporal patterns, step-length and speed parameters forms a gross characterization. From this, one can then generate the kinematic behavior of the gait - i.e. displacement, velocity and acceleration trajectories for the various angles. The motion of the upper part of the body is likewise investigated. The trunk motion together with the kinematic information specify the ground reactions. This leads to the determination of effective moments, reactions at the joints and other dynamic quantities. To facilitate adaptation of the walking program, feedback of information at various levels is indicated. The linearity of the initial feasible region as discussed in e. would certainly be of value in adaptive design. Such an optimal design procedure takes into account the dynamic and kinematic details of the gait. This appears to be much more realistic than the algorithmic approach taken by McGhee, Frank and Tomovic in their investigations [45-48].

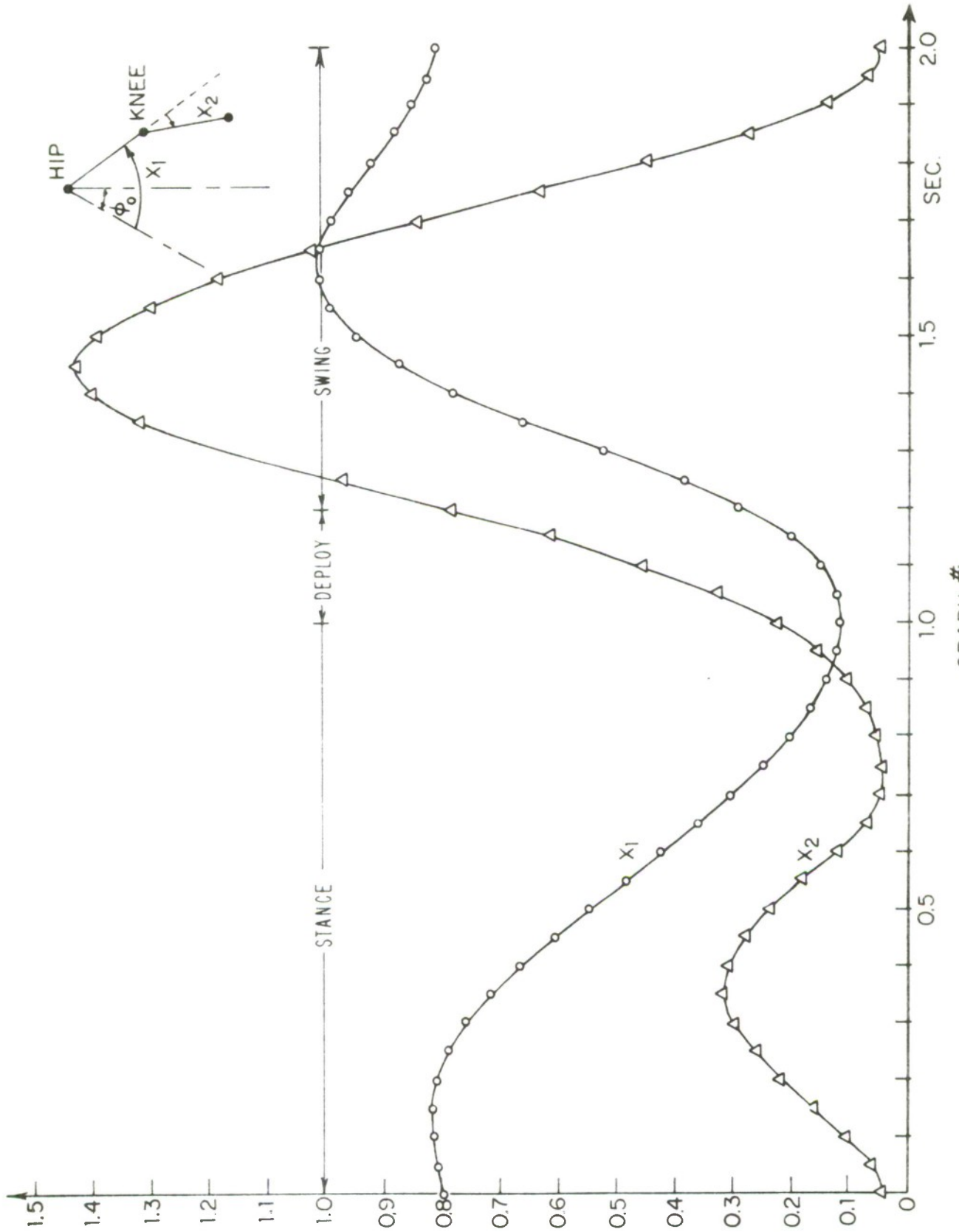

GRAPH #1

ANGULAR DISPLACEMENT OF HIP AND KNEE

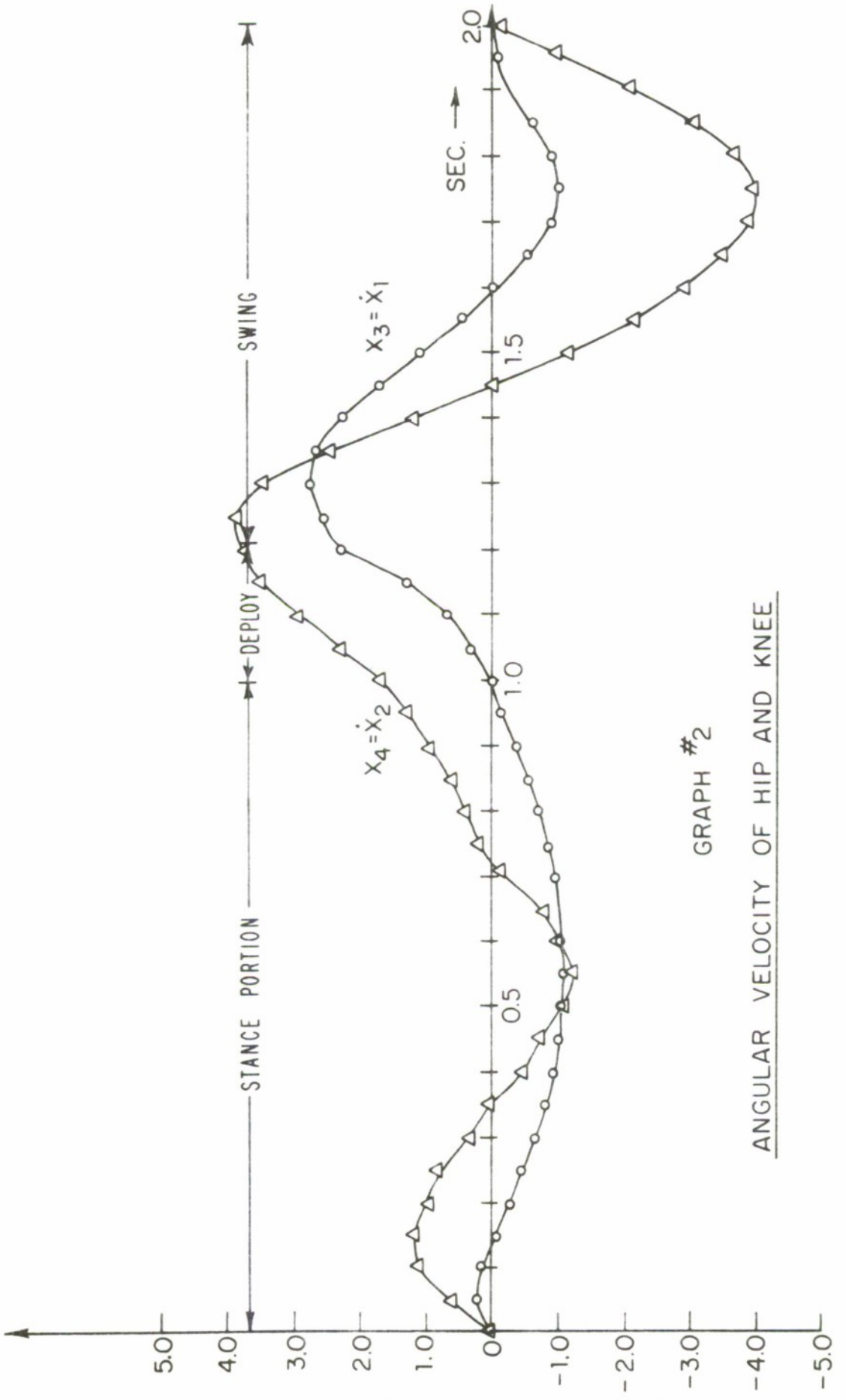

GRAPH #2

ANGULAR VELOCITY OF HIP AND KNEE

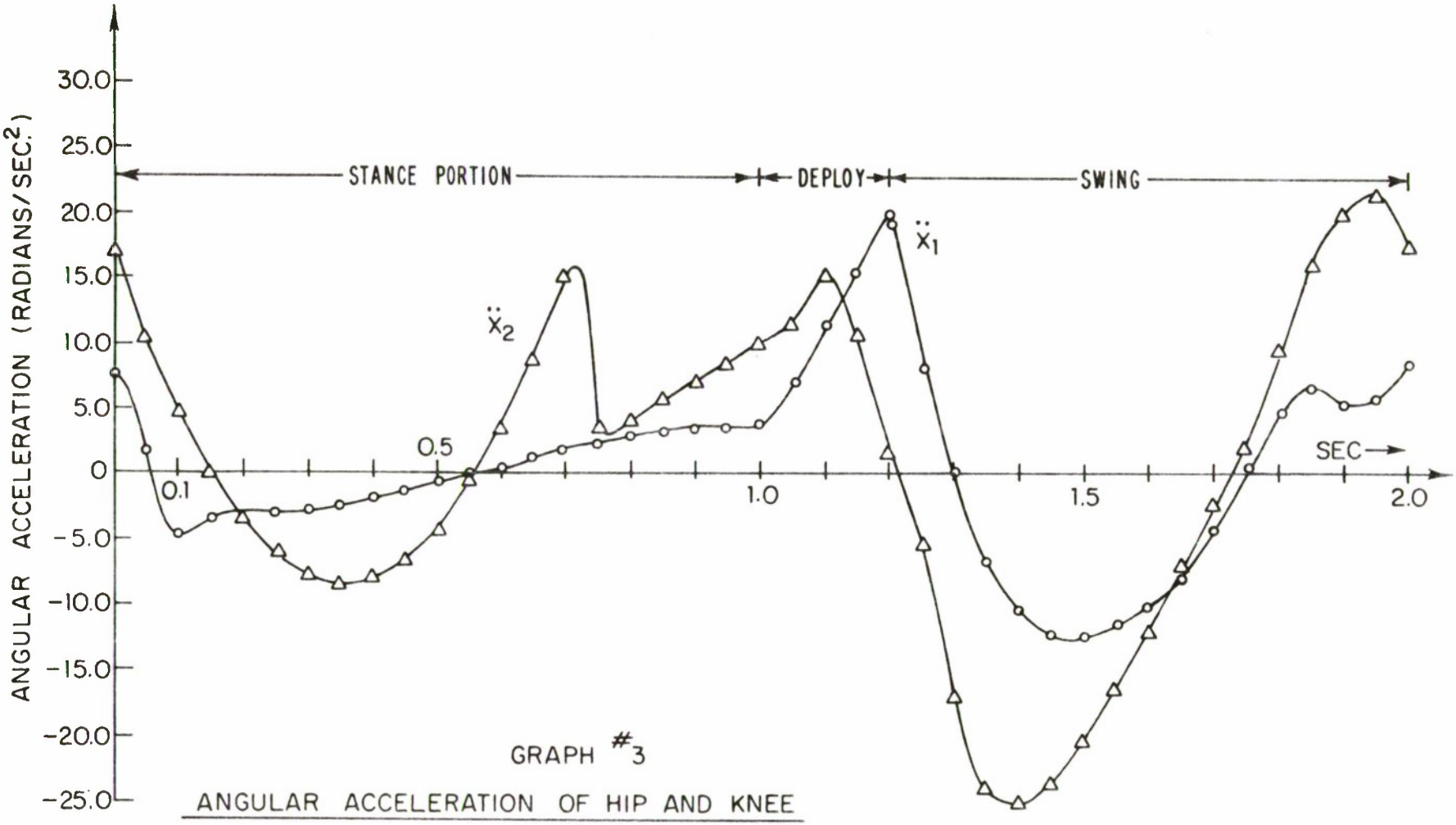

GRAPH #3

ANGULAR ACCELERATION OF HIP AND KNEE

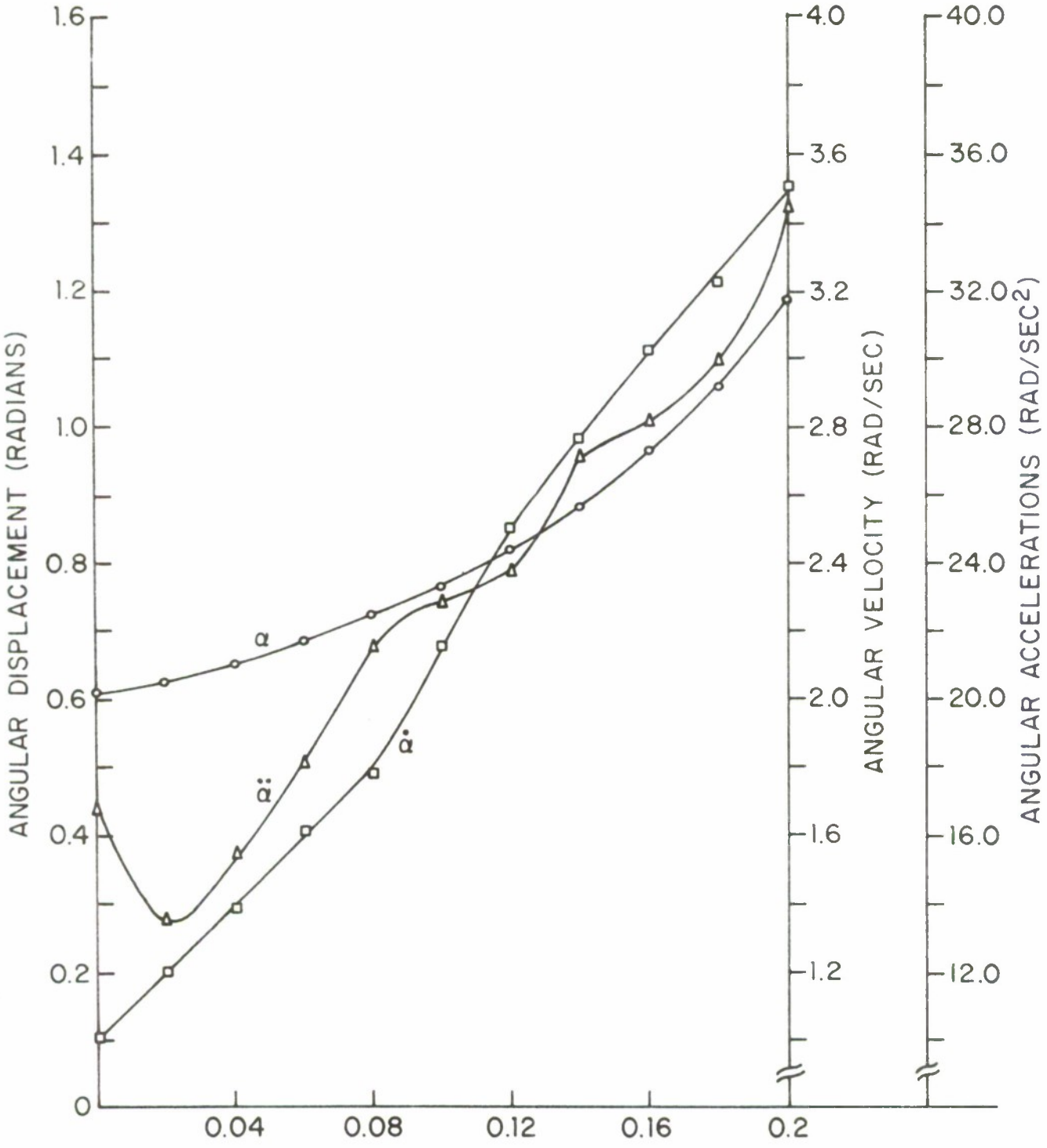

GRAPH #4

ROTATION OF THE FOOT IN DEPLOY PORTION

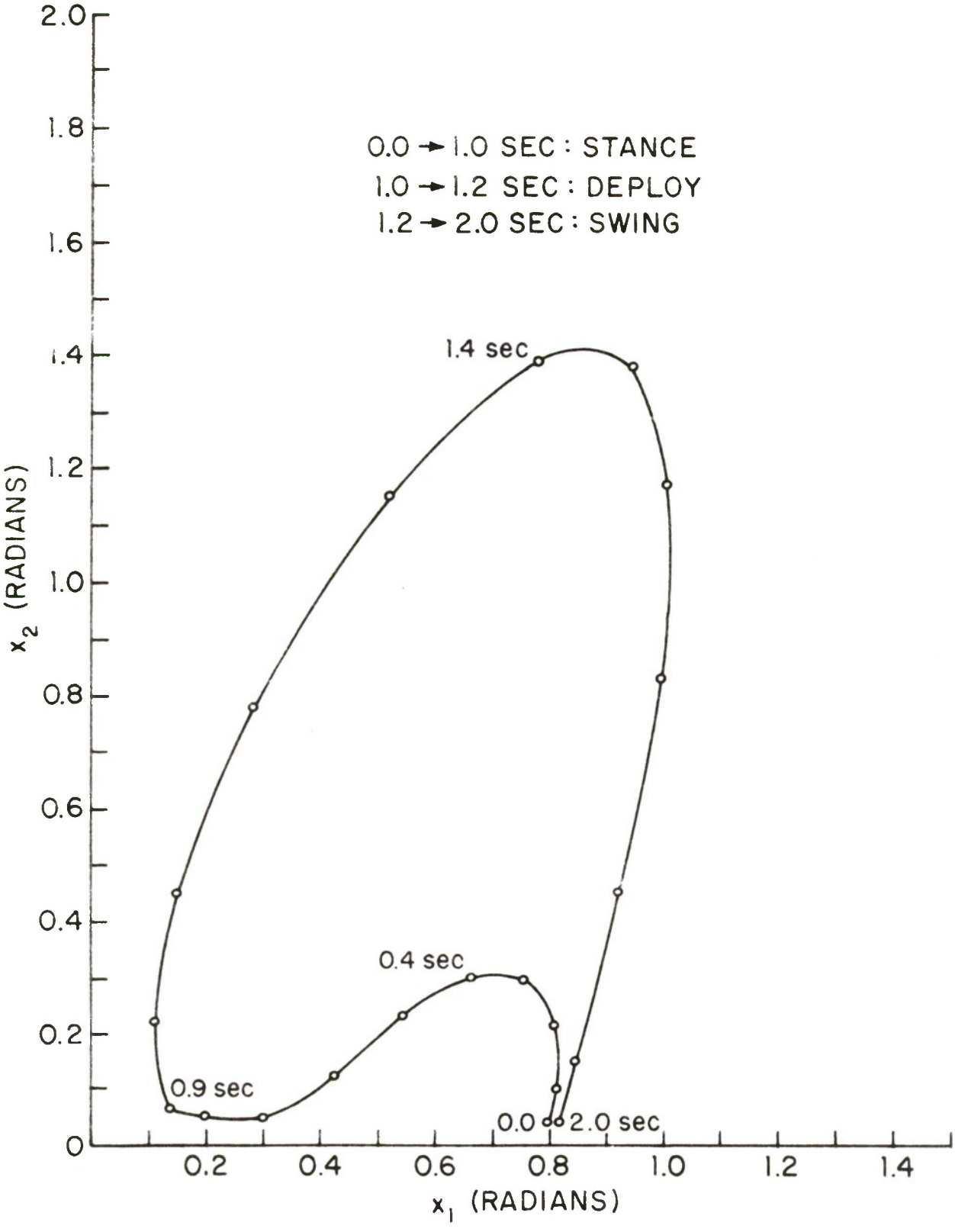

GRAPH #5

"PHASE PLANE" DIAGRAM OF HIP AND KNEE ANGLES IN A DOUBLE-STEP

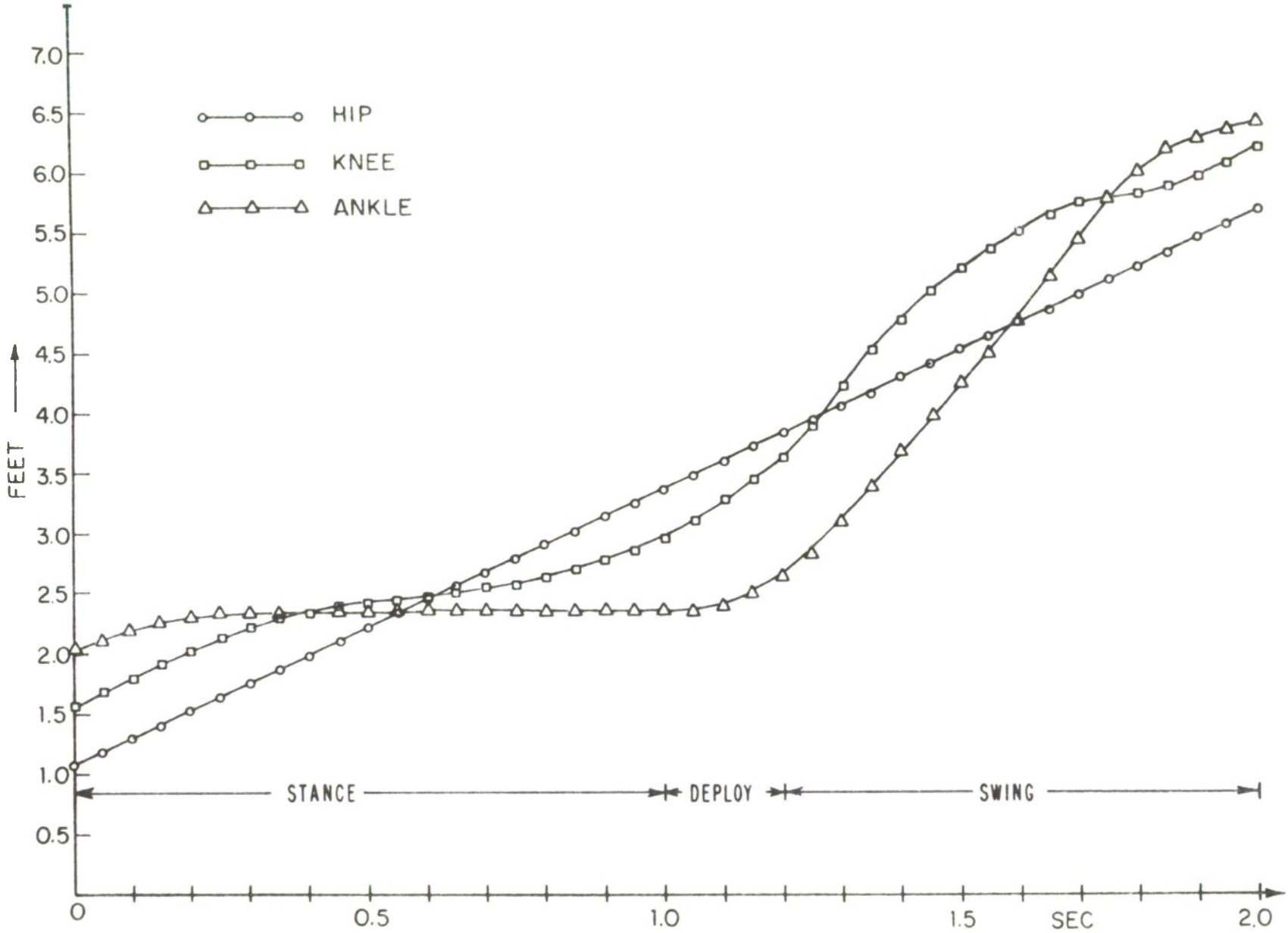

GRAPH #6

HORIZONTAL DISPLACEMENT OF THE JOINTS

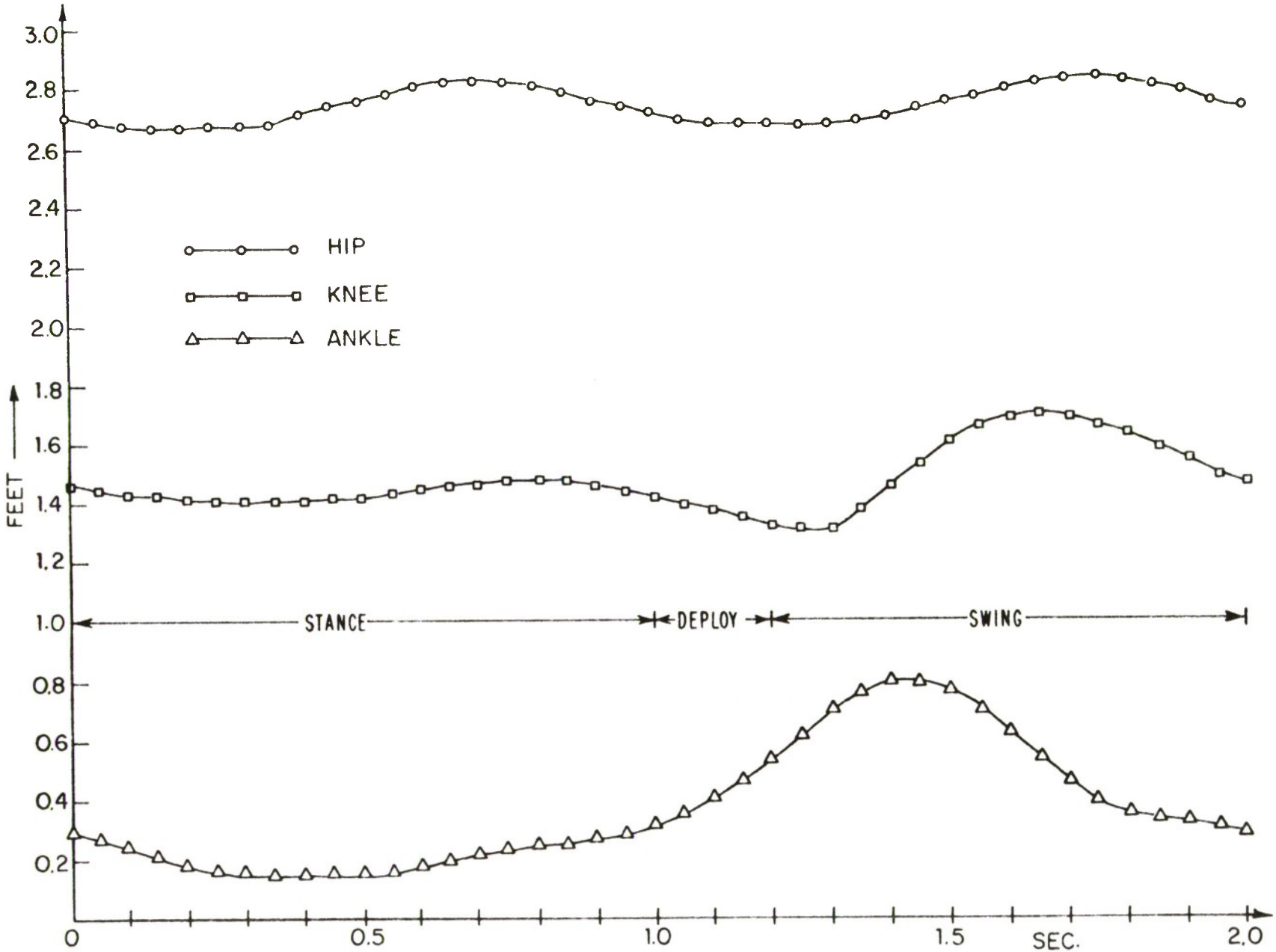

GRAPH #7

VERTICAL DISPLACEMENT OF THE JOINTS

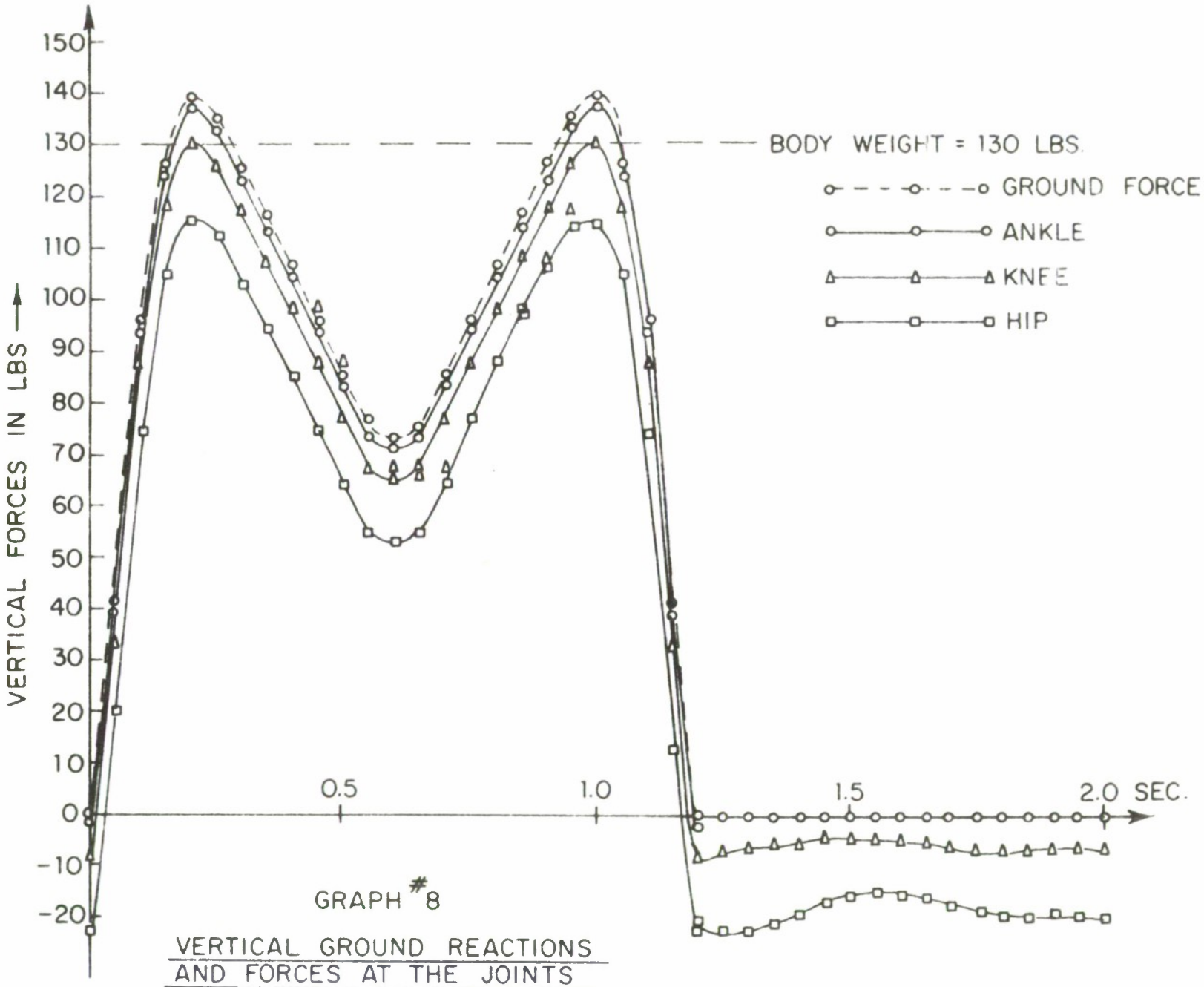

GRAPH #8

VERTICAL GROUND REACTIONS AND FORCES AT THE JOINTS

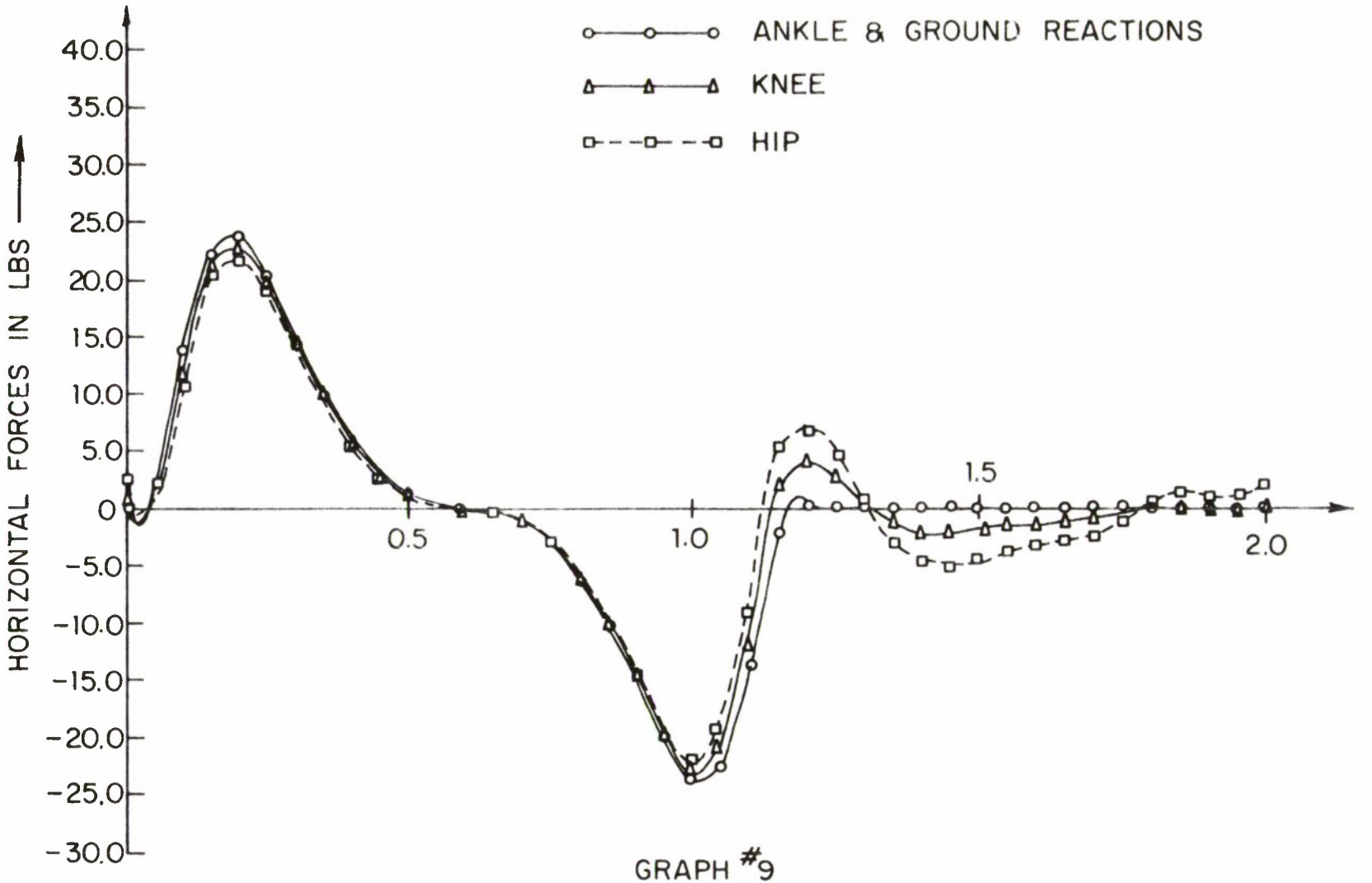

GRAPH #9

HORIZONTAL GROUND REACTIONS AND FORCES AT THE JOINTS

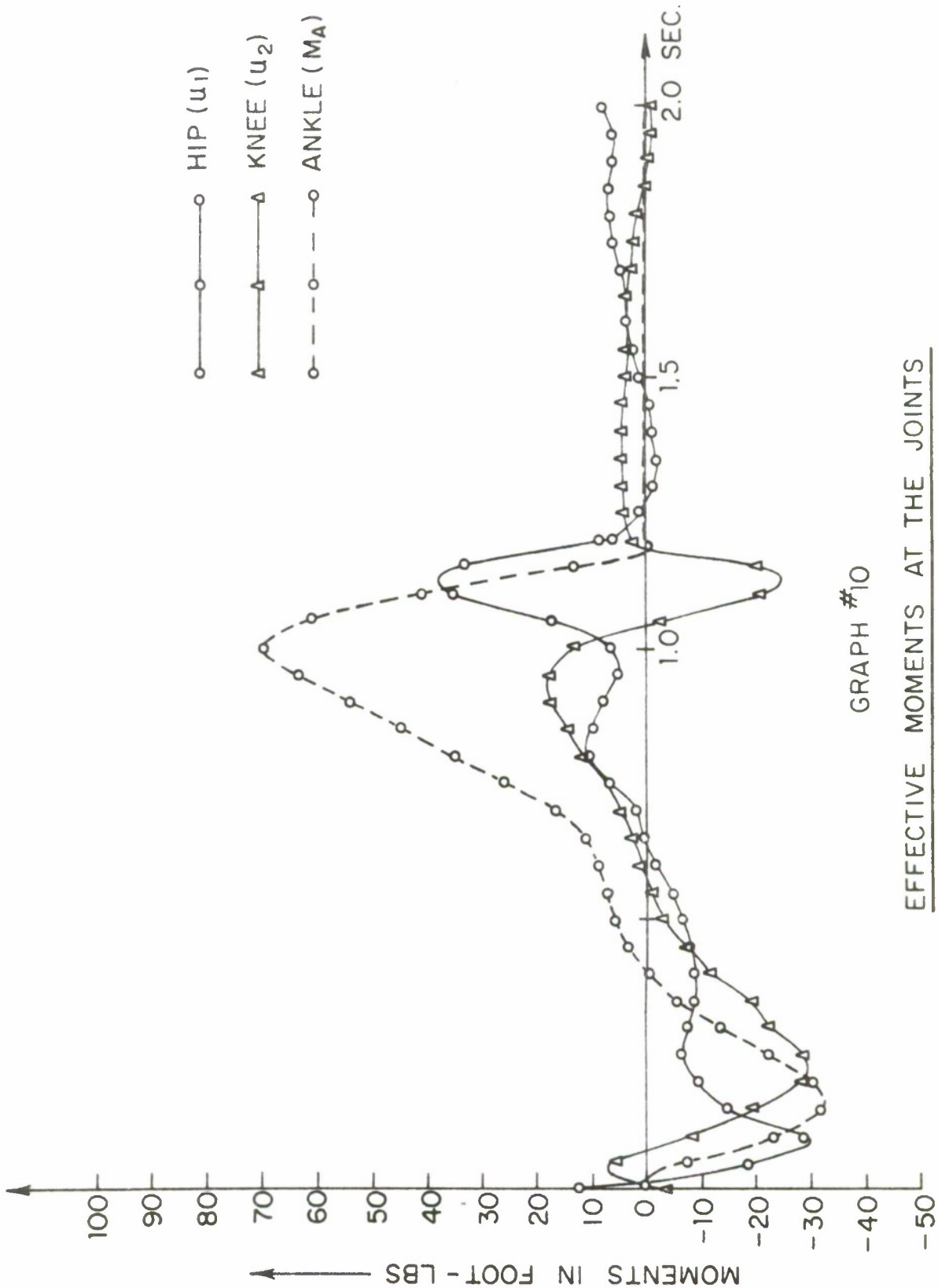

GRAPH #10

EFFECTIVE MOMENTS AT THE JOINTS

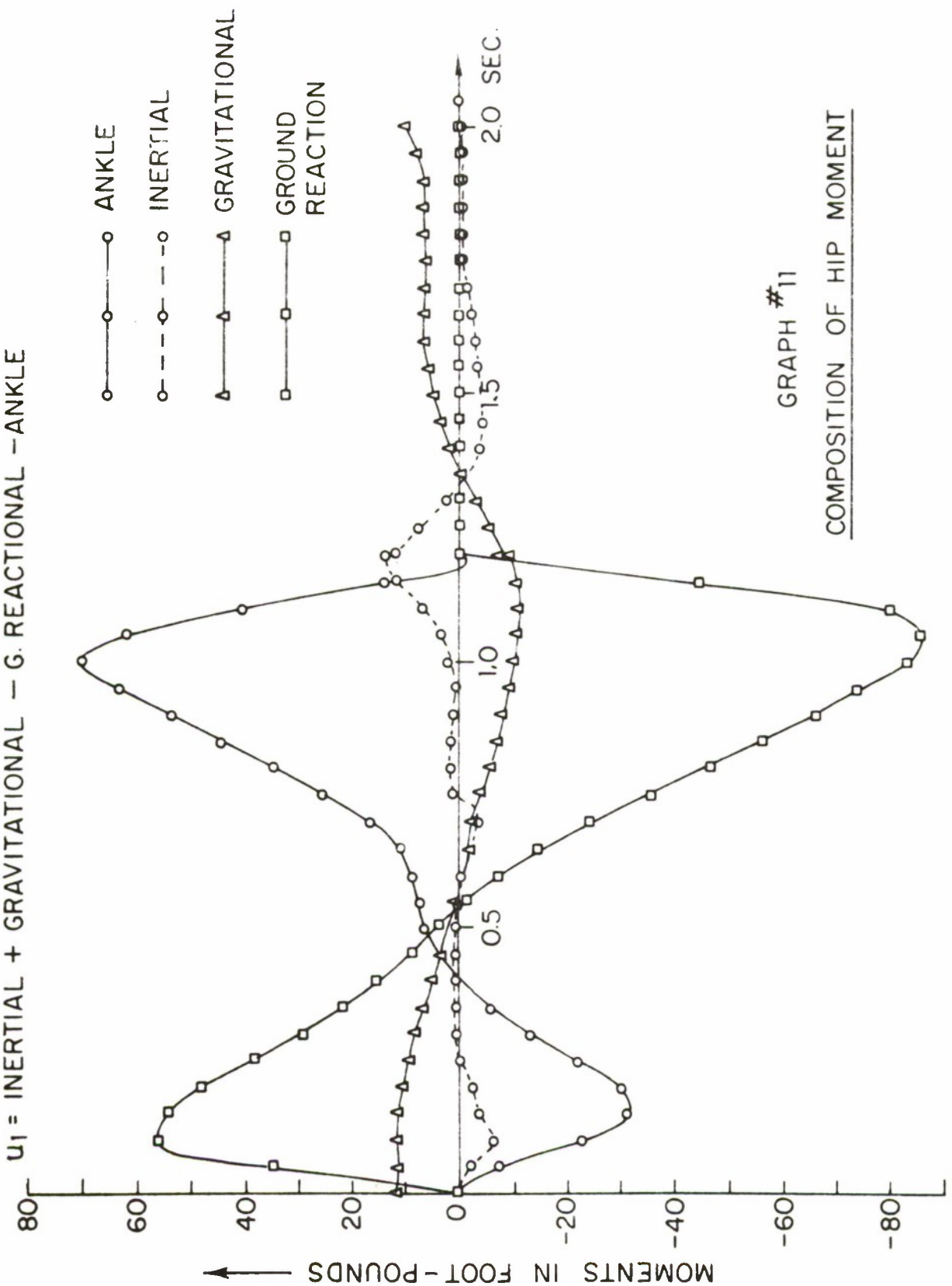
COMPOSITION OF HIP MOMENT
GRAPH #11
ANKLE
INERTIAL
GRAVITATIONAL
GROUND REACTION
u_1 = INERTIAL + GRAVITATIONAL − G. REACTIONAL − ANKLE
MOMENTS IN FOOT-POUNDS
80
60
40
20
0
-20
-40
-60
-80
0.5
1.0
1.5
2.0 SEC.

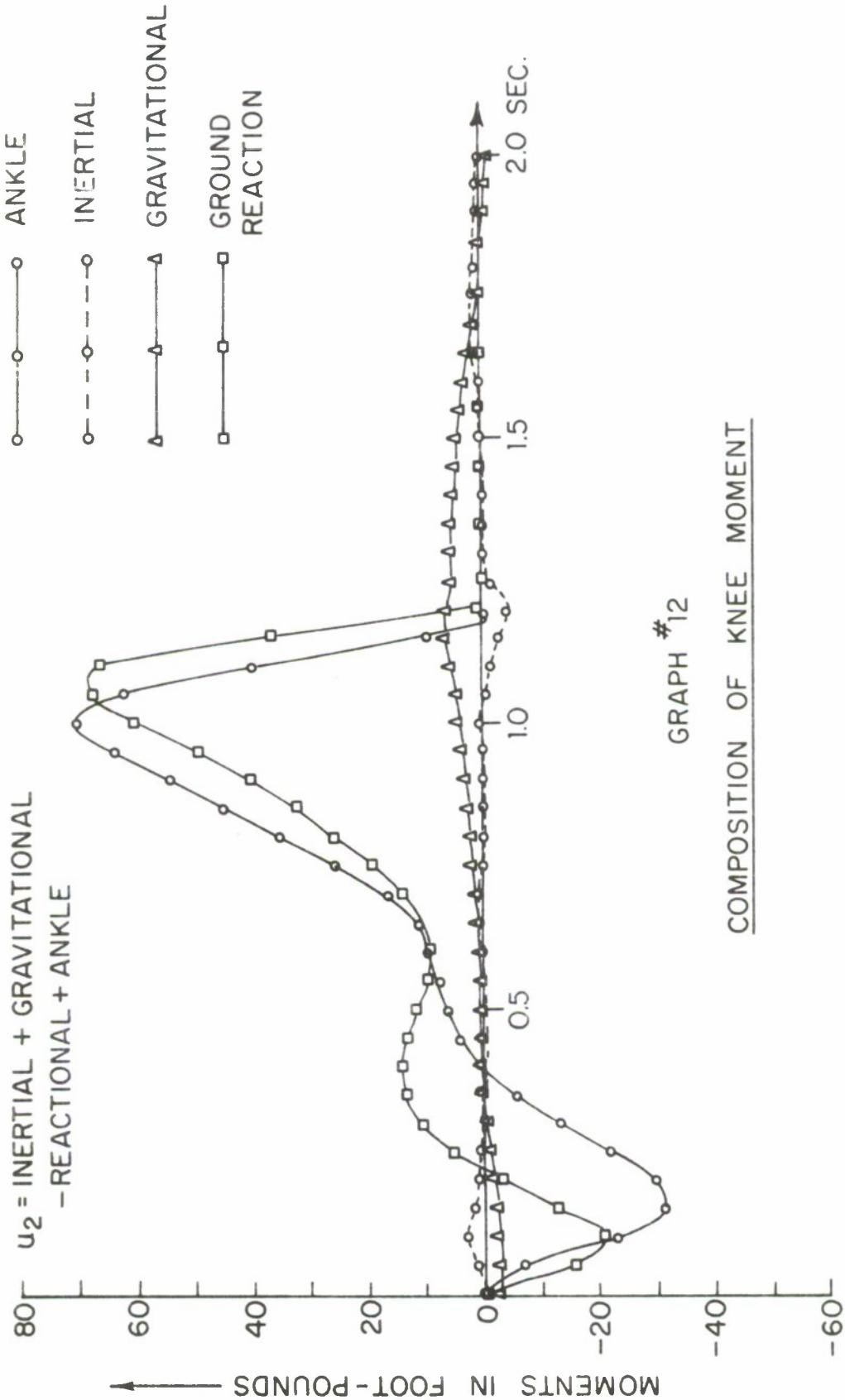
ANKLE
INERTIAL
GRAVITATIONAL
GROUND REACTION
u_2 = INERTIAL + GRAVITATIONAL
−REACTIONAL + ANKLE
MOMENTS IN FOOT-POUNDS
80
60
40
20
0
-20
-40
-60
0.5
1.0
1.5
2.0 SEC.
GRAPH #12
COMPOSITION OF KNEE MOMENT

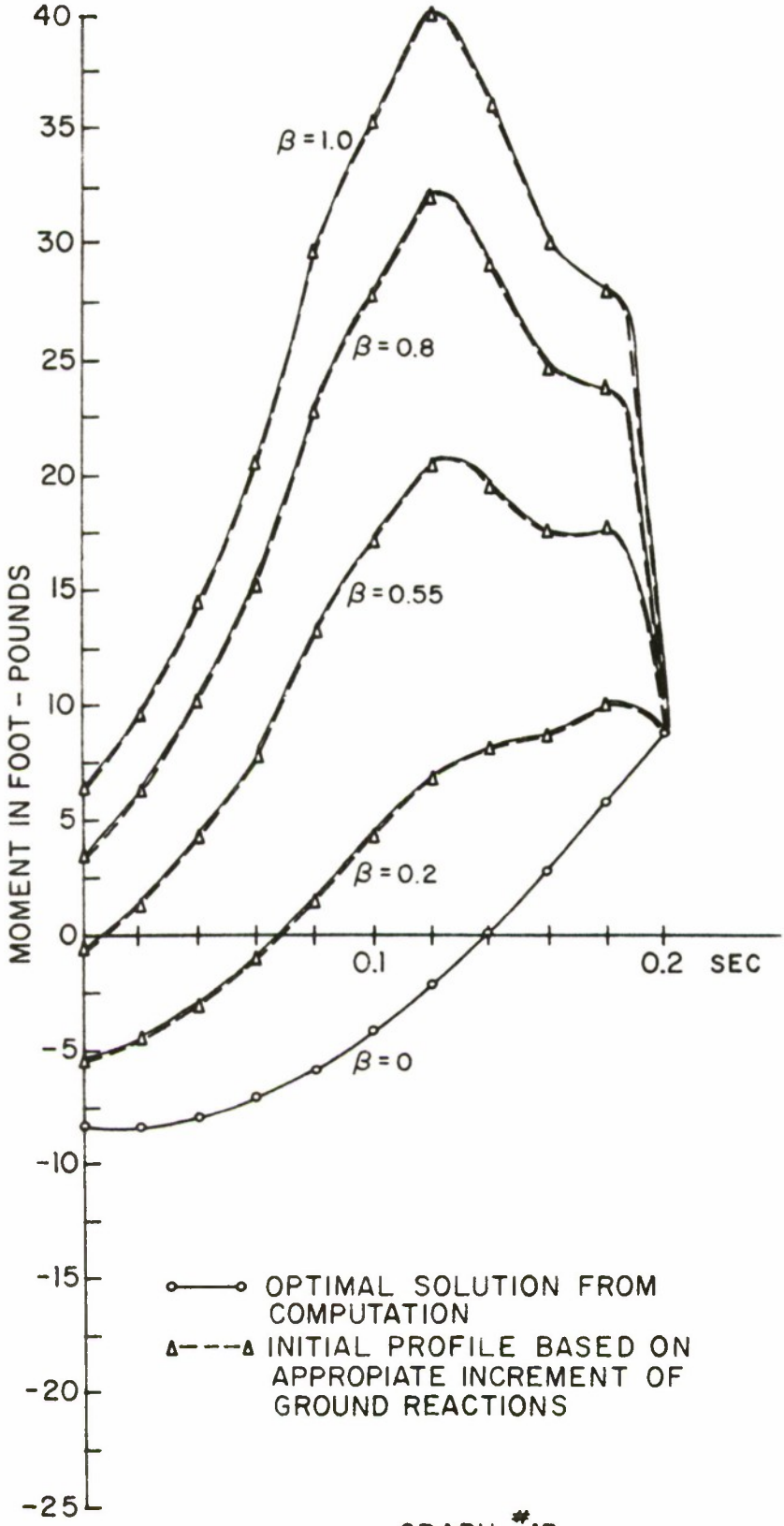

GRAPH #13

HIP MOMENT FOR VARIOUS PORTIONS (β) OF GROUND REACTIONS AT DEPLOY

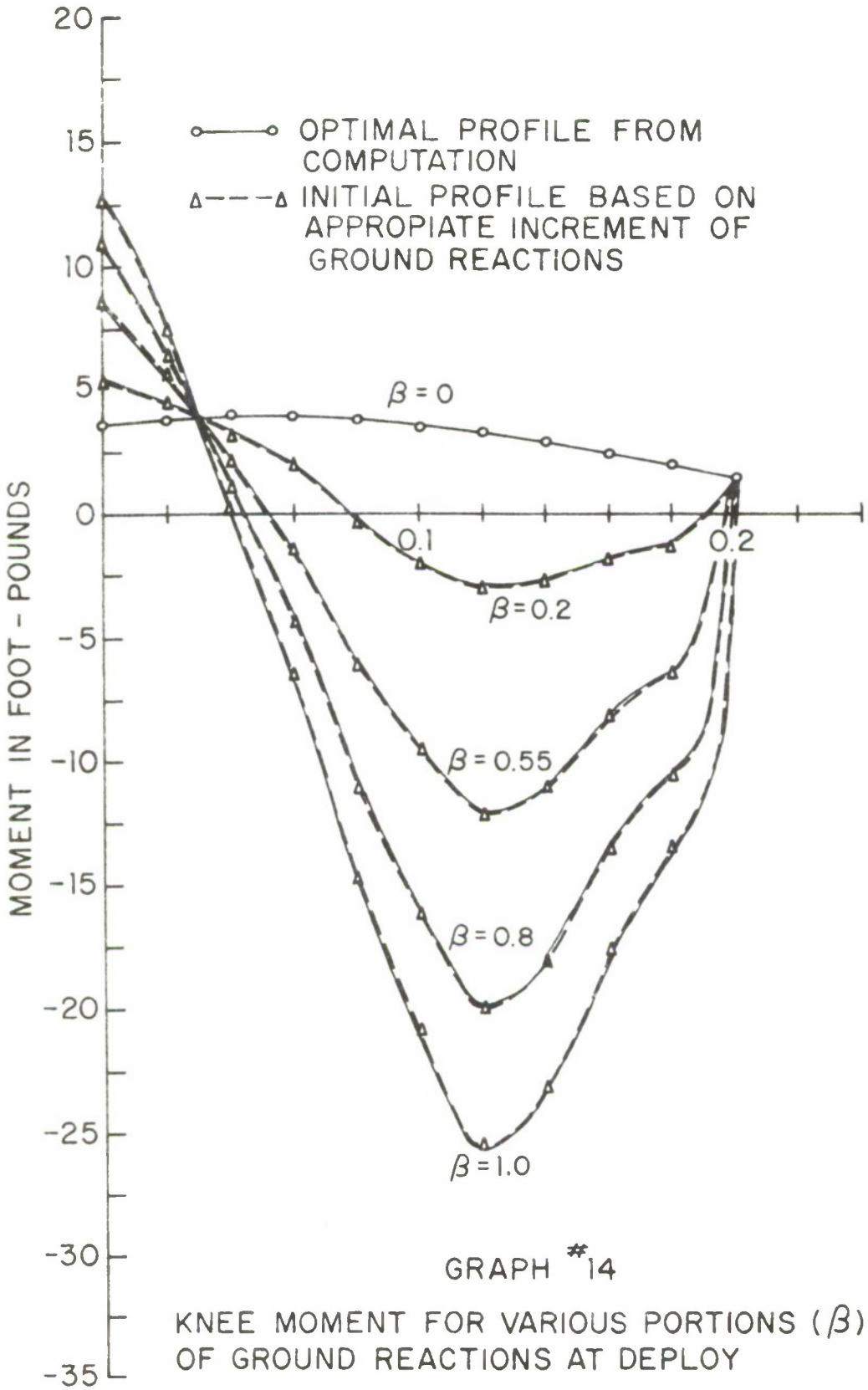

GRAPH #14

KNEE MOMENT FOR VARIOUS PORTIONS (β) OF GROUND REACTIONS AT DEPLOY

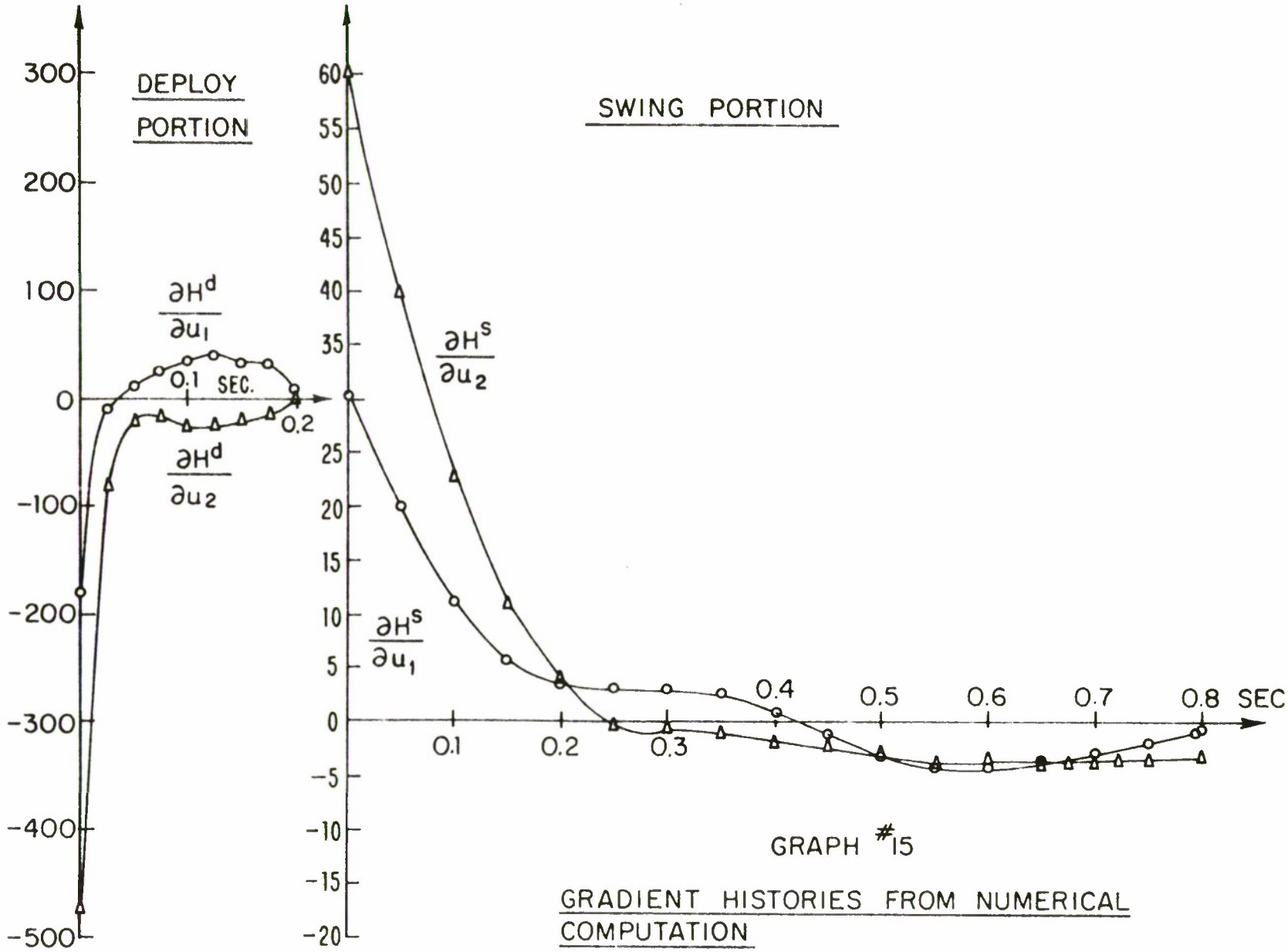

GRAPH #15

GRADIENT HISTORIES FROM NUMERICAL COMPUTATION

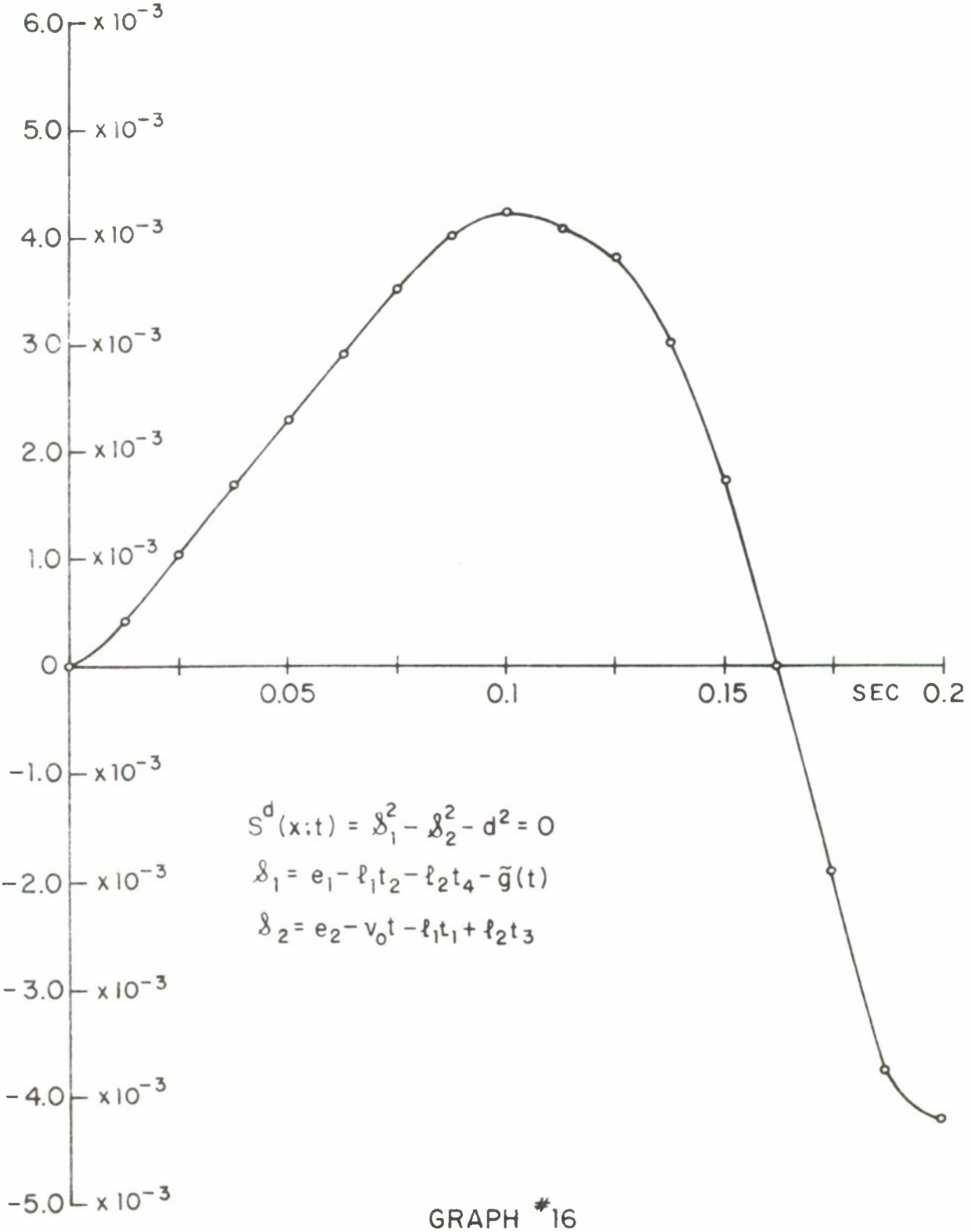

GRAPH #16

STATE EQUALITY CONSTRAINT IN DEPLOY PORTION

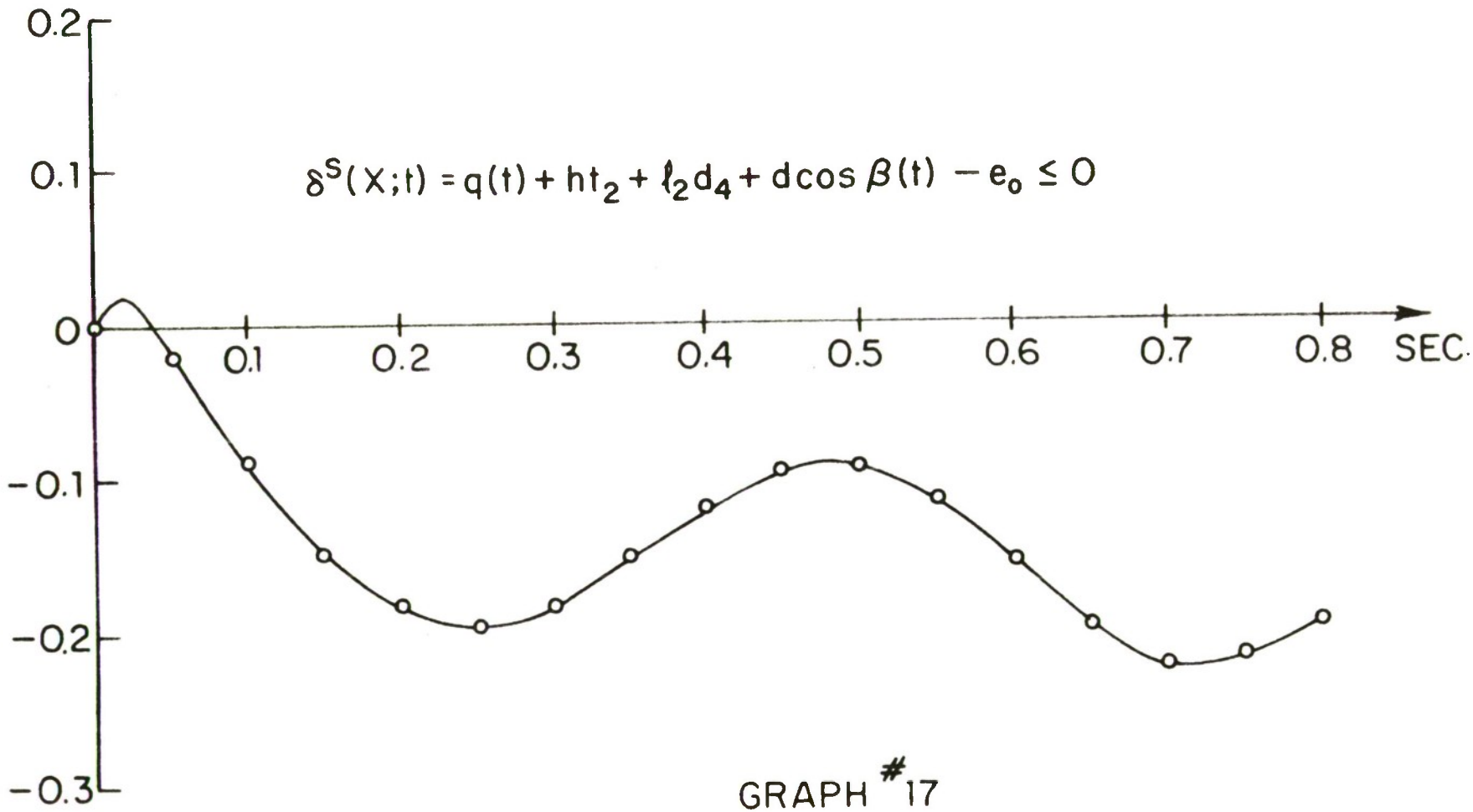

GRAPH # 17

STATE INEQUALITY CONSTRAINT FOR
SWING PORTION

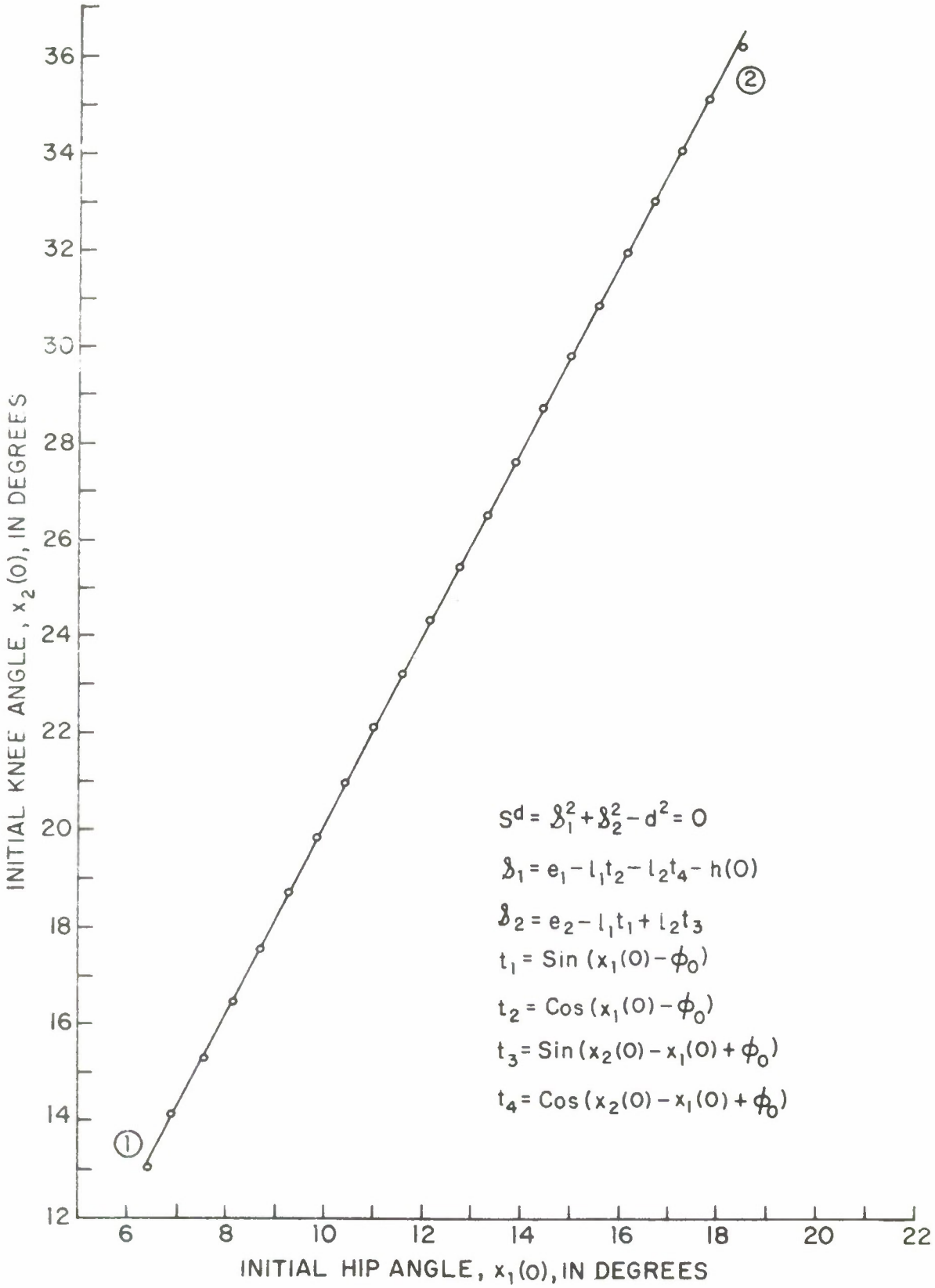

GRAPH #18
THE SET OF INITIAL ANGLES $(x_1(0), x_2(0))$
WHICH SATISFIES THE ENTRY CONDITION

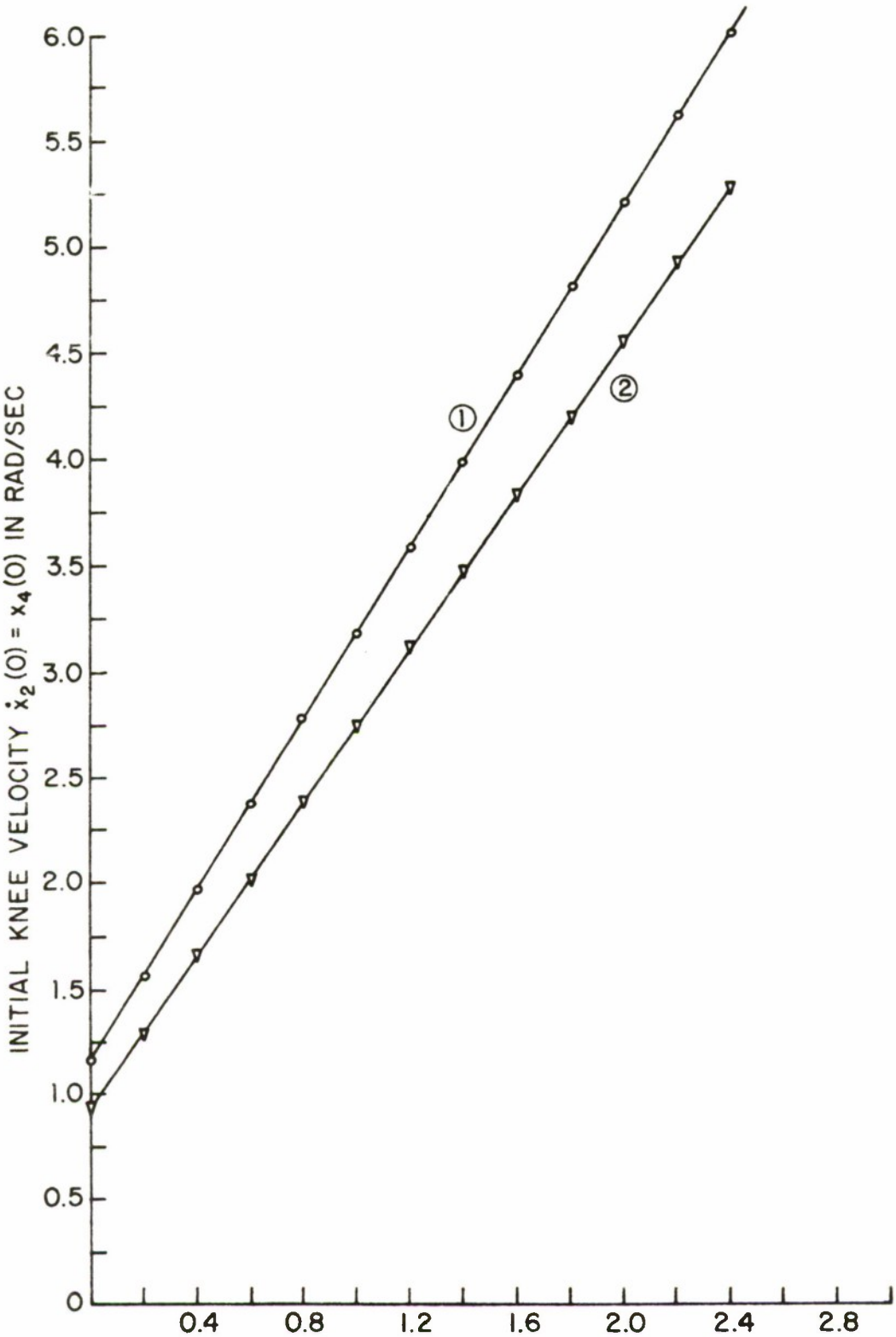

GRAPH #19

THE SET OF INITIAL VELOCITIES WHICH SATISFIES $\dot{S}^d\Big|_{t=0} = 0$

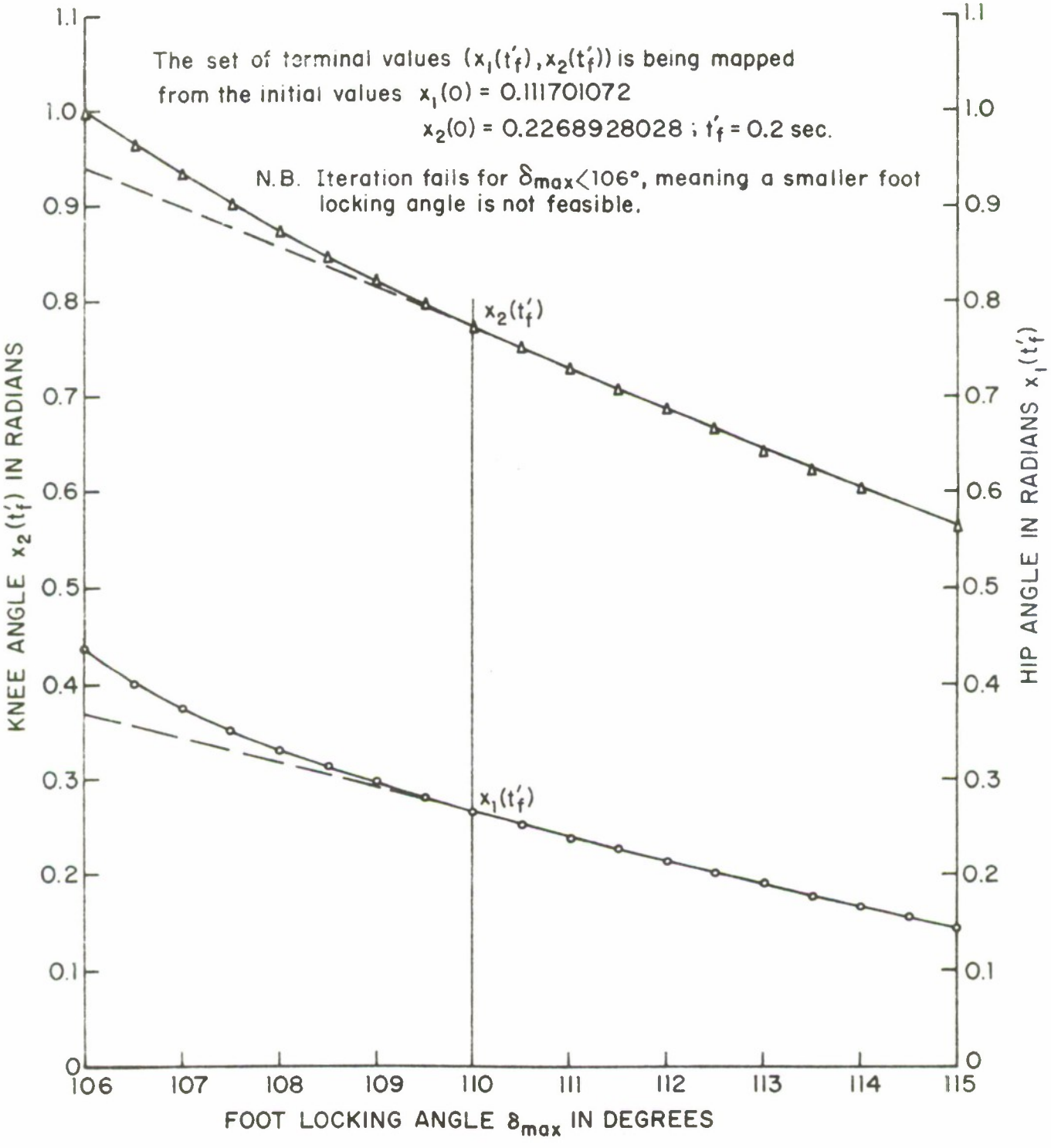
The set of terminal values $(x_1(t_f'), x_2(t_f'))$ is being mapped
from the initial values $x_1(0) = 0.111701072$
$x_2(0) = 0.2268928028$; $t_f' = 0.2$ sec.
N.B. Iteration fails for $\delta_{max} < 106°$, meaning a smaller foot locking angle is not feasible.
$x_2(t_f')$
$x_1(t_f')$
KNEE ANGLE $x_2(t_f')$ IN RADIANS
HIP ANGLE IN RADIANS $x_1(t_f')$
FOOT LOCKING ANGLE δ_{max} IN DEGREES
0
0.1
0.2
0.3
0.4
0.5
0.6
0.7
0.8
0.9
1.0
1.1
106
107
108
109
110
111
112
113
114
115

GRAPH #20

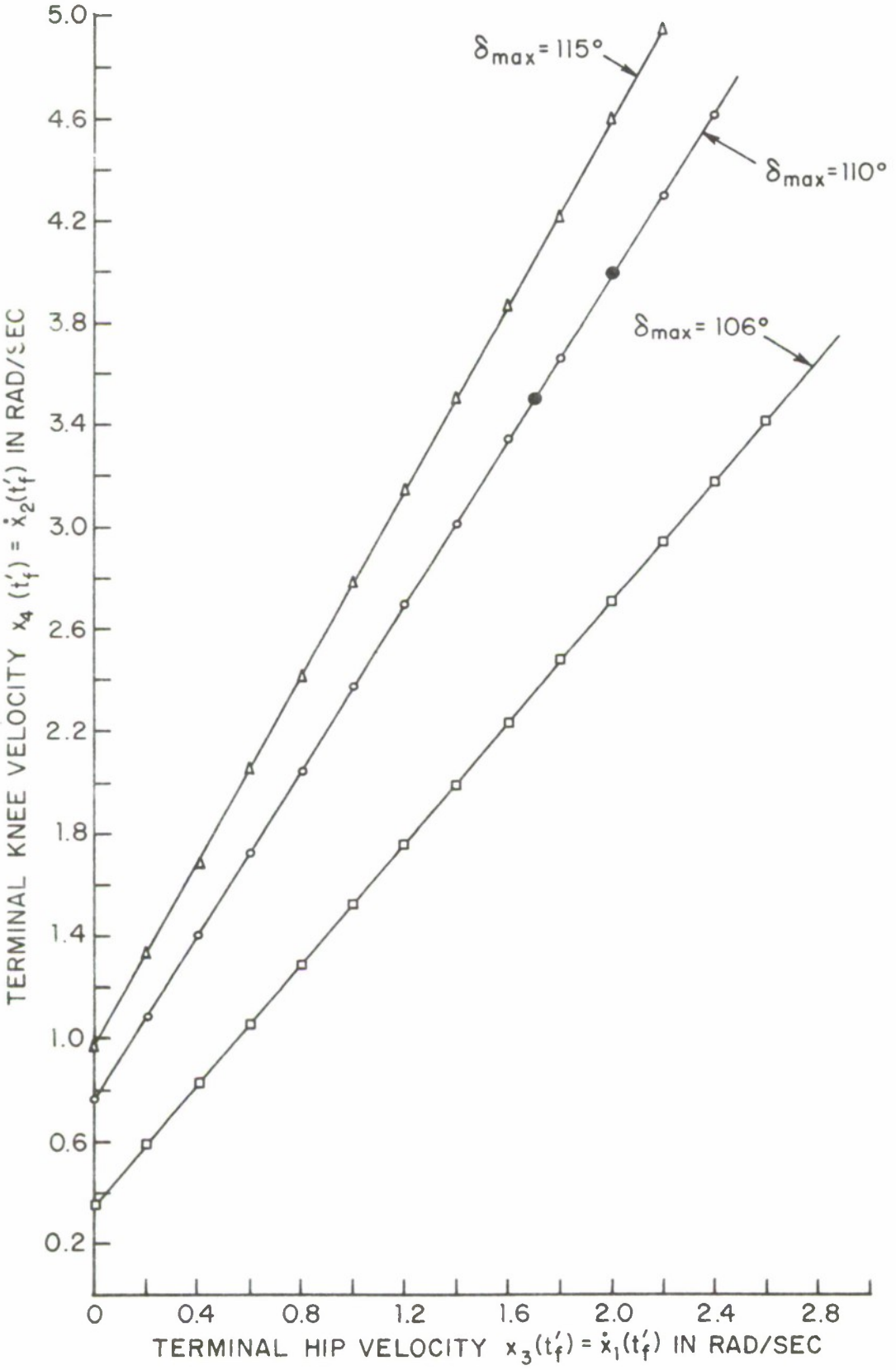
5.0
4.6
4.2
3.8
3.4
3.0
2.6
2.2
1.8
1.4
1.0
0.6
0.2
TERMINAL KNEE VELOCITY $x_4(t_f') = \dot{x}_2(t_f')$ IN RAD/SEC
$\delta_{max} = 115°$
$\delta_{max} = 110°$
$\delta_{max} = 106°$
0
0.4
0.8
1.2
1.6
2.0
2.4
2.8
TERMINAL HIP VELOCITY $x_3(t_f') = \dot{x}_1(t_f')$ IN RAD/SEC

GRAPH #21

F. Conclusions

A new quantitative study of the human locomotion problem has been developed using the methods of optimal programming and control theory. The multi-arc formulation is based on the qualitative properties of the biped gait. Results of the numerical experiment indicate that the theory is highly relevant and agrees well with experimental results to-date. Because of the flexibility of the method, the theory can certainly be used to study various types of gait, normal or pathological. The quantitative method should find importance in prosthetic design. Eventually, it is hoped, through systematic studies like the one described, locomotion by programmed stimulation will be realized.

References

1. Bernstein, N., Popova and Mogilansky, "Technique of the Study of Movements", Moscow, Gossidat, 1934.

2. Fenn, W. O., "The Mechanics of Muscular Contraction in Man", J. App. Physio. 9, p. 165+, 1938.

3. Ibid., "Work Against Gravity and Work Due to Velocity Changes in Running", Am. J. Physiol., No. 93, p. 433+, 1930.

4. Steindler, A., "Mechanics of Normal and Pathological Locomotion" (book), Springfield, Ill., Charles C. Thomas, Publisher, 1935.

5. Elftman, H., "Biomechanics of Muscle", J. of Bone and Joint Surgery, Vol. 48-A No. 2, March, 1966.

6. Ibid., "The Basic Pattern of Human Locomotion", Annals of New York Acad. Science, No. 51, p. 1207+, 1951.

7. Ibid., "Skeletal and Muscular Systems: Structure and Function", In Medical Physics (book), p. 1420+, Chicago, Year Book Publishers, 1944.

8. Ibid., "Forces and Energy Changes in the Leg During Walking", Am. J. Physiol., No. 125, pp. 339-356, 1939.

9. Liberson, W. T., "Biomechanics of Gait: A Method of Study", Archives of Physical Medicine and Rehabilitation, Jan., 1965.

10. Wilson, P. D. and Klopsteg, P. E. (Editors), "Human Limbs and Their Substitutes", McGraw-Hill, New York, 1968.

11. Close, J. R., "Motor Function in the Lower Extremity", American Lecture Series Publication No. 551, Charles C. Thomas, Publisher, Springfield, Ill., 1964.

12. College of Engineering, University of California (Berkeley), "Fundamental Studies of Human Locomotion and Other Information Relating to Design of Artificial Limbs", Rep. to National Research Council Artificial Limbs, 1947.

13. Bresler, B. and Frankel, J. P., "The Forces and Moments in the Leg During Level Walking", Trans. of American Soc. of Mechanical Engineers, p. 27+, Jan., 1950.

14. Crochetierre, W. J., Vodvnik, L., Reswick, J. B., "Electrical Stimulation of Skeletal Muscle - A Study of Muscle as an Actuator", Medical and Biological Engineering, Vol. 5, pp. 111-125, 1967.

15. Ibid., "Control of a Skeletal Joint by Electrical Stimulation of Antagonists", Vol. 5, pp. 97-109, 1967.

16. Scott, R. N., "Myo-electric Control Systems" in S. Levine (Ed.) "Advances in Biophysics and Bio-engineering" (book), Prentice-Hall, 1969.

17. Milner, M., Quanbury, A. O. and Edwards, E. P., "Progress Report No. 1-Human Locomotion by Ordered Electro-Stimulation of the Available Musculature", LTR-CS-6, April, 1969, Control Systems Lab., National Research Council, Ottawa, Canada.

18. Ibid., "Progress Report No. 2-Human Locomotion by Ordered Electro-Stimulation of the Available Musculature", LTR-CS-11, September, 1969. NRC, Ottawa, Canada.

19. Ibid., "Progress Report No. 3-Analysis of Footswitch Data in Walking", LTR-CS-26, January, 1970, NRC, Ottawa, Canada.

20. Ibid., "Progress Report No. 4-Analysis of Muscle Activities at Various Speeds and Pace Periods from EMG's with Indwelling Electrodes", LTR-CS-33, June 1970, NRC, Ottawa, Canada.

21. Mountcastle, V. B. (Editor), "Medical Physiology" (book), Vol. 2, C. V. Mosby, St. Louis, 1968.

22. Vukobratovic. M., Juričić, D., "Contribution to the Synthesis Biped Gait", IEEE Trans. on Bio-Medical Engineering, Vol. BME-16 No. 1, January. 1969.

23. Vukobratovic. M., Frank, A. A., Juričić D., "On the Stability of Biped Locomotion", IEEE Trans. on Bio-Medical Engineering. Vol. BME-17, No. 1, January, 1970.

24. Tomovic, R., "Outline of a Control Theory of Prosthetics", IFAC Proceedings, Basle, Switzerland, 1963.

25. Ralston, H. J., "Energy-Speed Relations and Optimal Speed During Level Walking", Int. S. Augew. Physiol. einschl Arbeitsphysio. Bd. 17, 277-283, 1958.

26. Cotes, J. E., and Meade, F., "The Energy Expenditure and Mechanical Energy Demand in Walking", Ergonomics, April, 1960.

27. Nubar, Y. and Contini, R., "A Minimal Principle in Bio-Mechanics", Bull. Math. Biophysics, No. 23, pp. 377-390. 1961.

28. Beckett, R. and Chang, K., "An Evaluation of the Kinematics of Gait by Minimum Energy", T. of Biomechanics, Vol. 1, pp. 147-159, 1968.

29. Vukobratovic, M., Marić, M. and Garvilovic, M., "An Approach to the Synthesis of Lower-Extremity Control", Proc. 2nd International Symp. on External Control of Human Extremities, Yugoslav Committee for Electronics (ETAN), Belgrade, pp. 206-211, 1967.

30. Hill, J. C., "A Model of the Human Postural Control System", 8th-IEEE Symp. on Adaptive Processes; Decision and Control, December, 1969.

31. Inman, V. T., "Human Locomotion", Canadian Medical Assoc. J., Vol. 94, pp. 1047-1054, 1966.

32. Lissner, H. R. and Williams, W., "Biomechanics of Human Motion" (book), W. B. Sanders, Philadelphia, Penn., 1962.

33. Galiana, H. L., "Modelling the Human Leg in Walking", M. Eng. Thesis, McGill Univ., Montreal, Quebec, Canada, August, 1968.

34. Wallach, J. and Saibel, E., "Control Mechanism Performance Criterion for an Above-Knee Leg Prosthesis", J. of Biomechanics, Vol. 3, pp. 87-97, 1970.

35. Lasdon, L. S., Waren, A. D. and Rice, R. K., "An Interior Penalty for Inequality Constrained Optimal Control Problems", IEEE Trans. on Automatic Control, Vol. AC-12, No. 4, August, 1967.

36. Wilkie, D. R., "Facts and Theories about Muscle", Prog. in Biophysics and Biophysical Chemistry, No. 4, p. 288+, 1954.

37. Ibid., "The Relation between Force and Velocity in Human Muscle", J. Physiol., No. 110, p. 249+, 1950.

38. Vickers, W., "A Physiologically Based Model of Neuromuscular System Dynamics", IEEE Trans. on Man-Machine Systems, Vol. MMS-9, No. 2, p. 21+, 1968.

39. McRuer, D. et al, "A Neuromuscular Actuation System Model", IEEE Trans. on Man-Machine Systems, Vol. MMS-9, No. 3, p. 61+, 1968.

40. Bigland, B. and Lippold, O. C. J., "The Relation between Force, Velocity and Integrated Electrical Activity in Human Muscle", J. Physiol., No. 123, p. 214+, 1954.

41. Stark, L., "Neurological Control Systems-Studies in Bioengineering" (book), Plenum Press, N. Y., 1968, (p. 302+).

42. Houk, J., "A Mathematical Model of the Stretch Reflex in Human Muscle Systems", M. S. Thesis, M. I. T., 1963. (Also appears in "The Application of Control Theory to Physiological Systems" book by T. Milhorn, Saunders, 1963, Chapter 17.

43. Bryson, A. E. and Ho, Y. C., "Applied Optional Control: Optimization, Estimation and Control" (book), Blaisdell Publishing Company, Waltham, Mass., 1968.

44. Lele, M. M. and Jacobson, D. H., "A Proof of the Convergence of the Kelley-Bryson Penalty Function Technique for State-Constrained Control Problems", J. Math. Anal. Appl., 1969.

45. McGhee, R. B., "Some Finite State Aspects of Legged Locomotion", Math. Biosciences, Vol. 2, No. 2, pp. 67-84, 1968.

46. McGhee, R. B. and Frank, A. A., "On the Stability Properties of Quadruped Creeping Gaits", Math. Biosciences, Dec., 1968.

47. Tomovic, R. and McGhee, R. B., "A Finite State Approach to the Synthesis of Bioengineering Control Systems", IEEE Trans. on Human Factors in Electronics, Vol. HFE-7, No. 2, June, 1966.

48. Tomovic, R., "Multi-level Control of Mechanical Multivariable Systems as Applied to Prosthetics", IEEE Trans. Automatic Control (short papers), Vol. AC-13, February, 1968.

Asst Director/Research (Rm 3C128)
Office of the Secretary of Defense
Pentagon
Washington, D. C. 20301

Technical Library
DDR and E
Room 3C-122, The Pentagon
Washington, D. C. 20301

Chief, R and D Division (340)
Defense Communications Agency
Washington, D. C. 20305

Director for Materials Sciences
ARPA
Room 3D179, The Pentagon
Washington, D.C. 20301

Major Richard J. Gowen
Tenure Associate Professor
Dept of Electrical Engineering
USAF Academy, Colorado 80840

Defense Documentation Center
Attn: DDC-TCA
Cameron Station
Alexandria, Virginia 22314 (40)

M. A. Rothenberg (STEPD-SD(SI)
Scientific Director
Dugway Test Center
Bldg 100, Soldiers' Circle
Fort Douglas, Utah 84113

Mr. H. E. Webb, Jr (EMPIS)
Rome Air Development Center
Griffiss Air Force Base, New York 13440

Central Intelligence Agency
Attn: CRS/ADD/PUBLICATIONS
Washington, D.C. 20505

Hq. USAF (AFRDDD)
The Pentagon
Washington, D.C. 20330

Hq. USAF (AFRDDG)
The Pentagon
Washington, D.C. 20330

Hq. USAF (AFRD3D)
The Pentagon
Washington, D.C. 20330
Attn: LTC C. M. Wreppy

Colonel E. P. Gaines, Jr
ACDA/FO
1901 Pennsylvania Avenue N.W.
Washington, D.C. 20451

Lt. Col. H. W. Jackson (SREE)
Chief, Electronics Division
Directorate of Engineering Sciences
Air Force Office of Scientific Research
Arlington, Virginia 22209 (5)

Dr. I. R. Mirman
Hq AFSC (SCGP)
Andrews Air Force Base
Washington, D.C. 20331

Commanding General
USACDC Institute of Land Combat
Attn: Technical Library, Rm 636
2461 Eisenhower Avenue
Alexandria, Virginia 22314

Rome Air Development Center
Attn: Documents Library (EMTLD)
Griffiss Air Force Base
New York 13440

MIT Lincoln Laboratory
Attn: Library A-082
P. O. Box 73
Lexington, Mass. 02173

Dr. L. M. Hollingsworth
AFCRL (CRN)
L. G. Hanscom Field
Bedford, Massachusetts 01730

VELA Seismological Center
300 North Washington Street
Alexandria, Virginia 22314

Hq. ESD (ESTI)
L. G. Hanscom Field
Bedford, Massachusetts 01730 (2)

Prof. R. H. Rediker
Electrical Engineering, Professor
MIT
Building 13-3050
Cambridge, Massachusetts 02139

AFAL (AVT) Dr. H. V. Noble
Electronics Technology Division
Air Force Avionics Laboratory
Wright-Patterson AFB, Ohio 45433

Director
Air Force Avionics Laboratory
Wright-Patterson AFB
Ohio 45433

AFAL (AVTA/R. D. Larson)
Wright-Patterson AFB
Ohio 45433

Director of Faculty Research
Dept. of the Air Force
U. S. Air Force Academy
Colorado Springs, Colorado 80840

Academy Library (DFSLB)
USAF Academy
Colorado Springs, Colorado 80840

Director
Aerospace Mechanics Sciences
Frank J. Seiler Research Lab. (OAR)
USAF Academy
Colorado Springs, Colorado 80810

Director, USAF PROJECT RAND
Via: Air Force Liaison Office
The RAND Corporation
Attn: Library D
1700 Main Street
Santa Monica, California 90406

HQ SAMSO (SMTAE/Lt. Belair)
AF Unit Post Office
Los Angeles, California 90045

Miss R. Joyce Harman
Project MAC, Room 810
545 Main Street
Cambridge, Mass. 02139

AUL3T-9663
Maxwell AFB, Alabama 36112

AFETR Technical Library
(ETV, MU-135)
Patrick AFB, Florida 32925

ADTC (ADBPS-12)
Eglin AFB, Florida 32542

Mr. B. R. Locke
Technical Adviser, Requirements
USAF Security Service
Kelly Air Force Base, Texas 78241

Hq. AMD (AMR)
Brooks AFB, Texas 78235

USAFSAM (SMKOM)
Brooks AFB, Texas 78235

Commanding General
Attn: STEWS-RE-L, Technical Library
White Sands Missile Range
New Mexico 88002 (2)

Hq. AESC (AETS)
Arnold AFS, Tennessee 37389

USAF
European Office of Aerospace Research
APO, New York 09667

Director
Physical and Engineering Sciences Div.
3045 Columbia Pike
Arlington, Virginia 22204

Commanding General
U. S. Army Security Agency
Attn: IARD-T
Arlington Hall Station
Arlington, Virginia 22212

Commanding General
U. S. Army Material Command
Attn: AMCRD-TP
Washington, D.C. 20315

Commanding Officer
Harry Diamond Laboratories
Attn: Dr. Reinhold Altman (AMXHD-TI)
Connecticut Avenue & Van Ness St. N.W.
Washington, D.C. 20438

Chief
Missile Electronic Warfare Tech Area
(AMSEL-WL-M)
U. S. Army Electronics Command
White Sands Missile Range
New Mexico 88002

Commanding Officer (AMXRD-BAT)
U. S. Army Ballistic Research Lab
Aberdeen Proving Ground
Aberdeen, Maryland 21005

Technical Director
U. S. Army Limited War Laboratory
Aberdeen Proving Ground
Aberdeen, Maryland 21005

Commanding Officer
U. S. Army Engineer Topographic Labs
Attn: STINFO Center
Fort Belvoir, Virginia 22060

U. S. Army Munitions Command
Attn: Science & Technology Info. Branch
Building 59
Picatinny Arsenal, SMUPA-RT-S
Dover, New Jersey 07801

U. S. Army Mobility Equipment Research
and Development Center
Attn: Technical Document Center
Building 315
Fort Belvoir, Virginia 22060

Commanding Officer (AMSEL-RI-WS-RI)
Atmospheric Sciences Laboratory
U. S. Army Electronics Command
White Sands Missile Range
New Mexico 88002

Dr. Herman Robl
Deputy Chief Scientist
U. S. Army Research Office (Durham)
Box CM, Duke Station
Durham, North Carolina 27706

Richard O. Ulsh (CRD-ARD-IP)
U. S. Army Research Office (Durham)
Box CM, Duke Station
Durham, North Carolina 27706

Technical Director
(SMUFA-A1100-107-1)
Frankford Arsenal
Philadelphia, Pa. 19137

Redstone Scientific Info. Center
Attn: Chief, Document Section
U. S. Army Missile Command
Redstone Arsenal, Alabama 35809

Commanding General
U. S. Army Missile Command
Attn: AMSMI-RR
Redstone Arsenal, Alabama 35809

Commanding General
U. S. Army Strategic Comm. Command
Attn: SCC-CG-SAE
Fort Huachuca, Arizona 85613

Commanding Officer
Army Materials and Mechanics
Research Center
Attn: Dr. H. Priest
Watertown Arsenal
Watertown, Mass. 02172

Commandant
U. S. Army Air Defense School
Attn: Missile Science Div., C&S Dept.
P. O. Box 9390
Fort Bliss, Texas 79916

Commandant
U. S. Army Command and General
Staff College
Attn: Acquisitions, Lib. Div.
Fort Leavenworth, Kansas 66027

Mr. Norman J. Field, AMSEL-RD-S
Chief, Office of Science & Technology
Research & Development Directorate
U. S. Army Electronics Command
Fort Monmouth, New Jersey 07703

Mr. Robert O. Parker, AMSEL-RD-S
Executive Secretary, TAC/JSEP
U. S. Army Electronics Command
Fort Monmouth, New Jersey 07703

Commanding General
U. S. Army Electronics Command
Fort Monmouth, New Jersey 07703
Attn: AMSEL-SC
DL
GG-DD
XL-D
XL-DT
BL-FM-P
CT-D
CT-R
CT-S
CT-L (Dr. W. S. McAfee)
CT-O
CT-I
CT-A
NL-D (Dr. H. Bennett)
NL-A
NL-C
NL-P
NL-P-Z
NL-R
NL-S
KL-D
KL-I
KL-E
KL-S
KL-SM
KL-T
VL-D
VL-F
WL-D

Dr. Alvin D. Schnitzler
Institute for Defense Analyses
Science and Technology Division
400 Army-Navy Drive
Arlington, Virginia 22202

Director (NV-D)
Night Vision Laboratory, USAECOM
Fort Belvoir, Virginia 22060

Commanding Officer
Atmospheric Sciences Laboratory
U. S. Army Electronic Command
White Sands Missile Range
New Mexico 88002

Code 8350
Mowry Center Library
Naval Research Laboratory
Washington, D. C. 20390

Dr. A. G. Jordan
Head of Dept. of Electrical Engineering
Carnegie-Mellon University
Pittsburgh, Pennsylvania 15213

Project Manager
NAVCOM
Attn: Herold H. Pehr (AMCPM-NS-TM)
Building 439
U. S. Army Electronics Command
Fort Monmouth, New Jersey 07701

Director, Electronic Programs
Attn: Code 427
Dept. of the Navy
Washington, D.C. 20360 (3)

Commander
Naval Security Group Command
Naval Security Group Headquarters
Attn: G43
3801 Nebraska Avenue
Washington, D.C. 20390

Director
Naval Research Laboratory
Washington, D.C. 20390
Attn: Code 2027 (6)
Dr. W. D. Hall, Code 7600 (1)
Dr. A. Brodzinsky (1)
Supt. Elec. Div.

Dr. G. M. R. Winkler
Director, Time Service Division
U. S. Naval Observatory
Washington, D.C. 20390

Naval Air Systems Command
AIR 03
Washington, D.C. 20360 (2)

Naval Ship Systems Command
SHIP 031
Washington, D.C. 20360

Naval Ship Systems Command
SHIP 035
Washington, D.C. 20360

U. S. Naval Weapons Laboratory
Dahlgren, Virginia 22448

Naval Electronic Systems Command
ELEX 01, Rm 2534 Main Navy Bldg.
Dept. of the Navy
Washington, D.C. 20360 (2)

Government Documents Dept.
University of Iowa Libraries
Iowa City, Iowa 52240

Commander
U. S. Naval Ordnance Laboratory
Attn: Librarian
White Oak, Maryland 21502 (2)

Director
Naval Research Laboratory
Attn: Library, Code 2029 (ONRL)
Washington, D.C. 20390 (2)

Hollander Associates
P. O. Box 2276
Fullerton, California 92633

Illinois Institute of Technology
Dept. of Electrical Engineering
Chicago, Illinois 60616

The University of Arizona
Dept. of Electrical Engineering
Tucson, Arizona 85721

Utah State University
Dept. of Electrical Engineering
Logan, Utah 84321

Case Institute of Technology
Engineering Division
University Circle
Cleveland, Ohio 44106

Capt E. Baum, Capt.
AFWL (WLRE)
Kirtland AFB, New Mexico 87117

Lenkurt Electric Co., Inc.
1105 County Road
San Carlos, California 94070
Attn: Mr. E. K. Peterson

Dr. F. R. Charvat
Union Carbide Corporation
Materials Systems Division
Crystal Products Dept.
8888 Balboa Avenue
P. O. Box 23017
San Diego, California 92123

Director
U. S. Army Advanced Materiel
Concepts Agency
Washington, D. C. 20315

Electromagnetic Compatibility
Analysis Center
(ECAC), Attn: ACOAT
North Severn
Annapolis, Maryland 21402

Dept. of Electrical Engineering
Rice University
Houston, Texas 77001

Research Laboratories for the
Engineering Sciences
School of Engineering and Applied
Science
University of Virginia
Charlottesville, Virginia 22903

Dept. of Electrical Engineering
Clippinger Laboratory
Ohio University
Athens, Ohio 45701

Lehigh University
Dept. of Electrical Engineering
Bethlehem, Pennsylvania 18015

Professor James A. Cadzow
Dept. of Electrical Engineering
State Univ. of New York at Buffalo
Buffalo, New York 14214

Director
Office of Naval Research Branch Office
495 Summer Street
Boston, Mass. 02210

Commander (AIR-)
Naval Air Development Center
Johnsville, Warminster, Pa. 18974
Attn: NADC Library

Commander (Code 753)
Naval Weapons Center
Attn: Technical Library
China Lake, California 93555

Commanding Officer
Naval Weapons Center
Corona Annex
Attn: Library
Corona, California 91720

Commanding Officer (563221)
U. S. Naval Missile Center
Point Mugu, California 93041

W. A. Eberspacher, Assoc. Head
Systems Integration Division
Code 5341A
U. S. Naval Missile Center
Point Mugu, California 93041

Commander
Naval Electronics Laboratory Center
Attn: Library
San Diego, California 92152 (2)

Deputy Director and Chief Scientist
Office of Naval Research Branch Office
1030 East Green Street
Pasadena, California 91101

Library (Code 2124)
Technical Report Section
Naval Postgraduate School
Monterey, California 93940

Glen A. Myers (Code 52 My)
Assoc. Prof. of Electrical Engineering
Naval Postgraduate School
Monterey, California 93940

Commanding Officer (Code 2064)
Navy Underwater Sound Laboratory
Fort Trumbull
New London, Conn. 06320

Commanding Officer
Naval Avionics Facility
Indianapolis, Indiana 46241

Dr. H. Harrison, Code RRE
Chief, Electrophysics Branch
National Aeronautics and Space Admin
Washington, D.C. 20546

NASA Lewis Research Center
Attn: Library
21000 Brookpark Road
Cleveland, Ohio 44135

Los Alamos Scientific Laboratory
Attn: Reports Library
P. O. Box 1663
Los Alamos, New Mexico 87544

Mr. M. Zane Thornton, Chief
Network Engineering, Communications
and Operations Branch
Lister Hill National Center for
Biomedical Communications
8600 Rockville Pike
Bethesda, Maryland 20014

U. S. Post Office Dept
Library - Room 6012
12th & Pennsylvania Ave. N.W.
Washington, D.C. 20260

Director
Research Laboratory of Electronics
M17
Cambridge, Mass. 02139

Mr. Jerome Fox
Research Coordinator
Polytechnic Institute of Brooklyn
333 Jay Street
Brooklyn, New York 11201

Director
Columbia Radiation Laboratory
Columbia University
538 West 120th Street
New York, New York 10027

Director
Coordinated Science Laboratory
University of Illinois
Urbana, Illinois 61801

Director
Stanford Electronics Laboratories
Stanford University
Stanford, California 94305

Director
Microwave Physics Laboratory
Stanford University
Stanford, California 94305

Director
Electronics Research Laboratory
University of California
Berkeley, California 94720

Director
Electronic Sciences Laboratory
University of Southern California
Los Angeles, California 90007

Director
Electronics Research Center
The University of Texas at Austin
Engineering-Sciences Bldg 110
Austin, Texas 78712

Division of Engineering and Applied Physics
190 Pierce Hall
Harvard University
Cambridge, Mass. 02138

Dr. G. J. Murphy
The Technological Institute
Northwestern University
Evanston, Illinois 60201

Dr. John C. Hancock, Head
School of Electrical Engineering
Purdue University
Lafayette, Indiana 47907

Dept. of Electrical Engineering
Texas Technological College
Lubbock, Texas 79409

Aerospace Corporation
P. O. Box 95085
Los Angeles, California 90045
Attn: Library Acquisitions Group

Professor Nicholas George
California Institute of Technology
Pasadena, California 91109

Aeronautics Library
Graduate Aeronautical Laboratories
California Institute of Technology
1201 E. California Blvd
Pasadena, California 91109

The Johns Hopkins University
Applied Physics Laboratory
Attn: Document Librarian
8621 Georgia Avenue
Silver Spring, Maryland 20910

Hunt Library
Carnegie-Mellon University
Schenley Park
Pittsburgh, Pa. 15213

Dr. Lee Young
Stanford Research Institute
Menlo Park, California 94025

Chairman, Electrical Engineering
Arizona State University
Tempe, Arizona 85281

Engineering & Mathematical
Sciences Library
University of California at L. A.
405 Hilgard Avenue
Los Angeles, California 90024

Sciences-Engineering Library
University of California
Santa Barbara, California 93106

Prof. Joseph E. Rowe
Chairman, Dept. of Electrical Engin.
The University of Michigan
Ann Arbor, Michigan 48104

Dr. W. R. LePage, Chairman
Syracuse University
Dept. of Electrical Engineering
Syracuse, New York 13210

Yale University
Dept. of Engineering and Applied Science
New Haven, Conn. 06520

Airborne Instruments Laboratory
Deerpark, New York 11729

Raytheon Company
Research Division Library
28 Seyon Street
Waltham, Massachusetts 02151

Dr. Sheldon J. Welles
Electronic Properties Information Center
Mail Station E-175
Hughes Aircraft Company
Culver City, California 90230

Dr. Robert E. Fontana
Dept. of Electrical Engineering
Air Force Institute of Technology
Wright-Patterson AFB, Ohio 45433

Dr. John R. Ragazzini, Dean
School of Engineering and Science
New York University
University Heights
Bronx, New York 10453

Sylvania Electronic Systems
Applied Research Laboratory
Attn: Documents Librarian
40 Sylvan Road
Waltham, Mass. 02154

Unclassified

Security Classification

DOCUMENT CONTROL DATA - R & D

Security classification of title, body of abstract and indexing annotation must be entered when the overall report is classified.

1. ORIGINATING ACTIVITY (*Corporate author*)
Division of Engineering and Applied Physics
Harvard University
Cambridge, Massachusetts

2a. REPORT SECURITY CLASSIFICATION
Unclassified

2b. GROUP

3. REPORT TITLE
STUDIES OF HUMAN LOCOMOTION VIA OPTIMAL PROGRAMMING

4. DESCRIPTIVE NOTES (*Type of report and inclusive dates*)
Technical Report (Interim)

5. AUTHOR(S) (*First name, middle initial, last name*)
C. K. Chow and D. H. Jacobson

6. REPORT DATE
October 1970

7a. TOTAL NO. OF PAGES

7b. NO. OF REFS
48

8a. CONTRACT OR GRANT NO.
N-00014-67-A-0298-0006

b. PROJECT NO.

c.

d.

9a. ORIGINATOR'S REPORT NUMBER(S)
Technical Report No. 617

9b. OTHER REPORT NO(S) (*Any other numbers that may be assigned this report*)

10. DISTRIBUTION STATEMENT
This document has been approved for public release and sale; its distribution is unlimited. Reproduction in whole or in part is permitted by the U. S. Government.

11. SUPPLEMENTARY NOTES

12. SPONSORING MILITARY ACTIVITY
Office of Naval Research

13. ABSTRACT

In this paper, a new approach to the study of "programmed" human locomotion is made using the methods of optimal programming and modern control theory.

Development of the problem structure relies closely on the phasic and temporal characteristics of the biped gait. The result is a multi-arc programming problem with three stages. Each stage involves appropriate dynamic constraints which reflect the particular nature of the phasic activity. Joining of the arcs is arranged in such a way as to maintain continuity of certain trajectories as well as repeatability of motion. A novelty of the approach is that the theory could be used to study walking behavior under different environmental conditions, such as walking up-stairs or over a hole.

A distinct feature of the present approach which differs from other studies is the presence of a minimizing performance criterion. Based on external characteristics of muscles and certain assumptions regarding normal locomotion, a simple quadratic type of criterion is proposed. This performance criterion is meaningful in that it is shown to be proportional to the mechanical work done during normal walking.

Invoking the necessary conditions of optimal control theory, a multi-point boundary value problem is obtained. A penalty function technique is employed for iterative numerical solution. Using the parameters available in the literature, simulation results are obtained which agree well with experimental studies. Furthermore, refined features are obtained which are not available in previous studies.

DD FORM 1 NOV 65 1473 (PAGE 1)

S/N 0101-807-6801

Unclassified

Security Classification

14 KEY WORDS	LINK A		LINK B		LINK C	
	ROLE	WT	ROLE	WT	ROLE	WT
Biped Locomotion						
Optimal Programming						
Human Locomotion						
Bio-Medical Engineering						
Mathematical Biosciences						
Mathematical Modelling						
Simulation						